2014-09-12

Remediation of a Salt-Affected, Macroporous Soil in Central Alberta, Canada

Callaghan, Michael Vincent

UNIVERSITY OF CALGARY

REMEDIATION OF A SALT-AFFECTED, MACROPOROUS SOIL IN CENTRAL ALBERTA, CANADA

by

MICHAEL V. CALLAGHAN

A THESIS

SUBMITTED TO THE FACULTY OF GRADUATE STUDIES

IN PARTIAL FULFILMENT OF THE REQUIREMENTS FOR THE

DEGREE OF DOCTOR OF PHILOSOPHY

DEPARTMENT OF GEOSCIENCE

CALGARY, ALBERTA

SEPTEMBER, 2014

Abstract

Salt-affected soil may be characterized by both elevated salinity and sodicity. High salinity levels impair plant growth and result in reduced plant yield. Leaching of salt from affected soil may be utilized to improve plant growth or to meet regulatory soil quality guidelines. As salinity levels decline during the leaching process recalcitrant elevated sodicity levels may result in clay swelling and disruption of soil structure. The accompanying reduction in soil permeability can produce poor soil drainage and reduced plant growth. The focus of this thesis is the remediation of salt-affected soil resulting from produced water releases associated with oil and gas production. Laboratory and field characterization and experiments were conducted on salt-affected soil at a former production facility in central AB, 35 km southwest of Edmonton. The objective of this thesis is to improve remediation outcomes using salt leaching in the relatively dry climate and fine-grained soil conditions typical of the Canadian prairies (CP). In addition, the effect of soil mineralogy on remediation of salt-affected soils is examined by quantifying the effect of gypsum and calcite dissolution on soil saturated paste extract (SPE) salinity and sodicity, as well as saline-sodic effects on hydraulic conductivity due to clay swelling.

Gypsum ($CaSO_4 \cdot 2H_2O$) was added to the soil as a Ca-amendment to ameliorate elevated Na levels. Calcite ($CaCO_3$) occurs naturally in this soil. Sulphate and HCO_3 mass in the SPE was compared to that in soil water samples collected from the field using suction lysimeters. Excess sulphate mass attributed to gypsum dissolution was measured in the SPE, while negligible excess calcite dissolution was determined. Excess gypsum dissolution occurred in 30 % of the soil samples. Gypsum dissolution in the saturated paste resulted in an overestimation of electrical conductivity (EC) by 22 % on average and an underestimation of sodium adsorption ration (SAR) by 7.6 % on average. The relative error increased as soil salinity and sodicity approached regulatory guidelines of 3 dS m^{-1} for EC and 4 for SAR. Following application of the correction for excess gypsum dissolution, the number of samples that met regulatory guidelines for both EC and SAR increased from 3 to 8, a 167 % increase.

Smectite, a swelling clay, is present in the soil under study, comprising 48 % of the clay-sized (<2 μm) fraction. Laboratory permeameter testing on intact soil cores demonstrated that 46 % of hydraulic conductivity reduction induced by clay swelling during leaching of moderately sodic conditions (SAR = 14) occurs following stabilization of effluent soil salinity. This time-dependent effect is attributed to slow diffusion of a small fraction of salt from smectite-bound pores. Additionally, variable degrees of recovery of hydraulic conductivity were observed upon application of high salinity permeant. This implies that saline-sodic swelling effects on pore structure are not fully reversible. Confined and intact subsoil shows greater sensitivity to saline-sodic induced reduction in hydraulic conductivity than repacked soils used in other research studies. Saline-sodic swelling effects represent a greater hazard to hydraulic conductivity to saline-sodic subsoils than surface soils for a similar swelling clay content.

A field irrigation experiment was conducted to increase leaching rates under naturally dry climate conditions. Supplementing natural precipitation with irrigation resulted in varying degrees of leaching from good to negligible, depending on the soil moisture condition. Efficient and timely leaching in fine-grained, macroporous soil is complicated by complex interaction between preferential flow in macropores and saline pore water stored within the soil matrix. Infiltration and drainage result in mixing of fresh water infiltrated through macropores with saline pore water within the aggregated soil matrix. Good leaching efficiency was achieved using repeated cycles of irrigation and drainage. In contrast, under continuous matrix-saturated moisture conditions, persistent fresh water flow in macropores bypassed the saline soil matrix resulting in negligible leaching efficiency. Control of infiltration and drainage cycles to produce good leaching efficiency are well suited to automated irrigation. Soil moisture conditions should be cycled between field capacity and saturation for optimal salt leaching.

Acknowledgements

I dedicate this thesis to my wife Christine and my children Elizabeth, Gabriel, Timothy, Kathryn, and my son Keswick who unfortunately passed to soon. I thank all the people with whom I worked on this project at the University of Calgary and everyone on whose assistance much of this work relied, including: Josh Bishop, Frank Head, Blake Hiebert, Jackie Randell, Simon Martin, Kristyn Adams, Alex Wilkinson, Farzin Malekani, and Aaron Booterbaugh. I also thank Imperial Oil Research (Dr. Michelle Young and Dr. Asfaw Bekele) and Surplus Properties Management (now Imperial Oil Environmental Services) for funding, in-kind support and access to their research site. Additional funding was supplied by Imperial Oil's University Research Awards Program. Funding and in-kind support was also provided by Environment Canada through Natural Resources Canada's Program for Energy Research and Development (PERD), managed by Dr. John Headley and Kerry Peru. Lastly but definitely not least, I thank my co-supervisors Dr. Laurence Bentley and Dr. Edwin Cey. Having two perspectives on my research definitely made it better. Supervisor funding came from the Natural Sciences and Engineering Research Council (NSERC) Collaborative Research and Development Grant Program. Additional funding was provided to me by the University of Calgary Open Scholarship Competition, the Engineers Canada scholarship program, and the Canadian Foundation for Geotechnique Graduate Scholarship program.

Table of Contents

List of Tables

List of Figures

CHAPTER 1: THESIS INTRODUCTION

Elevated levels of salt in soil result in a decrease in osmotic potential between plant roots and the surrounding soil water. Plants compensate for this decrease in osmotic potential by expending energy to increase internal solute concentrations (Hanson et al., 2006). A plant therefore expends more energy per unit of water uptake under saline soil conditions than under non-saline conditions, resulting in decreased energy expenditure on growth and reduced plant yield under saline conditions (Lauchli and Grattan, 2011). The associated negative effects on plant growth are of particular concern in agricultural soils, where decreased yield has direct associated costs, such as lost income from crop production.

Elevated levels of sodium in soil are often correlated with elevated salinity, where the salt of concern is dominantly NaCl in composition. Clay bearing soils are at increased susceptibility to clay swelling and dispersion in the presence of high sodium and low salinity levels (Shainberg and Singer, 2011). Clay swelling can result in decreased size or continuity of conductive soil pores, while dispersed clay can result in pore clogging with fines. The effect of both processes is a decrease in soil permeability, which may have deleterious consequences for water infiltration and drainage in soils. Sodic-effects on soil may result in waterlogging due to poor internal drainage and surface sealing by dispersed clay, resulting in reduced seedling emergence (Quirk, 2001).

Salt-affected soils are particularly common in arid and semi-arid areas (Hanson et al., 2006). Dryland salinity affects 2 Mha of land in the Canadian prairies (CP) or 5% of the total area under cultivation (Alberta Agriculture and Rural Development, 2013; Natural Resources Canada, 2013). Salt-affected soils are also a common environmental issue encountered as a result oil and gas operations (Merrill et al., 1990; Leskiw et al., 2012). As part of this thesis, site characterization and field experiments were conducted at a former oil and gas production facility located in central Alberta, Canada, 35 km southwest of Edmonton. The dominant land use in the area is agricultural, including cattle rearing, miscellaneous specialty farming, and grain/oilseed crop production (Alberta Agriculture and Rural Development, 2006). Production facilities at the site included two wellheads with flare pits, a small tank

farm and associated pipelines. Oil and gas was produced with a fraction of highly saline wastewater, so-called "produced water". Produced water is dominantly NaCl in composition with total dissolved solids (TDS) of 180 g L^{-1}. Major ion chemistry for the produced water is contained in Table 1.1. Salt-affected soil and shallow groundwater resulted from produced water releases to the environment due to historic disposal in the unlined flare pits and a pipeline break. Production facilities were removed from the site sometime prior to 1976.

Leaching of salt from the plant rooting zone is a common method of reclaiming salt-affected soil to improve crop yield (Ayers and Westcot, 1994). Successful reclamation of salt-affected soil results in reduction of soil salinity within the plant rooting zone to levels below the salinity threshold for a given crop (Keren and Miyamoto, 2011). In contrast, remediation of salt-affected soils at industrial sites is typically conducted within a regulatory framework. This thesis was prepared within a context of remediation of salt-affected soils resulting from oil and gas operations within the province of Alberta. Therefore, objectives of this research are framed within an applicable regulatory framework. Remediation of salt contamination at industrial sites in Alberta is prescribed by the document titled *Salt Contamination Assessment & Remediation Guidelines* (Alberta Environment, 2001). In contrast to reclamation where the goal is improved plant growth, remediation is deemed to be successful when soil quality meets guidelines for salinity and sodicity levels. In Alberta, salinity is measured as the electrical conductivity (EC) of a soil saturated paste extract (SPE), and sodicity is measured as the sodium adsorption ratio (SAR) of the same extract, where $SAR = Na / [(Mg + Ca)/2]^{1/2}$, with aqueous cation concentrations in $mmol_c\ L^{-1}$ [United States Salinity Laboratory (USSL) Staff, 1954].

In 2003, a tile drain system was installed at the study site by Imperial Oil Limited under 2 ha of the most salt-affected soil. The tile drain system was designed to collected saline leachate from the rooting zone and route it for disposal by deep well injection. The tile drains were installed near the base of the rooting zone at 2 m depth and 10 m spacing. The site is planted with a mix of perennial grasses and legumes typical of forage species but is not in use for agricultural purposes. Since 2003, a number of research projects have been conducted by University of Calgary, Department of Geoscience researchers at

the site. Time-lapse electrical resistivity tomography (ERT) geophysical surveys demonstrated higher rates of salt leaching above tile drains and in local micro-topographic depressions (Hayley, 2010). Modeling of salt leaching under natural precipitation produced a prediction of >100 yrs to leach the in situ salts out of the soil profile (Smith, 2008). This long timeline for remediation motivated the current phase of research to enhance salt leaching using irrigation. As part of the current phase of work a tracer study using 2,6-Difluorobenzoic acid was conducted to characterize preferential flow processes in the fine-grained, macroporous soil at the site (Bishop, 2012). Additional time-lapse geophysical characterization was performed coincident with this study by Head (2013). This thesis represents the final contribution to the most recent phase of research into salt leaching at the study site. The content of this thesis focuses on three distinct but related issues associated with remediation of salt-affected soils, explained below.

1.1 Mineral Dissolution during Preparation of the Saturated Paste Extract

The soil SPE methodology is the standard method for determination of soluble salts in soil [United States Salinity Laboratory (USSL) Staff, 1954]. Preparation of the saturated paste requires addition of distilled or deionized water to a dry soil sample, which is mixed and allowed to stand for a period of several hours to overnight (Rhoades, 1982). The degree of saturation is deemed sufficient if the surface glistens and flows freely. Extraction of the soil water and soluble salts is effected using low-vacuum or pressure filtration. Use of the SPE methodology is motivated by it being the lowest soil-to-water ratio that can be easily extracted under low vacuum or pressure, and due to good correlation between SPE salinity and plant response (Robbins and Wiegand, 1990). The amount of water added during preparation of the SPE is almost always in excess of the field-saturated moisture content. Due to this addition of excess water to the soil during preparation of the SPE, it is recognized that dilution during preparation of soil extracts introduces some error in ionic ratios resulting from mineral dissolution, ion hydrolysis, and cation exchange relative to field moisture conditions (Robbins and Wiegand, 1990).

Two of the aforementioned sources of error in the SPE determination of EC and SAR are investigated in this thesis: dissolution of sparingly soluble minerals; and, cation exchange. Sparingly

soluble minerals gypsum ($CaSO_4 \cdot 2H_2O$) and calcite ($CaCO_3$) are potential sources of excess ion contribution to EC measurements and Ca contribution to SAR. Gypsum is both commonly used as a soil amendment to ameliorate elevated soil sodicity (Ashworth et al., 1999) and is present naturally as a precipitate in soils of the CP (Chang et al., 1982; Hendry et al., 1986; Keller et al., 1991). Calcite is a common mineral in glacial sediments on which soils of the CP have developed (Pawluk and Bayrock, 1969). The degree to which gypsum and calcite dissolution within the soil saturated paste contributes to EC and SAR remains unquantified in the literature. Qualitatively, dissolution of gypsum and calcite within the soil saturated paste is expected to result in an overestimation of EC through contribution of additional ions and an underestimation of SAR due to additional contribution of Ca. Decisions on remedial success are made by comparing measured EC and SAR to soil quality guidelines. Therefore, improved accuracy in determination of these parameters may have direct implications on the evaluation of remedial success.

1.2 Clay Swelling Effects on Soil Hydraulic Conductivity during Leaching

Clay minerals of the smectite and vermiculite groups are swelling clays with documented effects on soil hydraulic conductivity under high sodicity and low salinity conditions (Quirk and Schofield, 1955; McNeal and Coleman, 1966). Smectite clay is the dominant swelling clay in soils in the CP (Curtin et al., 1994; Kohut and Dudas, 1995). Decreased hydraulic conductivity during leaching is of concern due to the relatively high leachability of soluble salts vs. adsorbed Na. Leaching of elevated Na from soil is somewhat retarded due to its adsorption on clays and organic matter (Curtin and Rostad, 1997). Of concern is that as salinity decreases during the leaching process persistent elevated Na levels may result in clay swelling and a corresponding decrease in hydraulic conductivity. If the decrease in hydraulic conductivity is substantial, it may have deleterious effects on the remediation effort, since the low hydraulic conductivity of fine-grained soils is already a limiting factor to infiltration and leaching. Due to variation in sensitivity of soils to saline-sodic swelling effects, soil-specific or region-specific studies are recommended (Rhoades, 1982).

1.3 Salt Leaching in Fine-Grained, Macroporous Soils in a Dry Climate

Leaching of salt from soil is effective, if there is sufficient water available to leach salts to depth. In the dry climate of the CP, average annual potential evapotranspiration is generally greater than precipitation. Therefore, the majority of precipitation that infiltrates into soil is either evaporated from the soil surface or transpired by plants. The consequence is that very little water is available under natural conditions to result in appreciable salt leaching. In dry climates, leaching rates are improved by augmenting precipitation with irrigation (Ayers and Westcot, 1994). Integrated irrigation and salt leaching studies in the CP are limited in geographic scope to southern Alberta (van Schaik and Milne, 1962; Rapp and Laliberte, 1968). These studies demonstrated that irrigation can be used successfully to leach salts from relatively coarse-grained soils (e.g., sands and sandy loams). Much less research has been performed on fine-grained soils. Good drainage of irrigated soils developed on glacial till in southern Alberta was attributed to small-scale weathering fractures (Hendry, 1982). There exists a need for detailed study of salt leaching in fine-grained soils that are the dominant soil cover in the CP. As part of this thesis, a plot-scale irrigation experiment was conducted at the aforementioned study site. A test plot, 20 m by 20 m was constructed over two tile drains, shown in Fig 1.1a. Irrigation water was applied by drip irrigation to the soil surface. The tile drains consist of slotted plastic pipe, with a slot size of 0.51 mm, wrapped in a non-woven geotextile filter fabric surrounded by a clean gravel pack (Fig. 1.1b). In addition to monitoring tile drain flow and effluent in a dedicated sump (Fig. 1a), the test plot was instrumented with soil moisture sensors, soil water suction lysimeters, and monitoring wells. Soil sampling and geophysical surveys were also utilized to track the movement of salts in the subsurface.

Infiltration, drainage and leaching in fine-grained soils are complicated by the occurrence of preferential flow in macropores, shown schematically in Fig. 1.2. Macropore flow occurs through pores that are substantially larger than the surrounding fine-grained matrix and include desiccation cracks, fractures resulting from pedogenic processes, and biopores such as wormholes and root holes (Flury et al., 1994). A major component of the research in this thesis focuses on the hydrologic controls on macropore

flow and the mechanism(s) of salt leaching. Macropore flow generation is highly sensitive to hydrologic conditions near the soil surface during infiltration. In general, under low intensity infiltration rates, macropore flow generation is less in relatively dry soils than in wet soils. This is demonstrated by a sharp increase in the depth of macropore flow penetration that occurs as macroporous soil approaches saturated moisture conditions. The range of soil water tension (SWT) between the relatively dry scenario (Fig. 1.3a) at SWT of 3.7 cm and the wet scenario (Fig. 1.3b) at SWT of 0.6 cm is narrow. Therefore, given the highly dynamic soil moisture conditions resulting from regular irrigation, it can be inferred that macropore flow generation is highly dynamic and will form a major control on salt leaching in our study.

1.4 Research Objectives

The objective of this research was to improve remediation of salt-affected soils in characteristic climate and soil conditions typical of the CP region. Efficient use of irrigation to increase leaching rates relative to those under natural precipitation conditions is investigated. Soil conditions in the CP are dominated by fine-grained glacially derived soils for which low soil permeability can be a limiting factor for timely leaching. Additionally, the presence of sparingly soluble minerals and swelling clays in soils of the CP has implications for remediation of salt-affected soils and is investigated.

1.5 Thesis Structure

This thesis is structured into six chapters, the middle four of which were prepared as stand-alone manuscripts for journal submission. Therefore, some degree of repetition exists between the individual manuscripts, primarily in the introduction to each chapter. The four chapters making up the body of this thesis fall under three aforementioned themes. Chapter 2 addresses mineral dissolution occurring during preparation of the saturated paste extract and its effect on soil salinity and sodicity determination. Chapter 3 addresses clay swelling effects on soil hydraulic conductivity during leaching of saline-sodic soil. Chapters 4 and 5 address hydrologic controls on leaching efficiency in fine-grained, macroporous soils.

Chapter 6 is a summary of the conclusions from each of the main body chapters, with recommendations for future research.

1.6 Author Contributions

Each of the four manuscripts prepared for this thesis, the authors on each, the journals they have been submitted to, and the contributions of each author to the manuscripts is given below:

1. *Gypsum and calcite dissolution effects on soil saturated paste extract electrical conductivity and sodium adsorption ratio*, Michael V. Callaghan (MVC), Edwin E. Cey (EEC), and Laurence R. Bentley (LRB), was originally submitted to the Journal of Environmental Quality and is currently being revised for resubmission. MVC lead the sample collection, analyzed and interpreted the data, and wrote the manuscript. LRB and EEC co-designed the sampling program, provided financial support, advised throughout, reviewed, and edited the manuscript.
2. *Hydraulic conductivity dynamics during salt leaching of a sodic, structured subsoil*, Michael V. Callaghan (MVC), Edwin E. Cey (EEC), and Laurence R. Bentley (LRB), accepted for publication in Soil Science Society of America Journal on 13 May 2014. MVC designed the experiment, lead the data collection, analyzed and interpreted the data, and wrote the manuscript. LRB and EEC provided financial support, advised throughout, reviewed, and edited the manuscript.
3. *Hydrologic controls on effective salt leaching in a fine-grained macroporous soil*, Michael V. Callaghan (MVC), Edwin E. Cey (EEC), Laurence R. Bentley (LRB), and Franklin A. Head (FAH), not yet submitted. MVC conducted the field experiment, lead collection of the hydrologic monitoring and samples, analyzed and interpreted the data, and wrote the manuscript. FAH participated in the electrical resistivity data collection, analyzed, and interpreted the electrical resistivity data. LRB and EEC provided financial support, advised throughout, reviewed, and edited the manuscript. LRB lead the electrical resistivity data collection and interpretation.

4. *Improving salt leaching efficiency in fine-grained, macroporous soil by controlling preferential flow using irrigation and drainage*, Michael V. Callaghan (MVC), Edwin E. Cey (EEC), and Laurence R. Bentley (LRB), not yet submitted. MVC developed the conceptual model, and wrote the manuscript. LRB and EEC provided financial support, advised throughout, reviewed, and edited the manuscript.

1.7 References

Alberta Agriculture and Rural Development. 2006. Alberta municipality profile 2006 census of agriculture, north west region. Government of Alberta., Edmonton, AB.

Alberta Agriculture and Rural Development. 2013. Salinity classification, mapping and management in Alberta. Government of Alberta. http://www1.agric.gov.ab.ca/$department/deptdocs.nsf/all/sag3267. (accessed 1 Aug. 2013).

Alberta Environment. 2001. Salt contamination and remediation guidelines. Environmental Sciences Division, Environmental Service, Pub. No. T/606, Edmonton, AB.

Ashworth, J., D. Keyes and J.L. Crepin. 1999. A comparison of methods for gypsum requirement of brine-contaminated soils. Can. J. Soil Sci. 79: 449-455.

Ayers, R.S. and D.W. Westcot. 1994. Water quality for agricultureFAO Irrigation and Drainage Paper No. 29 Rev. 1, Rome, Italy.

Beven, K. and P. Germann. 1982. Macropores and water flow in soils. Water Resour. Res. 18: 1311-1325.

Bishop, J.M. 2012. The influence of macropores on flow and transport to subsurface drains in low permeability, salt affected soils. M.Sc. diss., University of Calgary, Calgary, AB.

Cey, E.E. and D.L. Rudolph. 2009. Field study of macropore flow processes using tension infiltration of a dye tracer in partially saturated soils. Hydrological Processes 23: 1768-1779.

Chang, C., S. Dubetz, T.G. Sommerfeldt and D.C. Mackay. 1982. Leaching fractions and salt status of two irrigated gypsum-rich soils in southern Alberta. Can. J. Soil Sci. 62: 97-103.

Curtin, D. and H.P.W. Rostad. 1997. Cation exchange and buffer potential of Saskatchewan soil estimated from texture, organic matter and pH. Can. J. Soil Sci. 77: 621-626.

Curtin, D., H. Steppuhn and F. Selles. 1994. Structural stability of chernozemic soils as affected by exchangeable sodium and electrolyte concentration. Can. J. Soil Sci. 74: 157-164.

Flury, M., H. Fluhler, W.A. Jury and J. Leuenberger. 1994. Susceptibility of soils to preferential flow of water - a field-study. Water Resour. Res. 30: 1945-1954.

Hanson, B.R., S.R. Grattan and A. Fulton. 2006. Agricultural salinity and drainageDivision of Agriculture and Natural Resources Publ. 3375, University of California, Davis, CA.

Hayley, K. 2010. Time lapse electrical imaging of salt affected soil and groundwater. Ph.D. diss., University of Calgary, Calgary, AB.

Head, F. 2013. Geophysical monitoring of salt remediation. M.Sc. diss., University of Calgary, Calgary, AB.

Hendry, M.J. 1982. Hydraulic conductivity of a glacial till in alberta. Ground Water 20: 162-169.

Hendry, M.J., J.A. Cherry and E.I. Wallick. 1986. Origin and distribution of sulfate in a fractured till in southern Alberta, Canada. Water Resour. Res. 22: 45-61.

Keller, C.K., G. van der Kamp and J.A. Cherry. 1991. Hydrogeochemistry of a clayey till .1. Spatial variability. Water Resour. Res. 27: 2543-2554.

Keren, R. and S. Miyamoto. 2011. Reclamation of saline, sodic, and boron-affected soils. In: W. W. Wallender and K. K. Tanji, editors, Agricultural salinity assessment and management, 2nd ed. ASCE Manuals and Reports on Engineering Practice No. 71. ASCE, Reston, VA. p. 655-686.

Kohut, C.K. and M.J. Dudas. 1995. Layer charge characteristics of smectites in salt-affected soils in Alberta, Canada. Clay Clay Miner. 43: 78-84.

Lauchli, A. and S.R. Grattan. 2011. Plant responses to saline and sodic conditions. In: W. W. Wallender and K. K. Tanji, editors, Agricultural salinity assessment and management, 2nd ed. ASCE Manuals and Reports on Engineering Practice No. 71. ASCE, Reston, VA. p. 169-205.

Leskiw, L.A., R.B. Sedor, C.M. Welsh and T.B. Zeleke. 2012. Soil and vegetation recovery after a well blowout and salt water release in northeastern British Columbia. Can. J. Soil Sci. 92: 179-190.

McNeal, B.L. and N.T. Coleman. 1966. Effect of solution composition on soil hydraulic conductivity. Soil Sci. Soc. Am. Proc. 30: 308-&.

Merrill, S.D., K.J. Lang and E.C. Doll. 1990. Contamination of soil with oil-field brine and reclamation with calcium-chloride. Soil Sci. 150: 469-475.

Natural Resources Canada. 2013. Prairies - Canada in a changing climate. Climate Change Publications. Government of Canada. http://www.nrcan.gc.ca/environment/resources/publications/impacts-adaptation/reports/backgrounder/10065. (accessed 1 Aug. 2013).

Quirk, J.P. 2001. The significance of the threshold and turbidity concentrations in relation to sodicity and microstructure. Aust. J. Soil Res. 39: 1185-1217.

Quirk, J.P. and R.K. Schofield. 1955. The effect of electrolyte concentration on soil permeability. J. Soil Sci. 6: 163-178.

Rapp, E. and G.E. Laliberte. 1968. Performance of tile drains under irrigation in southern Alberta. Canadian Agricultural Engineering 10: 64-69.

Rhoades, J.D. 1982. Reclamation and management of salt-affected soils after drainage. First Annual Western Provincial Conference, Rationalionalization of Water and Soil Research and Management: Soil Salinity. Lethbridge, AB.

Rhoades, J.D. 1982. Soluble salts. In: A.L Page, R.H. Miller, and D.R. Keeney, editors, Methods of soil analysis, Part 2, Chemical and Microbiological Properties, 2nd ed. Agron. Monogr. 9. ASA and SSSA, Madison, WI. p. 167–179.

Robbins, C.W. and C.L. Wiegand. 1990. Field and laboratory measurements. In: K. K. Tanji, editor Agricultural salinity assessment and management. ASCE Manuals and Reports on Engineering Practice No. 71. ASCE, New York, NY. p. 201-219.

Shainberg, I. and M.J. Singer. 2011. Soil response to saline and sodic conditions. In: W. W. Wallender and K. K. Tanji, editors, Agricultural salinity assessment and management, 2nd ed. ASCE Manuals and Reports on Engineering Practice No. 71. ASCE, Reston, VA. p. 139-168.

Smith, A.D. 2008. Evaluating tile drainage systems as a method of salt remediation in Alberta. M.Sc. diss., University of Calgary, Calgary, AB.

United States Salinity Laboratory (USSL) Staff. 1954. Diagnosis and improvement of saline and alkali soils. U.S. Gov. Print. Office, Washington, DC.

van Schaik, J.C. and R.A. Milne. 1962. Reclamation of a saline-sodic soil with shallow tile drainage. Can. J. Soil Sci. 42: 43-48.

1.8 Figures and Tables

Fig. 1.1. Photographs of: (a) the irrigated test plot, showing surface projection of tile drains and tile drain collection sump; and, (b) an excavated tile drain of slotted PVC 102-mm diameter, within a clean gravel pack and wrapped in non-woven geotextile.

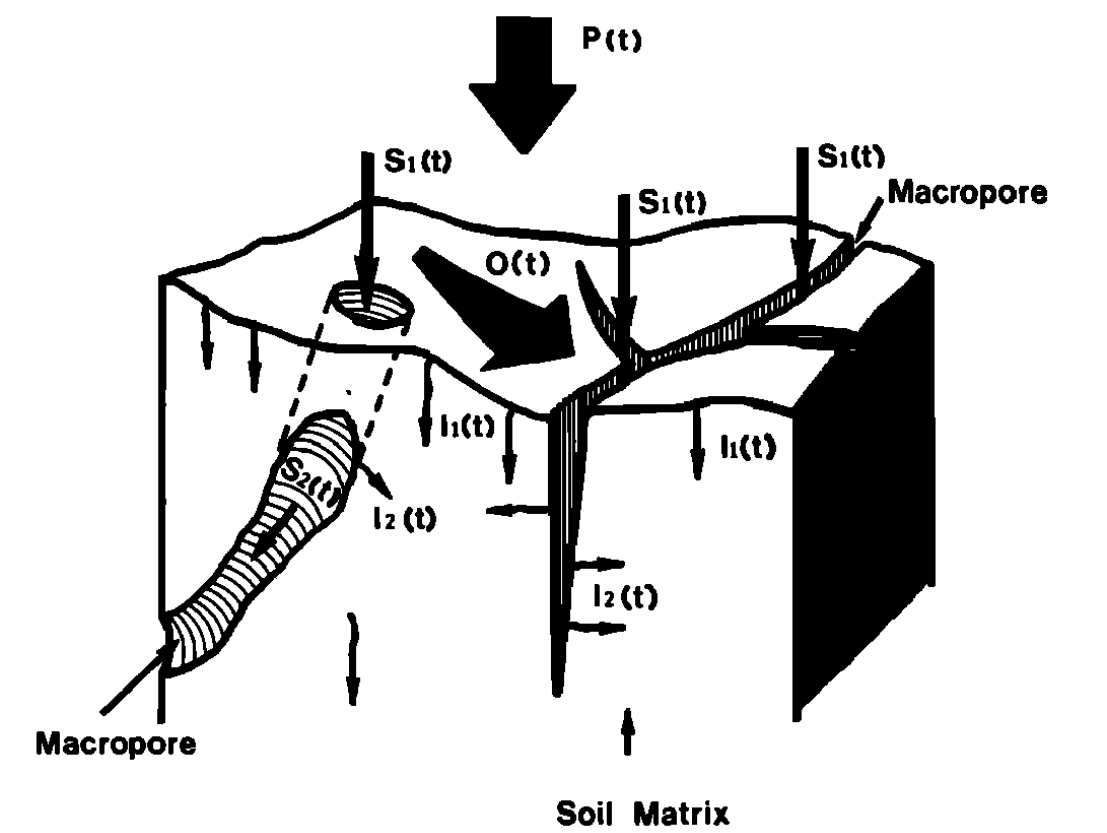

Fig. 1.2. Schematic for water flow during infiltration into a macroporous soil. P(t), water applied as rainfall or irrigation; $I_1(t)$, direct infiltration into the matrix from the soil surface; $I_2(t)$, lateral infiltration into the matrix through the walls of the macropores; $S_1(t)$, seepage into macropores at the soil surface; $S_2(t)$, macropore flow; O(t), overland flow; t, time (after Germann, 1980).

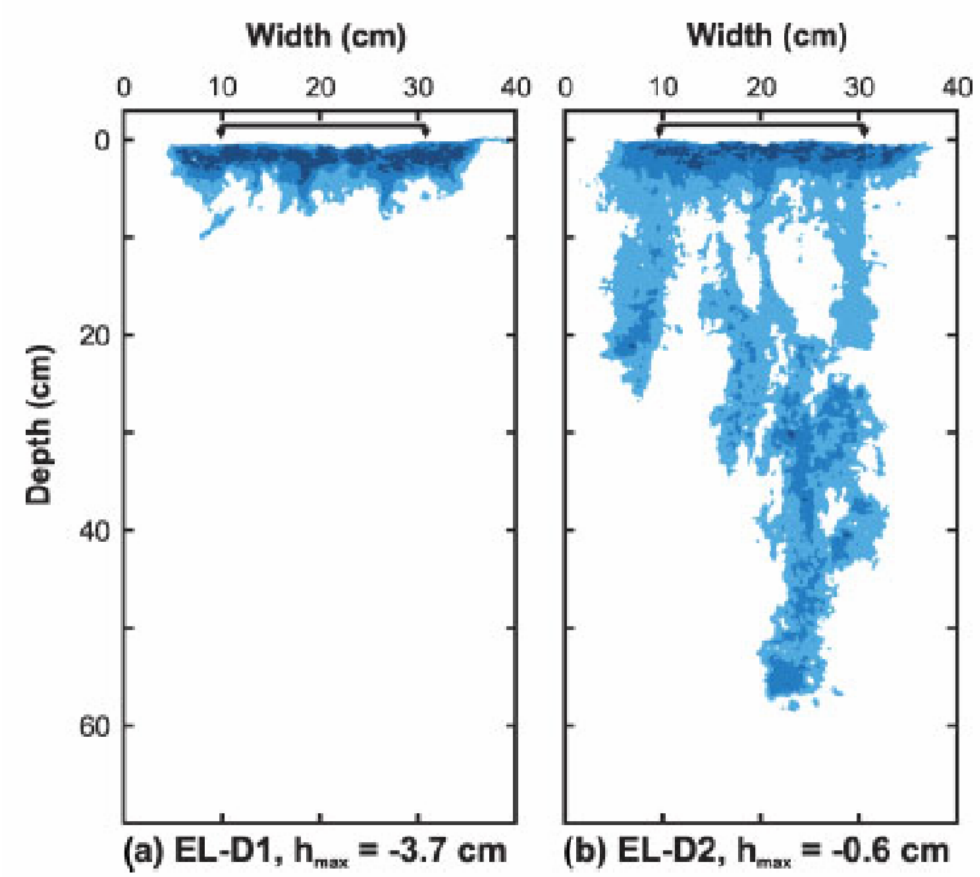

Fig. 1.3. Classified dye staining patterns for vertical sections in a fine-grained, macroporous soil showing: (a) limited deep preferential flow during infiltration of 1 L of dyed water into a relatively dry soil at a tension of 3.7 cm for 152 min; and, (b) relatively deep dye penetration as a result of preferential flow during infiltration of 2 L of dyed water into a relatively wet soil at a tension of 0.6 cm for 22 min (after Cey and Rudolph, 2009).

Table 1.1. Major ion chemistry of produced water from the Leduc Oilfield, Nisku Fm.[z]

Cl	SO_4	Alkalinity as HCO_3	Na	Ca	Mg	K	pH
$g\ L^{-1}$	$g\ L^{-1}$	$g\ L^{-1}$	$g\ L^{-1}$	$g\ L^{-1}$	$g\ L^{-1}$	$g\ L^{-1}$	-
120	1.08	0.087	45.0	13.0	2.50	2.70	6.2

[z] Water sample was collected on 9 Sep. 2009 near Leduc, AB.

CHAPTER 2: GYPSUM AND CALCITE DISSOLUTION IN THE SOIL SATURATED PASTE EXTRACT AND ITS EFFECT ON ELECTRICAL CONDUCTIVITY AND SODIUM ADSORPTION RATIO

2.1 Introduction

Reclamation of salt-affected soil restores land capability for the growth of agricultural or natural plant species. The goal of reclamation is to reduce salinity to mitigate deleterious osmotic effects on plants, and to reduce sodicity to mitigate soil swelling or dispersion and thus maintain soil permeability (Keren, 1990). In contrast to the reclamation of natural or agriculturally-related saline-sodic soils, the remediation of industrial impacts may be required to meet regulatory standards. Industrial sources of soil salinity include the unintended release of oilfield brines (so-called produced water) or saline geothermal fluids (Jury and Weeks, 1978; Merrill et al., 1990; Leskiw et al., 2012).

The saturated paste extract (SPE) methodology is recommended as the standard method of determining soil salinity and sodicity [United States Salinity Laboratory (USSL) Staff, 1954] and is often the method to which other methods of salinity appraisal (e.g., fixed soil:water ratio extractions and immiscible liquid extractions) are compared (Hogg and Henry, 1984; Kohut and Dudas, 1994; Korshandi and Yazdi, 2011). The SPE methodology uses the lowest diluted soil:water ratio on which low pressure or vacuum filtration can be readily accomplished, while providing improved correlation with plant-salinity response (Robbins and Wiegand, 1990). The saturated paste is prepared by the addition of distilled or deionized water to a dry soil sample to achieve a saturated condition. Water added to the soil sample is almost always in excess of the field-saturated water content. In soils bearing soluble minerals, such as gypsum and calcite ($CaSO_4 \cdot 2H_2O$ and $CaCO_3$, respectively), this dilution effect promotes additional mineral dissolution beyond what is normally found in soil water under field conditions. The period of time allowed for moisture equilibration of the saturated paste may affect the amount of calcite dissolved in the SPE .

The amount of mineral dissolution in a soil-water mixture increases with the amount of water added relative to a fixed amount of soil. Sulfate concentrations in 1:1 (mass of dry soil:mass of water) extracts in excess of gypsum saturation levels have been attributed to salt and gypsum dissolution (Nadler and Magaritz, 1986). In practice, the difference between sulfate concentrations in a dilute soil-water extract and the SPE is used to calculate soil gypsum content (Loeppert and Suarez, 1996). Likewise, Levy (1981) demonstrated increased dissolution of calcite in 1:10 soil extracts compared to less dilute 1:1 soil extracts. Bicarbonate concentrations in soil-water suspensions have been observed to increase to a constant concentration over a period of 20 d (Suarez and Rhoades, 1982). This implies that addition of distilled water during preparation of a saturated paste for calcareous soil may dissolve calcite, but the process is slow in relation to the time of extraction, which is typically 4 hrs to overnight (Rhoades, 1982).

Fixed ratio extracts (e.g., 1:1, 1:2, 1:5, 1:10) are sometimes used in lieu of saturated paste extracts due to the ease of automation of the extract procedure (Visconti and de Paz, 2012). However, due to the widespread use of the SPE methodology, it is often desirable to convert fixed ratio extract data to an SPE basis. Since dissolution of gypsum is known to occur in dilute soil-water mixtures, adjustment of fixed ratio extract data is often undertaken in gypsiferous soils. One method of adjusting for excess mineral dissolution is to use soil-specific or region-specific regression equations to estimate SPE electrical conductivity (EC) from fixed ratio extract data (Khorsandi and Yazdi, 2007). Another method is to use geochemical modeling to adjust fixed ratio extract data for the effects of dilution, mineral dissolution, and cation exchange (USSL, 2007). Visconti and de Paz (2012) showed that EC data from 1:5 extracts from a gypsiferous and calcareous soil, corrected for dilution only, resulted in an estimated mean SPE EC of 8 dS m^{-1}, relative to an observed mean of 4.4 dS m^{-1}. Use of detailed geochemical modeling improved the estimate of SPE EC to 4.3 dS m^{-1}. These regression and geochemical modeling methods account for excess gypsum dissolution that occurs during preparation of the fixed ratio extract, but do not include further adjustment for excess mineral dissolution within the SPE. In gypsiferous soils, EC of the SPE may be up to 1 to 3 dS m^{-1} higher than if gypsum were not present (Hanson et al., 2006). Even though the general effects of mineral dissolution on the salinity of the SPE are well known, explicit methods to

account for this effect are not commonly applied. The adjustment method presented here can be considered a simple form of geochemical model, in which excess mineral dissolution is determined from the apparent solubility limit. One advantage of this method is that it is simple enough to use within a spreadsheet software program. The accuracy of determination of soil salinity and sodicity may have important implications for evaluating the state of progress of soil remediation. Whether remediation of salt-affected soils is prescribed within a regulatory framework varies by governmental jurisdiction. In Alberta, Canada, environmental regulators have based their guidelines for assessment and remediation of salt-affected soils on the SPE methodology (Alberta Environment, 2001). Soil salinity is measured as EC, and sodicity is measured as sodium adsorption ratio (SAR). The salinity scale used for topsoil follows that recommended by the United States Salinity Laboratory (USSL Staff, 1954), while the salinity scale for subsoil is marginally higher. For example, the guideline for remediation of soil of "Good Quality" is an EC < 2 dS m^{-1} for topsoil and < 3 dS m^{-1} for subsoil, and for sodicity a SAR < 4 (mmol L^{-1})$^{1/2}$ is used for both topsoil and subsoil (Table 2.1). It is common practice to omit the units for SAR, which is done hereafter. Decisions regarding remedial requirements or progress are made by comparing soil sampling results to the guideline values. Dissolution of sparingly soluble minerals such as gypsum and calcite can reasonably be expected to increase ion content in the SPE relative to levels at field water content. In addition, an increase in Ca concentrations results in a lower SAR than would be measured in the absence of additional dissolution. Therefore, EC and SAR unadjusted for excess mineral dissolution occurring within the SPE could affect decisions regarding remedial progress. The objectives of this study are: to identify effects of gypsum and calcite dissolution in the SPE; and to quantify the difference on EC and SAR resulting from excess mineral dissolution.

2.2 Materials and Methods

2.2.1 Site Description and Field Sampling

Soil samples were collected from a salt-affected soil in central Alberta, Canada. The dominant land use in the area is agricultural, and the study site is vegetated with mixed forage plant species, mainly

grasses. Soil in the study area is mapped as Navarre silt loam developed on slightly saline glaciolacustrine material (Bowser et al., 1962). It is classified as an Orthic Black Chernozem in the Canadian soil classification system (Soil Classification Working Group, 1998). The soil profile is comprised of topsoil, 0–0.15 m, silt to silt loam subsoil (B and C horizons), 0.15–2.4 m, overlying glacial till to a depth exceeding the maximum depth of investigation of 7.5 m. The plant rooting zone, the upper 2.4 m, is the target interval for remediation. Below 2.4 m, the dense glacial till is resistant to root penetration. The site is a former oil and gas production battery that conducted operations between 1949 and 1962 and was decommissioned by 1976. Salt-affected soil resulted from historical surface releases of brine during oil and gas production. Produced water from oil wells in the area was dominantly sodium chloride in composition, with a total dissolved solids concentration of 180 g L^{-1} and a SAR of 95. The most heavily affected area covers approximately 2 ha, with salt-affected soil extending to a depth of approximately 7 m.

In 2003, a remedial tile drain system was installed at 2 m depth for collection of saline leachate from the rooting zone. The collected leachate is routed for disposal by deep well injection. In 2008, a field experiment was initiated to investigate the use of irrigation to increase the rate of salt flushing. Two test plots, 20 by 20 m in dimension, were constructed. One of the test plots was irrigated, while the other was used as an unirrigated control. Results of the irrigation experiment are not presented in this paper; however, some of the soil salinity monitoring results reported here were collected from the irrigated test plot area. This has implications for soil water content used in the calculation of soil pore water concentrations reported in the results section. Soil salinity was monitored by borehole sampling in August 2008, October 2008, November 2009, and October 2010. Soil samples were taken from 32 mm diameter soil cores collected using a direct-push drilling rig. Soil core was sampled in 150 to 200 mm lengths.

A commercial analytical laboratory in Calgary, AB conducted soil SPE analysis. Procedural details for preparation of the SPE are given in Rhoades (1982). The general procedure is to add deionized water to a know mass of air dry soil while mixing. Sufficient water is added such that a saturated condition is

reached, at which point the soil flows freely and its surface glistens. The sample is allowed to stand for 4 hrs to overnight after which the saturated condition is checked again. Additional soil or water is added to the soil paste, if necessary to re-attain the saturated condition. The mass of water added to the known mass of soil is calculated as the saturation percentage of the paste. Electrical conductivity of the SPE was measured by EC electrode. Major ion concentrations (Na, Ca, Mg, K, and SO_4) were determined by inductively couple plasma-atomic emission spectroscopy (ICP-AES). Chloride was determined by ion chromatography (IC) with EC detection, and carbonate alkalinity was determined by strong acid titration. Soil pH was measured in the supernatant of a 1:2, mass of dry soil to mass of 0.01 M aqueous $CaCl_2$ mixture. The average charge balance error for the four sampling events ranged from a minimum of 2% for the October 2010 event to a maximum of 6% for the August 2008 event. Samples with charge balance error greater than 10 % were culled from the dataset. Over the range of observed pH, 7.3–8.1, carbonate alkalinity is assumed to consist mainly of bicarbonate and is reported as such.

Field soil water was sampled using suction lysimeters (Model SW-071, Soil Measurement Systems). The suction lysimeters are 50 mm in diameter with a porous stainless steel sampling interval, 100 mm in length. The stainless steel body of the lysimeters was installed within a hand cored 50 mm diameter access hole and was backfilled with a fine silica flour slurry to improve hydraulic contact between the lysimeters and native soil. The suction lysimeters were installed at four depths in two locations ranging from 0.15–0.9 m below ground surface, for a total of eight sampling points. The two uppermost lysimeters at 0.15 and 0.3 m depth were installed at a 45° angle to the vertical to aid interception of vertical infiltration, while those at deeper depths were installed vertically. Each lysimeter was installed within a plastic access tube backfilled with hydrated bentonite to minimize preferential infiltration. A partial vacuum of approximately 50–60 kPa was applied to the lysimeters with a hand pump. Due to the relatively low hydraulic conductivity of the soil, leachate was allowed to collect overnight before sampling. Soil water samples collected from the suction lysimeters were analyzed for EC, major ions, and alkalinity at the University of Calgary. Electrical conductivity was measured with a handheld probe and digital conductivity meter. Major ion concentrations (Cl, SO_4, Na, Ca, Mg, and K)

were determined by IC with EC detection, and alkalinity was determined by titration with dilute sulfuric acid. The average charge balance error for soil water samples was 4 %. Samples with charge balance error greater than 10 % were culled from the dataset. Sample pH was determined and alkalinity titrations were performed using a handheld pH meter.

2.2.2 Soil Mineral and Cation Exchange Characterization

Gypsum was applied to the soil surface in 2003 as a source of Ca to ameliorate elevated SAR levels. The presence of naturally occurring gypsum at the study site has not been investigated. Qualitative analysis for gypsum was performed on 1:2 dilute soil extracts by precipitation with acetone (USSL Staff, 1954). Equal parts of dilute soil extract and acetone were mixed, and the presence of gypsum was indicated by the formation of a white precipitate. Based on a visual assessment of the opacity of the precipitate in suspension, each sample was assigned a level of high, moderate or low gypsum content.

Quantification of calcium carbonate in soil was performed using the pressure-calcimeter method of Nelson (1982). The method was modified to use a handheld pressure transducer and readout, instead of a mercury manometer. A quantity of soil was reacted with strong hydrochloric acid in a sealed container. The resulting pressure increase in the container is linearly related to the carbonate content. A calibration curve (not shown) was developed to convert container pressure to equivalent calcium carbonate content. Both calcite and dolomite, $(CaMg)(CO_3)_2$, produce a reaction with hydrochloric acid. Separate determination of calcite and dolomite content was not performed, and results are reported as calcium carbonate equivalent.

For purposes of adjusting measured SAR values for excess Ca resulting from mineral dissolution, effective cation exchange capacity (CEC) and the Na–Ca selectivity coefficient were determined. Gypsum, calcite and silicate dissolution during CEC determination can result in over or underestimation of CEC depending on whether excess dissolved cations affect the saturating or extracting step of the procedure (Rhoades, 1982). To improve the accuracy of CEC determination, the methodology of Amrhein and Suarez (1990) Modified Method A was used to correct for gypsum and calcite dissolution by

measuring SO_4 and HCO_3 in both the saturating and extracting solutions. Excess SO_4 and HCO_3 in the extracting solution are assumed to be the result of mineral dissolution. The saturating cation solution was a mixture of NaCl–$CaCl_2$ salts, ranging in concentration from 2–300 $mmol_c\ L^{-1}$ and SAR from 5–60. A 500 $mmol_c\ L^{-1}$ $MgNO_3$ solution was used to extract the exchangeable cations. Both the saturation and extraction steps were conducted at ambient pH of the soil-solution mixture. Cation and anion concentrations were determined in the decantate of the saturating and extracting solutions. Effective CEC was calculated as the sum of exchangeable Na and Ca (NaX and CaX, respectively). The Na–Ca selectivity coefficient was determined simultaneously as CEC. Cation saturation and extraction steps were performed at the University of Calgary, from which ion concentrations were determined at a commercial analytical laboratory (Maxxam) in Calgary, AB. In the decanted saturating and extracting solutions: concentrations of Na, Ca, Mg, K, and SO_4 were determined by ICP-AES; Cl was determined by automated colorimetry; and HCO_3 alkalinity was determined by strong acid titration. The charge balance error for the saturating solution was 4% on average and for the extracting solution was 1% on average. Samples with charge balance error greater than 10 % were culled from the dataset.

2.3 Results and Discussion

2.3.1 Calcite and Gypsum in Soil

For gypsum and calcite dissolution to appreciably affect the EC and SAR of the SPE, these minerals must be present in soil at levels that contribute significant excess amounts of Ca, SO_4, and HCO_3. The relative solubility of these minerals control the degree to which dissolution occurs. There is also a contextual aspect to developing and applying adjustments to SPE EC and SAR for excess mineral dissolution. In the context of salt-affected soil reclamation, the goal may be to improve land productivity, and not necessarily to achieve a target EC or SAR. However within a regulatory framework, remediation of salt-affected soil may be required to meet specific soil quality guidelines for salinity and sodicity. Therefore an increased level of accuracy of determination of EC and SAR is useful in the remediation context.

Calcium carbonate content in soil ranged from 7–83 g kg^{-1} over the sampling interval from 0.30–2.25 m (Fig. 2.1a). With limited sampling, calcium carbonate content is higher in the upper 0.75 m of the soil profile (up to 83 g kg^{-1}) and lower from 1.0–2.25 m depth (up to 25 g kg^{-1}). Over a similar depth interval, 0.075–2.0 m, HCO_3 concentrations in the SPE range from 0.23–8.1 $mmol_c$ L^{-1}, decreasing with depth (Fig. 2.2a). If calcite dissolution were occurring in the SPE, to such a degree that the SPE reaches saturation with respect to calcite, concentrations would be expected to show a distinct solubility limit. However, saturated paste extract HCO_3 concentrations do not exhibit a uniform maximum concentration with depth, suggesting calcite dissolution has not reached the solubility limit. This is likely due to the slower kinetics of the calcite dissolution reaction relative to gypsum dissolution. This does not preclude that calcite is dissolving in the soil saturated paste; however, it is indicative that HCO_3 concentrations in the saturated paste are likely not in equilibrium with the mineral phase.

The presence of gypsum was qualitatively determined by the soil water extract-acetone method. Soil samples collected from the uppermost 0.4 m of the soil profile produced the highest proportion of gypsum precipitate, decreasing to moderate levels by 2.4 m depth. Additional insight into the depth distribution of gypsum comes from examination of the SPE SO_4 concentration depth profile (Fig. 2.3a). Sulfate concentrations are highest in the upper 1.0 m of the soil profile and decrease below that depth. Sulfate concentrations reach an apparent solubility limit of 40 $mmol_c$ L^{-1}, defined as the maximum concentration attained in the 0 to 1.0 m depth interval. Therefore, it is likely that excess gypsum dissolution in the SPE is occurring over this depth interval.

2.3.2 Evidence of Mineral Dissolution in the SPE

To further explore the relative effect of mineral dissolution on HCO_3 and SO_4 concentrations, it is useful to examine the SPE data on a pore water basis calculated at field water content. This enables comparison of calculated pore water concentrations to measured soil water concentrations and serves to validate whether substantial dissolution of calcite or gypsum is occurring.

During preparation of the soil saturated paste, water is added to the dried soil sample. Pore water concentrations at field water content, C_{field} ($mmol_c\ L^{-1}$), are calculated from SPE data as (adapted from Rhoades and Corwin, 1990):

$$C_{field} = \frac{C \cdot SP \cdot \rho_b}{\rho_w \theta} \quad [2.1]$$

where C is the concentration of a single anion in the SPE ($mmol_c\ L^{-1}$), SP is the water saturation percentage of the saturated soil paste expressed as a decimal fraction ($kg\ kg^{-1}$), ρ_b is the soil dry bulk density ($kg\ L^{-1}$), ρ_w is the density of water (taken as 1.00 $kg\ L^{-1}$), and θ is the volumetric field water content ($m^3\ m^{-3}$). An average SP of 0.73 $kg\ kg^{-1}$ was determined for topsoil samples (0–0.15 m) and 0.63 $kg\ kg^{-1}$ for subsoil samples (0.15–2.4 m) for the 2010 dataset. Individual SP values were used in the calculation of C_{field} for each soil sample. Bulk density and water content used in the calculation are summarized in Table 2.2. Field-saturated water content was assumed when applying Eq. [2.1], to enable comparison of pore water concentrations calculated from SPE data to concentrations measured in soil water samples from suction lysimeters within the irrigated test plot. Soil tension was measured at one location inside and at two locations outside the irrigated test plot. Soil within the irrigated test plot was maintained near saturation throughout the irrigation season, while generally unsaturated conditions prevailed outside the irrigated plot.

The solubility limit for gypsum is taken to be 40 $mmol_c\ L^{-1}$ based on the maximum SO_4 concentration measured in the SPE (Fig. 2.3a). This apparent solubility limit is in agreement with gypsum solubility calculated using chemical equilibrium modeling using the software program GEOCHEM, accounting for formation of the $CaSO_4^0$ neutral charge complex and ionic strength effects on activity coefficients (Sposito and Traina, 1987). In the absence of sufficient data to calibrate the chemical equilibrium model, uncertainty in model coefficients results in a similar level of uncertainty to that resulting from use of a fixed solubility limit. Therefore, a fixed solubility limit was used instead of a more

complex activity coefficient model. Soil water SO_4 concentrations measured in lysimeter samples, 21.2–36.4 $mmol_c\ L^{-1}$, do not exceed 40 $mmol_c\ L^{-1}$ (Fig. 2.3b). In comparison, calculated pore water SO_4 concentrations (using Eq. [2.1]) are above 40 $mmol_c\ L^{-1}$, mainly in the upper 1 m of the soil profile. The overestimation of pore water sulfate concentrations from SPE results is attributed to gypsum dissolution occurring during preparation of the SPE. Maximum calculated SO_4 concentrations (up to 118 $mmol_c\ L^{-1}$) exceed 40 $mmol_c\ L^{-1}$ at the following depths: 0.075, 0.225, 0.5, 1.0, and 2.0 m, while median and 75th percentile concentrations exceed at depths of 0.225 and 0.5 m. Therefore, measured SPE SO_4 concentrations at depths of 0.225 and 0.5 m are the most heavily affected by excess gypsum dissolution.

Pore water HCO_3 concentrations were calculated from SPE concentrations using Eq. [2.1]. Over the common sampling interval, from near surface to 1 m depth, maximum pore water concentrations calculated from SPE results exceed HCO_3 concentrations measured in the suction lysimeter samples (Fig. 2.2b). However, the small sample size for measured soil water concentrations leads to a high degree of uncertainty in the comparison of mean and variance to that of the calculated pore water concentrations. The relative magnitude of excess SPE HCO_3 is small in comparison to excess SO_4. For example, for the 0.56 m depth lysimeter sample, the HCO_3 concentration in soil water was measured as 3.4 $mmol_c\ L^{-1}$, while the maximum HCO_3 concentration at 0.5 m, calculated from the SPE is 9.7 $mmol_c\ L^{-1}$. This difference of 6.3 $mmol_c\ L^{-1}$ is approximately 6 % of the maximum difference (97 $mmol_c\ L^{-1}$) between SO_4 pore water concentrations calculated from the SPE and the apparent gypsum solubility limit. Therefore, given a lack of strong evidence for calcite dissolution in the SPE and the relatively small potential error introduced by calcite dissolution relative to gypsum dissolution, adjustment for calcite dissolution was not included.

2.3.3 Excess Gypsum Dissolution in the SPE

Excess gypsum dissolution in the SPE is demonstrated by calculated field pore water concentrations in excess of the apparent solubility limit of 40 $mmol_c\ L^{-1}$ (Fig. 2.3b). Sulfate can be used as a tracer for gypsum dissolution and to adjust EC and SAR for any excess. Maximum SO_4

concentrations in the SPE are calculated from the apparent solubility limit at field water content. Rearranging the terms in Eq. [2.1] and replacing the field pore water concentration with the solubility limit concentration, the maximum SPE concentration, $SO_{4\,max}$, is calculated as:

$$SO_{4\,max} = \frac{SO_{4\,limit}\rho_w\theta}{SP \cdot \rho_b} \quad [2.2]$$

in which $SO_{4\,limit}$ is the apparent maximum concentration for gypsum in pore water (taken to be 40 $mmol_c\ L^{-1}$).

Excess sulfate concentration in the SPE can then be calculated as:

$$SO_{4\,excess} = 0, \text{ if } SO_4 \le SO_{4\,max} \quad [2.3]$$

$$SO_{4\,excess} = SO_4 - SO_{4\,max}, \text{ if } SO_4 > SO_{4\,max}$$

Under field conditions, dissolved gypsum mass is assumed to be maximum when soil is at field-saturated water content. At lower field water contents, the mass of gypsum dissolved is lower due to its solubility limit. The calculations contained herein were performed at field-saturated water content. This results in the highest possible contribution of field-dissolved gypsum to the SPE and thereby the lowest magnitude of calculated excess.

For the 2010 dataset, 25 of 82 samples, 30%, from the 0–2.4 m depth interval contained excess SO_4 determined by Eq. [2.3]. For the 25 samples, the average excess SO_4 concentration was 11 $mmol_c\ L^{-1}$, with a range from 0.33–22 $mmol_c\ L^{-1}$. The determined excess SO_4 concentration is used to calculate an EC adjustment in the following section. In addition to adjusting the SPE EC, the excess SO_4 in the SPE can be used to estimate the soil gypsum content. Gypsum content can be estimated by the difference between that dissolved in a dilute soil-water extract (e.g., 1:5, 1:10) and that of the SPE (Loeppert and

Suarez, 1996). The purpose of using the dilute water extract is to ensure that gypsum dissolves completely in the mixture and dissolution is not limited by saturation. For the method of Loeppert and Suarez (1996), the SPE serves as the measure of soluble salts in pore water and excess gypsum dissolved in the SPE is not corrected for. Here, gypsum content was determined as the difference between gypsum dissolved in the SPE and gypsum-saturated pore water at field-saturated water content. The gypsum content (g kg^{-1}) can therefore be determined from the excess sulfate in the SPE, calculated using Eq. [2.3]:

$$\text{Gypsum content} = \frac{\text{SO}_{4\ \text{excess}}\,\text{SP} \cdot M(\text{CaSO}_4 \cdot 2\text{H}_2\text{O})}{\rho_w z} \qquad [2.4]$$

where $M(CaSO_4 \cdot 2H_2O)$ is the molar mass of gypsum (taken to be 0.1722 g $mmol^{-1}$), and z is the molar charge for sulfate (2 $mmol_c$ $mmol^{-1}$). Not all gypsum in the soil sample may have dissolved in the saturated paste. Therefore, for soil saturated pastes that are saturated with respect to gypsum, this calculation yields only a minimum gypsum content and not the true gypsum content. For the 2010 dataset, SO_4 concentrations in the SPE generally did not reach the apparent saturation limit of 40 $mmol_c$ L^{-1}. Out of 25 samples with demonstrated excess gypsum dissolved in the SPE, 12 have SO_4 concentrations >30 $mmol_c$ L^{-1} and four have SO_4 concentrations >35 $mmol_c$ L^{-1}. Therefore, it is assumed that the majority of gypsum dissolved during preparation of the soil saturated paste. Three samples of this subset of 25 were split and extracted at a more dilute soil-water ratio of 1:2. Resulting SO_4 concentrations in the 1:2 extract ranged from 9.2–13.5 $mmol_c$ L^{-1}, well below the saturation limit for gypsum. Two of the three samples yield gypsum contents in the SPE that are 26 and 44 % lower than the contents determined from the 1:2 extract, while the third sample has a content in the SPE that is 67 % higher than that determined from the 1:2 extract. Based on this limited confirmatory dataset, gypsum content determined from the SPE by Eq. [2.4] is considered to produce an estimate of gypsum content within 50 % of that produced using a more dilute extract. In the upper 1 m of the soil profile, for samples containing gypsum, the average gypsum content is 0.29 g kg^{-1}, up to 1.60 g kg^{-1}, shown in Fig. 2.1b.

2.3.4 Electrical Conductivity Adjustment

To adjust SPE EC for excess gypsum dissolution a relationship between SO_4 concentration and EC is needed. Total anion concentration was calculated as the sum of Cl, SO_4, and HCO_3 ion concentrations in the SPE. The relationship between total anion concentration and EC is shown in Fig. 2.4, and the best-fit line determined by linear least squares regression is:

$$EC = 0.0945(Cl + SO_4 + HCO_3) + 0.163,\ R^2 = 0.991 \quad [2.5]$$

where anion concentrations are given in units of $mmol_c\ L^{-1}$. Anion concentrations shown in Fig. 2.4, up to 300 $mmol_c\ L^{-1}$, generally have a large contribution from chloride, since the maximum concentration observed in the SPE for SO_4 was 40 $mmol_c\ L^{-1}$ and for HCO_3 was 8.2 $mmol_c\ L^{-1}$. To obtain a more representative relationship between EC and $SO_4 + HCO_3$ concentrations, the dataset was culled to include only samples with low Cl concentrations. Data were selected with Cl concentrations that were on the order of 10% or less of $SO_4 + HCO_3$ concentrations. The residual contribution of chloride to EC was removed using the slope of the best fit line in Eq. [2.5]:

$$EC_{SO4+HCO3} = EC - 0.0945\ Cl \quad [2.6]$$

The relationship between $SO_4 + HCO_3$ and $EC_{SO4+HCO3}$ is not linear (Fig. 2.5). The $SO_4 + HCO_3$ to $EC_{SO4+HCO3}$ relationship starts to deviate from linear at a combined concentration of approximately 12 to 13 $mmol_c\ L^{-1}$. The HCO_3 ion contributes a relatively minor amount compared to SO_4. The average HCO_3 contribution for the data plotted in Fig. 2.5 is 3.7 $mmol_c\ L^{-1}$, which is approximately 10% of the maximum combined concentration. Therefore the non-linearity in the relationship is assumed to be associated with formation of lower charge complexes of sulfate [e.g., $CaSO_4^0$ (Sposito and Traina, 1987)].

The 2nd order polynomial equation for the best fit line for EC from SO_4 + HCO_3 concentration was determined through least squares regression and is given as:

$$EC_{SO4+HCO3} = -6.53\times10^{-4}C^2 + 9.84\times10^{-2}C + 3.83\times10^{-2},\ R^2 = 0.995 \quad [2.7]$$

where C is the combined concentration of SO_4 and HCO_3 ($mmol_c\ L^{-1}$).

The contribution of excess SO_4 to EC, hereafter termed EC_{excess} (dS m^{-1}), is calculated as the difference between $EC_{SO4\ +\ HCO3}$ from Eq. [2.7], using the concentration of SO_4 + HCO_3 measured in the SPE, less the $EC_{SO4\ +\ HCO3}$ from Eq. [2.7], using the concentration of HCO_3 measured in the SPE plus the maximum SO_4 concentration from Eq. [2.2].

$$EC_{excess} = EC_{SO4+HCO3}(C) - EC_{SO4+HCO3}(C_{max}) \quad [2.8]$$

Adjusted EC values, EC_{adj} (dS m^{-1}), are calculated by subtracting the contribution of excess SO_4 from the measured EC:

$$EC_{adj} = EC - EC_{excess} \quad [2.9]$$

Saturated paste extract EC results from the 2010 dataset were adjusted for excess gypsum dissolution by applying Eq. [2.9]. The relative measurement difference for the 25 samples containing excess SO_4 in the SPE was calculated as $(EC - EC_{adj})/EC_{adj}$. The average relative difference attributed to excess dissolved gypsum in the SPE is 22 %, with a range of 0.31–87 %. The data shows a general trend of relative difference increasing with decreasing EC (Fig. 2.6). Therefore, the importance of adjusting for excess gypsum in the SPE increases as remediation progresses and soil salinity decreases towards the remediation target.

2.3.5 Sodium Adsorption Ratio Adjustment

Equilibrium between exchangeable cations and cations in the soil solution has been expressed using a number of conventions. By the Gapon convention, the equilibrium exchange of sodium and calcium is given as (Shainberg and Letey, 1984):

$$Na^{+} + Ca_{0.5}X \leftrightarrow NaX + 1/2\,Ca^{2+} \qquad [2.10]$$

where Na^{+} and Ca^{2+} represent the aqueous phase sodium and calcium ions, and NaX and CaX represent the adsorbed or exchangeable cations. The equilibrium exchange coefficient, referred to as the Gapon coefficient [$(\text{mmol L}^{-1})^{-1/2}$] is given as:

$$K_G = \frac{NaX \cdot Ca^{1/2}}{Ca_{1/2}X \cdot Na} \qquad [2.11]$$

where concentrations are given in mmol L^{-1} for the aqueous cations and the exchangeable cation concentrations are equal to their molar charge fractions. The units of K_G are often omitted and are not included hereafter.

Two commonly used measures of sodicity: SAR for aqueous solution cations; and, exchangeable sodium ratio (ESR) for adsorbed cations, can be used to simplify the notation. SAR is a measure of the relative concentration of monovalent sodium to divalent calcium and magnesium cations (USSL, 1954):

$$SAR = \frac{Na}{\sqrt{(Ca + Mg)/2)}} \qquad [2.12]$$

where Na, Ca, and Mg are aqueous concentrations ($mmol_c\ L^{-1}$). ESR is the relative amount of sodium on soil cation exchange sites. The proportion of sodium to other adsorbed cations can be expressed as (Amrhein and Suarez, 1990):

$$ESR = \frac{NaX}{(CEC - NaX)} \quad [2.13]$$

where CEC is the effective cation exchange capacity ($mmol_c\ kg^{-1}$), which is taken to be the total of extracted cations at the unadjusted pH of extraction, which ranged 6.9–8.2. Effective CEC corrected for gypsum and calcite dissolution was determined to be 220 $mmol_c\ kg^{-1}$ on samples collected from the silt loam subsoil from 0.3–2.4 m depth (Table 2.2). The silt loam subsoil (B and C horizons) has an average clay-sized (<2 μm) fraction of 14 % by volume. The sand fraction is relatively small, < 5 %, with the remainder composed of silt-sized material. Smectite clay is the main mineral component in the clay-sized fraction (48 %), with lesser illite (23 %), kaolinite (17 %), chlorite (5 %) and quartz (6 %). In comparison, use of the single-step $BaCl_2$ extraction method of Hendershot et al. (1993), which does not correct for mineral dissolution, resulted in an overestimation of effective CEC by 59 % on average.

If the selectivity for Mg is assumed to be equal to that of Ca, ESR can be expressed in terms of the K_G and SAR of the aqueous solution (Shainberg and Letey, 1984):

$$ESR = K_G SAR \quad [2.14]$$

The Gapon selectivity coefficient was determined through least squares regression and is taken to be equal the slope of the best fit line of ESR, determined via Eq. [2.13], vs. SAR. The slope of the regression line (not shown) is 0.0125. The coefficient of determination for the regression line was 0.967.

Dissolution of gypsum within the saturated paste produces excess Ca in solution. For the soil under study, contribution of Ca from excess calcite dissolution is considered negligible. Excess Ca from

gypsum is not conserved within the bulk soil solution due to cation exchange. The exchange reaction produces new equilibrium cation concentrations within the saturated paste. The net effect is a lower SAR than would be measured in the absence of mineral dissolution; however, the effect is somewhat buffered by Ca exchange for Na resulting in a decrease of Ca in solution and an increase in Na in solution. Therefore, SAR values require adjustment for both mineral dissolution and subsequent cation exchange. The principle assumption of this method is that excess total Ca equals excess SO_4 calculated by Eq. [2.3]. The contribution of excess Ca is then removed from the total molar mass of Ca, including that in solution and on the cation exchange sites. Cation exchange modeling using spreadsheet software was used to determine the adjusted SAR via an iterative solution included in Appendix A.

Adjustment for gypsum dissolution was conducted on subsoil samples only. Separate determination of CEC and K_G was not conducted on topsoil samples, thus topsoil samples have been excluded from the analysis. Of the 68 subsoil samples, 22 contained excess sulfate in the SPE as determined by Eq. [2.3]. Measured SAR underestimates SAR_{adj} by 7.6 %, ranging from 0.18–21 %. As with EC, the magnitude of the relative difference increases with decreasing SAR (Fig. 2.6), as the soil progresses closer to the remediation target. However, the magnitude of the relative difference for SAR is lower than that for EC. On average, the magnitude of the SAR relative measurement difference is 33 % of that for EC.

2.3.6 Evaluation of Adjusted Values against Remediation Targets

In the context of soil remediation, a measure of the importance of data adjustment is whether it influences decision making on the progress of remediation. For example, does a soil sample meet the remediation target or not, and does remediation need to continue or not? Within the regulatory framework for Alberta, given as an example in Table 2.1, the applicable remediation guidelines for subsoil of "Good Quality" are an EC < 3 dS m^{-1} and SAR < 4 in the SPE (Alberta Environment, 2001). Saturated paste extract EC and SAR for the 22 subsoil samples exhibiting excess dissolved gypsum within the 2010 dataset are plotted in Fig. 2.7, along with the aforementioned remediation targets. Adjustment for excess gypsum dissolution results in an increase in the number of samples that meet the EC target of 3 dS m^{-1}

from 5 to 11, more than a two-fold increase. In comparison, the number of samples that meet the SAR target of 4, decreased from 11 to 10. The adjustment for gypsum dissolution in the SPE resulted in an overall increase in the number of subsoil samples meeting both remediation targets for EC and SAR. Prior to adjustment, three out of 22 samples met both targets. Following application of the adjustment, the number of samples meeting both targets increased to eight, a 167 % increase.

Gypsum applied as a soil amendment has demonstrated beneficial effects, such as reducing soil sodicity and maintaining soil permeability (Keren, 1990). Gypsum is therefore a valuable tool for use in remediation and reclamation of saline-sodic soils. As a soil amendment, gypsum dissolves in soil water and thereby contributes to soil salinity. What has been demonstrated in this paper is that additional dissolution of gypsum occurs during preparation of the saturated soil paste prior to extraction of soluble salts. This excess dissolved gypsum increases the measured EC and decreases the SAR of the SPE sufficiently to potentially affect the classification of individual soil samples relative to regulatory guidelines. This has implications for the cost and time required for remediation. Not accounting for the excess gypsum effect may result in continued remediation, when it is not necessary, and/or discontinued remediation of elevated SAR when additional remediation may be justified. The method of adjusting SPE EC and SAR presented here can be used by remediation practitioners or regulatory agencies to evaluate the magnitude of the excess-gypsum effect and make informed decisions regarding the progress of remediation.

2.4 Conclusions

Excess dissolution of gypsum is shown to occur in soil saturated paste extracts. Comparison of SO_4 concentrations measured in the SPE to soil water concentrations from field soil water samples demonstrates that gypsum dissolution produces excess Ca and SO_4 in the SPE. The relative excess dissolution effect observed for calcite in the SPE is considered negligible. Saturated paste extract EC data was adjusted by subtracting excess SO_4 concentrations from the analytical results and accounting for its contribution to EC. Saturated paste extract SAR data was adjusted by subtraction of excess Ca from total

Ca, and its relative effect on SAR was determined by equilibrium cation exchange modeling. Adjustment produces a decrease in EC and an increase in SAR relative to that measured in the SPE. As EC and SAR levels decrease towards remediation target levels, the magnitude of the measurement difference increases, hence the relative importance of adjusting for excess gypsum dissolution also increases. Adjusting for gypsum dissolution in the SPE increases the accuracy of measurement of soluble salts (as EC) and sodicity (as SAR), and thereby improves the reliability of data interpretation relative to remediation guidelines.

2.5 References

Alberta Environment. 2001. Salt contamination assessment and remediation guidelines. Environmental Sciences Division, Environmental Service, Pub. No. T/606. Edmonton, AB.

Amrhein, C., and D.L. Suarez. 1990. Procedure for determining sodium-calcium selectivity in calcareous and gypsiferous soils. Soil Sci. Soc. Am. J. 54:999–1007.

Bowser, W.E., A.A. Kjearsgaard, T.W. Peters, and R.E. Wells. 1962. Soil survey of Edmonton sheet (83-H). Canada Department of Agriculture. University of Alberta Bulletin No. SS-4. Alberta Soil Survey Report No. 21. Edmonton, AB.

Hanson, B.R., S.R. Grattan, and A. Fulton. 2006. Agricultural salinity and drainage. University of California Irrigation Program, Division of Agriculture and Natural Resources Publication 3375. Davis, CA.

Hendershot, W.H., H. Lalande, and M. Duquette. 1993. Ion exchange and exchangeable cations. In: M.R. Carter, editor, Soil sampling and methods of analysis. Canadian Society of Soil Science. CRC Press Inc., Boca Raton, FL. p. 167–176.

Hogg, T.J., and J.L. Henry. 1984. Comparison of 1:1 and 1:2 suspensions and extracts with the saturation extract in estimating salinity in Saskatchewan soils. Can. J. Soil Sci. 64:699–704.

Jury, W.A., and L.V. Weeks. 1978. Solute travel-time estimates for tile-drained fields: III. Removal of a geothermal brine spill from soil by leaching. Soil Sci. Soc. Am. J. 42:679–684.

Keren, R. 1990. Reclamation of saline, sodic, and boron-affected soils. In: K.K. Tanji, editor, Agricultural salinity assessment and management. ASCE Manuals and Reports on Engineering Practice No. 71. ASCE, New York, NY. p. 410–431.

Khorshandi, F., and F.A. Yazdi. 2007. Gypsum and texture effects on the estimation of saturated paste electrical conductivity by two extraction methods. Commun. Soil. Sci. Plant Anal. 38:1105–1117.

Khorsandi, F., and F.A. Yazdi. 2011. Estimation of saturated paste extracts' electrical conductivity from 1:5 soil/water suspension and gypsum. Commun. Soil. Sci. Plant Anal. 42:315–321.

Kohut, C.K., and M.J. Dudas. 1994. Comparison of immiscibly displaced soil solution and saturated paste extracts from saline soils. Can. J. Soil Sci. 74:409–419.

Leskiw, L.A., R.B. Sedor, C.M. Welsh, and T.B Zekele. 2012. Soil and vegetation recovery after a well blowout and salt water release in northeastern British Columbia. Can. J. Soil Sci. 92:179–190.

Levy, R. 1981. Effect of dissolution of aluminosilicates and carbonates on ionic activity products of calcium carbonate in soil extracts. Soil Soc. Am. J. 45:250–255.

Loeppert, R.H., and D.L. Suarez. 1996. Carbonate and gypsum. In: D.L. Sparks, editor, Methods of Soil Analysis, Part 3, Chemical methods. SSSA Book Series no. 5. SSSA, Madison, WI. p. 437–474.

Merrill, S.D., K.J. Lang, and E.C. Doll. 1990. Contamination of soil with oilfield brine and reclamation with calcium chloride. Soil Sci. 150:469–475.

Microsoft. 2003. Microsoft Office Excel. Microsoft Corporation, Redmond, WA.

Nadler, A., and M. Magaritz. 1986. Long-term effects of extensive gypsum amendment applied with sodic water irrigation on soil properties and soil solution chemical composition. Soil Sci. 142:196–202.

Nelson, R.E. 1982. Carbonate and gypsum. In: A.L Page, R.H. Miller, and D.R. Keeney, editors, Methods of Soil Analysis, Part 2, Chemical and Microbiological Properties, 2nd ed. Agron. Monogr. 9. ASA and SSSA, Madison, WI. p. 181–197.

Rhoades, J.D. 1982. Soluble salts. In: A.L Page, R.H. Miller, and D.R. Keeney, editors, Methods of soil analysis, Part 2, Chemical and microbiological properties, 2nd ed. Agron. Monogr. 9. ASA and SSSA, Madison, WI. p. 167–179.

Rhoades J.D., and D.L. Corwin. 1990. Soil electrical conductivity: Effects of soil properties and application to soil salinity appraisal. Commun. Soil. Sci. and Plant Anal. 21:837–860.

Robbins, C.W., and C.L. Wiegand. 1990. Field and laboratory measurements. In: K.K. Tanji, editor, Agricultural salinity assessment and management. ASCE Manuals and Reports on Engineering Practice No. 71. ASCE, New York, NY. p. 201–219.

Shainberg, I. and J. Letey, 1984. Response of soils to sodic and saline conditions. Hilgardia 52:1–57.

Soil Classification Working Group. 1998. The Canadian system of soil classification, 3rd ed. Agric. and Agri-Food Can. Publ. 1646, NRC Research Press, Ottawa, ON.

Sposito, G. and S.J. Traina. 1987. An ion-association model for highly saline sodium chloride-dominated waters. J. Environ. Qual. 16:80–85.

Suarez, D.L., and J.D. Rhoades. 1982. The apparent solubility of calcium carbonate in soils. Soil Sci. Soc. Am. J. 46:716–722.

U.S. Salinity Laboratory. 2007. ExtractChem Model. Release 2.0. USSL, Riverside, CA.

U.S. Salinity Laboratory Staff. 1954. Diagnosis and improvement of saline and alkali soils. U.S. Gov. Print. Office, Washington, DC.

van Genuchten, M. Th. 1980. A closed-form equation for predicting the hydraulic conductivity of unsaturated soils. Soil Sci. Soc. Am. J. 44:892–898.

Visconti, F., and J.M. de Paz. 2012. Prediction of the soil saturated paste extract salinity from extractable ions, cation exchange capacity, and anion exclusion. Soil Res. 50:536–550.

2.6 Figures and Tables

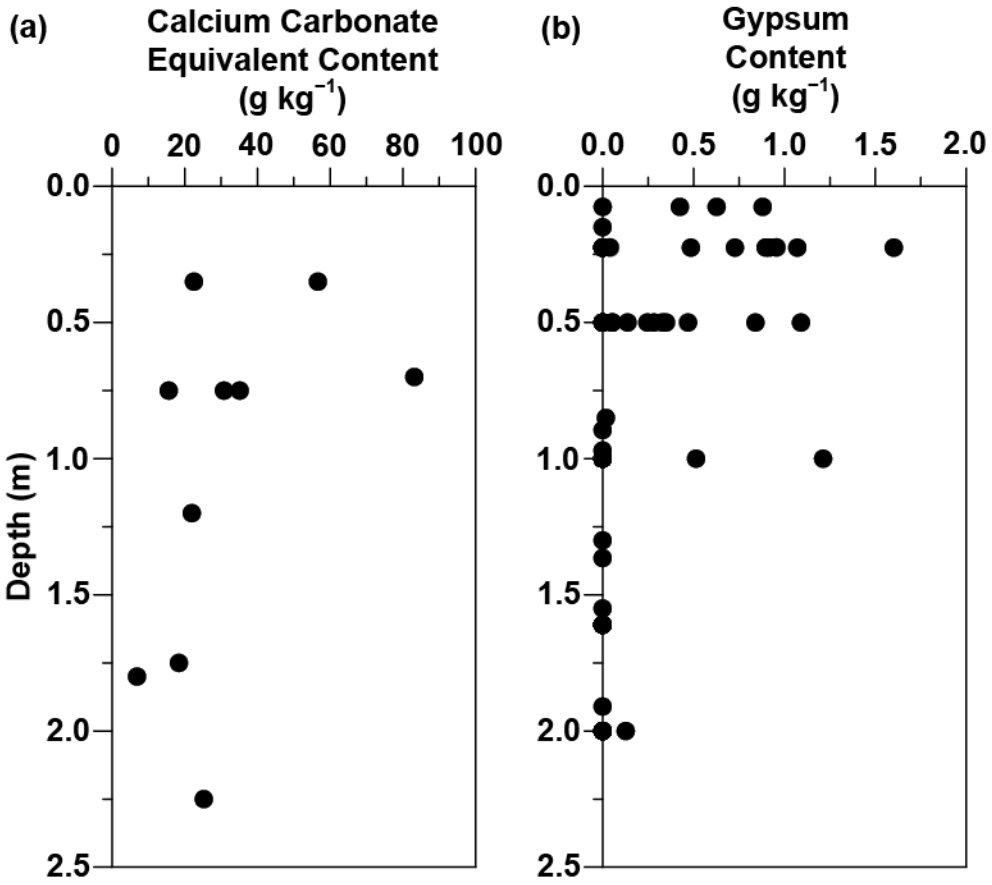

Fig. 2.1. Depth distribution of (a) calcium carbonate equivalent content, and (b) gypsum content in soil.

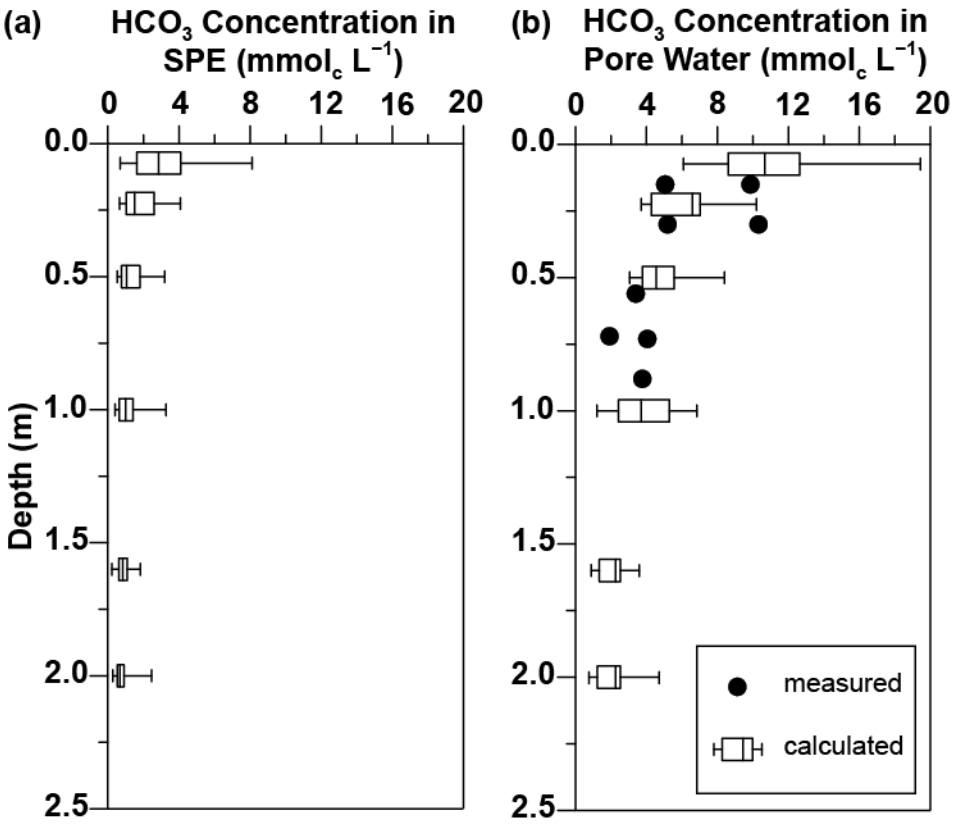

Fig. 2.2 Bicarbonate concentration with depth (a) measured in saturated paste extracts (SPE) from 2008-2010, and (b) calculated from 2010 SPE data. Bicarbonate concentrations measured in soil water samples collected from suction lysimeters are shown in (b) for comparison. Ends of the box plots define the upper and lower quartiles of the sample data, while the vertical line within the box is the sample median. Maximum and minimum values are indicated by the ends of the whiskers. The number of data for each box plot ranges from 11 to 56.

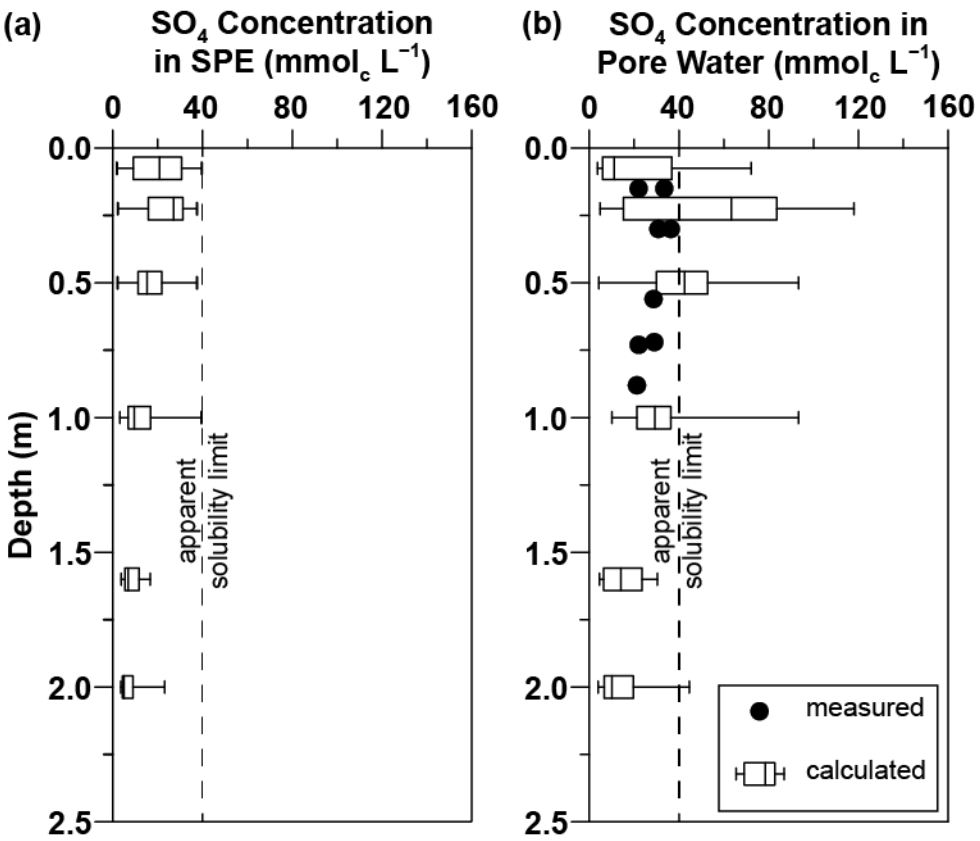

Fig. 2.3. Sulfate concentration with depth (a) measured in saturated paste extract (SPE) from 2008–2010, and (b) calculated from 2010 SPE data. Sulfate concentrations measured in soil water samples collected from suction lysimeters are shown in (b) for comparison. Ends of the box plots define the upper and lower quartiles of the sample data, while the vertical line within the box is the sample median. Maximum and minimum values are indicated by the ends of the whiskers. The number of data for each box plot ranges from 14 to 57.

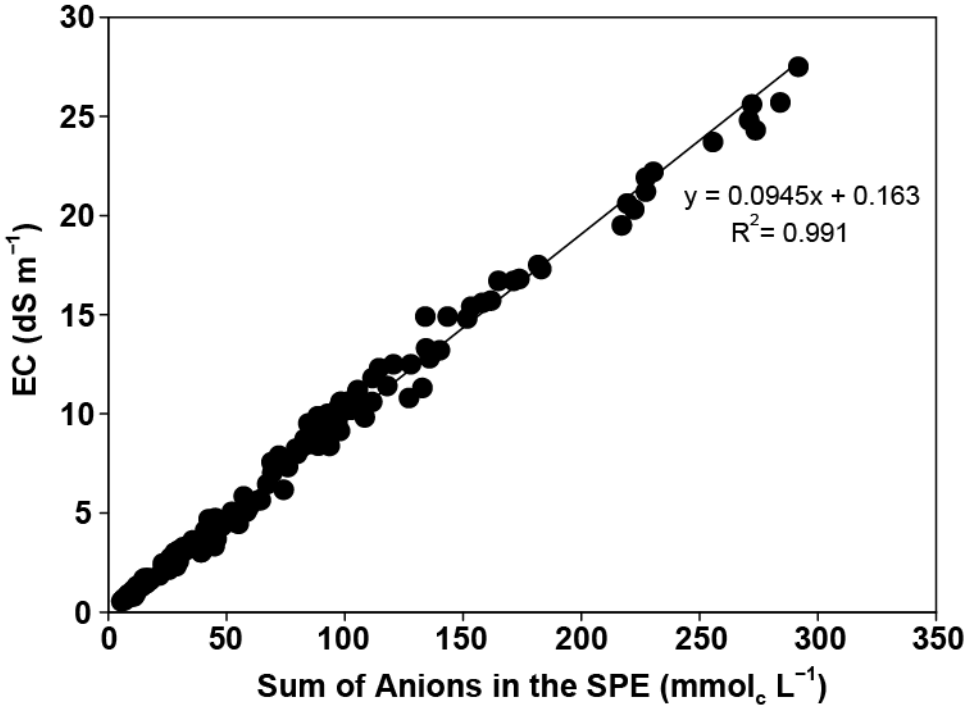

Fig. 2.4. Electrical conductivity (EC) of the saturated paste extract (SPE) vs. sum of major anions ($Cl + SO_4 + HCO_3$) in the SPE for the 2010 dataset, samples from depth 0–7.5 m. The best-fit line was determined through least squares regression.

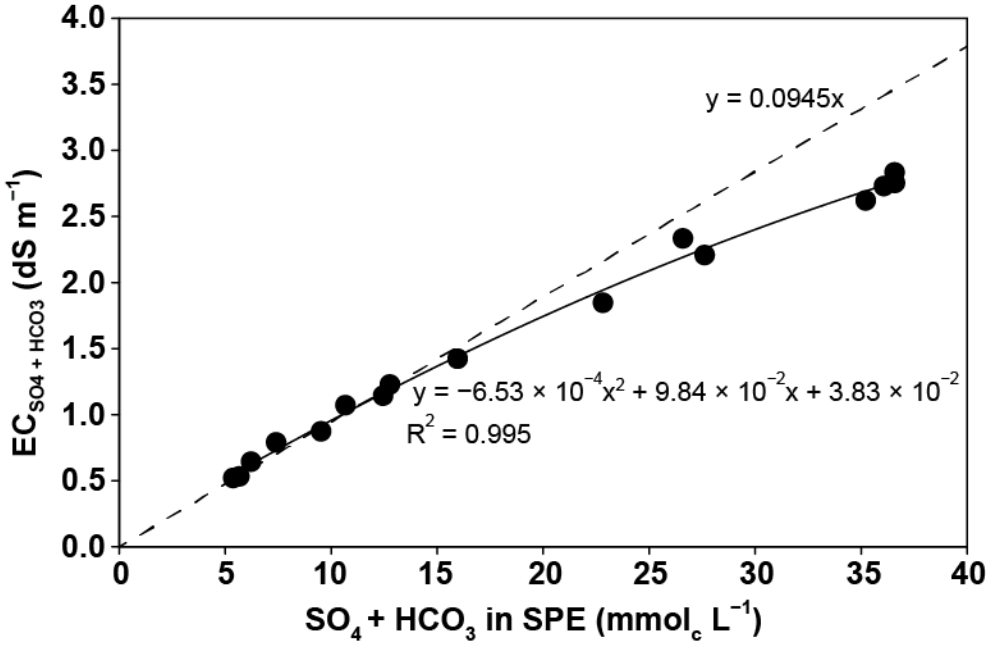

Fig. 2.5. Calculated electrical conductivity (EC) of the SO_4 + HCO_3 component in the saturated paste extract (SPE) vs. SO_4 + HCO_3 concentration in the SPE for the 2010 dataset, samples from depth 0–7.5 m. The line of constant slope y = 0.0945x is included for comparison, and represents the slope of the EC vs. (Cl + SO_4 + HCO_3) best-fit line.

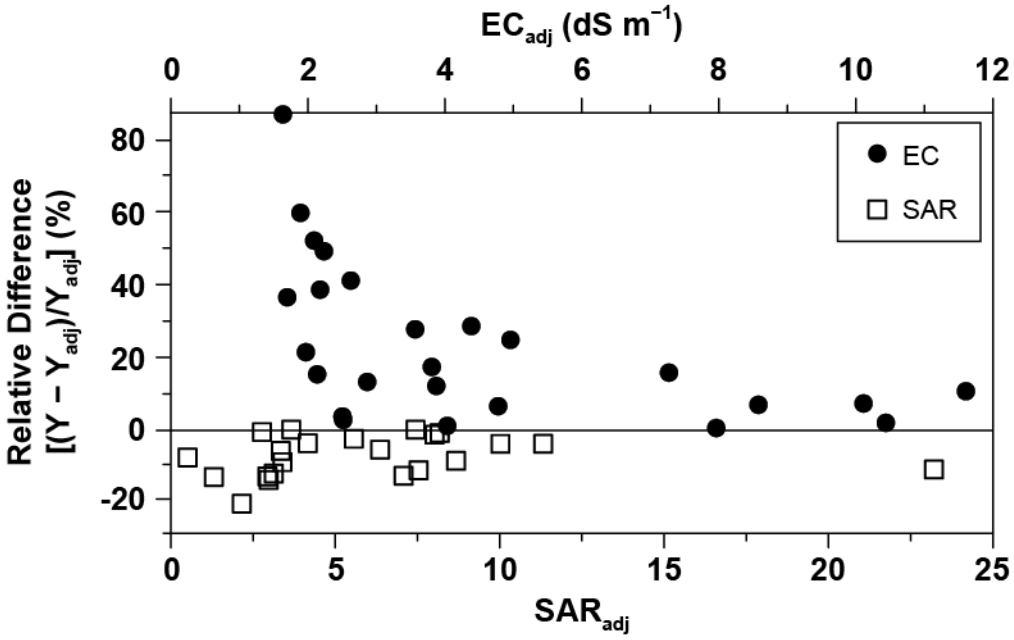

Fig. 2.6. Relative difference on electrical conductivity (EC) and sodium adsorption ratio (SAR) in the saturated paste extract due to gypsum dissolution. Y variable represents either EC or SAR.

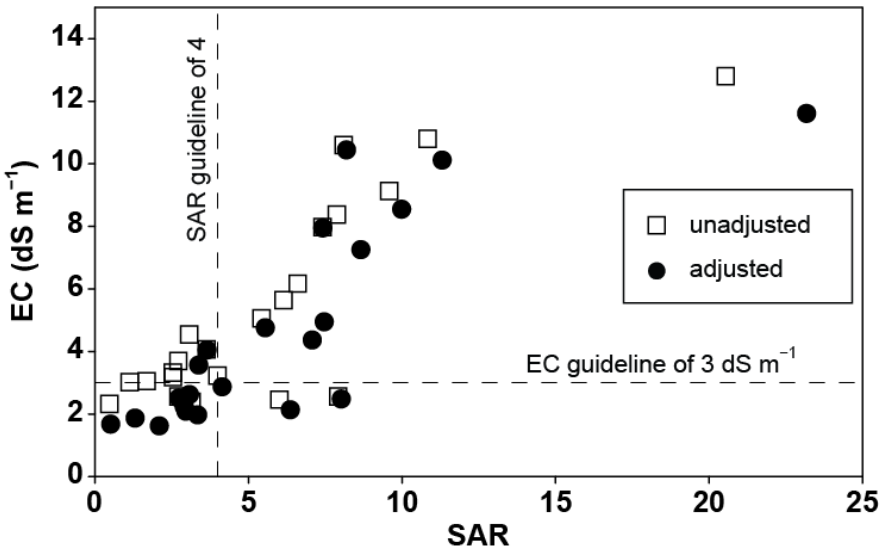

Fig. 2.7. Electrical conductivity (EC) vs. sodium adsorption ratio (SAR), unadjusted and adjusted for excess gypsum dissolved in the saturated paste extract from the 2010 samples from depth 0.15–2.4 m.

Table 2.1. Soil quality guidelines for salinity and sodicity for unrestricted land use. Adapted from Alberta Environment (2001).

Parameter	Rating Categories			
	Good	**Fair**	**Poor**	**Unsuitable**
Topsoil				
EC dS m^{-1}	<2	2–4	4–8	>8
SAR	<4	4–8	8–12	>12
Subsoil				
EC dS m^{-1}	<3	3–5	5–10	>10
SAR	<4	4–8	8–12	>12

Table 2.2. Select soil physical and chemical properties

Layer	Depth	Texture	OM	ρd	θs	pH	CECy	KGy
	m		%	kg L^{-1}	m^3 m^{-3}		$mmol_c$ kg^{-1}	
Topsoil	0–0.15	NT[z]	15.4	1.42	0.45	7.4	NT[z]	NT[z]
Subsoil	0.15–1.25	SIL[x]	NT	1.60	0.40	7.6	220	0.0125
Subsoil	1.25–2.40	SIL[x]	NT	1.46	0.45	7.6	220	0.0125

[z]NT, not tested.

[y]CEC and K_G were determined on samples from the subsoil interval 0.15–2.4 m.

[x]SIL = silt loam.

CHAPTER 3: HYDRAULIC CONDUCTIVITY DYNAMICS DURING SALT LEACHING OF A SODIC, STRUCTURED SUBSOIL

3.1 Introduction

Excessively high levels of salts in agricultural soils can impair plant growth and degrade soil structure (Abrol et al., 1988). The causes of soil salinization are varied. High evaporative demand in arid or semi-arid climates or natural groundwater discharge can concentrate salts close to the soil surface (Brown et al., 1982). Irrigation with water of marginal quality or low leaching rates are common causes of salinization in agricultural soils (Hanson et al., 2006). Additionally, industrial operations can result in accidental release of saline water to surface, such as oil field brines or saline geothermal fluids (Jury and Weeks, 1978; Merrill et al., 1990; Leskiw et al., 2012). Subsequently, reclamation of salt-affected soils may be required to restore land capability (Keren and Miyamoto, 2011), or remediation of industrial impacts may be required to meet regulatory guidelines for soil and shallow groundwater (Alberta Environment, 2001).

One method of reclaiming salt-affected soil is by leaching excess salts from the soil profile using fresh water, either with irrigation or natural rainfall (Abrol et al., 1988). Reclamation of saline-sodic soils by leaching with low-salinity water presents an increased risk for adverse effects on water infiltration and soil drainability due to saline-sodic disruption of soil structure (Suarez, 2011). This deleterious effect on soil structure is a result of high levels of soil-bound sodium coupled with low salinity levels in infiltrating water that produce a spectrum of effects, including: clay swelling, soil aggregate breakdown, clay dispersion, and pore clogging (Quirk, 2001). In low permeability soils, hydraulic conductivity is an important limiting factor in the time required to leach salt from the plant rooting zone. The hydraulic conductivity of a structured soil is controlled to a large degree by the presence of macroporosity including inter-aggregate pores, root holes, worm holes, fractures, etc. (Beven and Germann, 1982). Loss of macroporosity through sodium-induced clay swelling, aggregate breakdown, or pore clogging with

dispersed clays may produce a decrease in hydraulic conductivity. Therefore, maintenance of intact soil structure, and thereby hydraulic conductivity, is key to timely salt leaching.

Hydraulic conductivity of sodic, swelling clay-bearing soils has been shown to be dependent on pore water salinity (Quirk and Schofield, 1955; McNeal and Coleman, 1966). The sensitivity of a soil to saline-sodic effects varies depending on a wide array of soil physical, chemical, and mineralogical properties, including: clay content, clay mineralogy, iron and aluminum oxide content, soil water pH, and degree of soil aggregation (McNeal et al., 1968; Suarez et al., 1984; Alperovitch et al., 1985; Abu-Sharar et al., 1987). The large number of factors that affect the sensitivity of a soil to saline-sodic effects inhibits the development of general relationships for the prediction of soil relative hydraulic conductivity. However, it may be possible to develop adequate relationships between salinity, sodicity, and hydraulic conductivity for soils within a specific locality (Suarez, 2011). It is for these reasons that soil-specific testing of salinity, sodicity, and hydraulic conductivity relationships is recommended for more accurate evaluation of the risk for adverse effects on field soils.

The most widely used method of studying saline-sodic effects on hydraulic conductivity is through laboratory permeameter studies on repacked soil columns (Quirk and Schofield, 1955; McNeal and Coleman, 1966; Shainberg et al., 1981; Curtin et al., 1994). Due to the highly disturbed nature of repacked soils, they would be expected to demonstrate substantially different soil structure than their intact counterparts. It has been recognized that increased research is needed with respect to examining saline-sodic effects on hydraulic conductivity on a more field-relevant basis (Shaw et al., 1998; Oster and Shainberg, 2001).

The objective of this study was to examine the dynamics of hydraulic conductivity decreases induced during salt leaching of sodic, structured subsoil, and identify the mechanism(s) causing the reduction. In addition, the relative sensitivity of the structured subsoil is evaluated against literature-derived thresholds for saline-sodic effects. Two permeameter experiments were conducted on intact soil cores to quantify hydraulic conductivity during salt leaching with and without addition of a Ca-

amendment. Measurements were made using intact soil cores to improve the accuracy of induced decreases in hydraulic conductivity, from a perspective of improving soil remediation.

3.2 Methods and Materials

3.2.1 Site Description

The study site is in an agricultural area located approximately 35 km southwest of Edmonton, AB, Canada. The soil is classified as an Orthic Black Chernozem in the Canadian System of Soil Classification (Soil Classification Working Group, 1998). The soil is developed on a parent material of silt loam texture and glaciolacustrine origin (Bowser et al., 1962). The silt loam subsoil (B and C horizons) has an average clay-sized (<2 μm) fraction of 14 % by volume. The sand fraction is relatively small, < 5 %, with the remainder composed of silt-sized material. Smectite clay is the main mineral component in the clay-sized fraction (48 %), with lesser illite (23 %), kaolinite (17 %), chlorite (5 %) and quartz (6 %). Select soil physical, mineralogical, and chemical properties are summarized in Table 3.1.

The study site is the location of a former oil and gas production facility, decommissioned and removed by 1976. Oil was produced along with a waste fraction of dominantly NaCl brine. Produced water from the same oil-bearing horizon has a total dissolved solids concentration of 180 g L^{-1} and is highly sodic with a sodium adsorption ratio (SAR) of 95, where SAR = Na / $[(Mg + Ca)/2]^{1/2}$, with aqueous cation concentrations in $mmol_c$ L^{-1}. Releases of oil-field brine have resulted in salt-affected soils over an area of approximately 2 ha. In 2003, a remedial tile drain system was installed at 2 m depth to collect saline leachate and route it for disposal by deep well injection.

Intact soil samples were collected in 2009 in cylindrical, thin-walled steel samplers (Shelby tubes), 76 mm in diameter and 500 mm in length. The Shelby tube samplers were hydraulically pushed into the ground using a drilling rig. A portion of the subsoil interval, from 0.7–1.6 m depth, was targeted due to its relatively high levels of salinity and sodicity. Subsequent to collection, samples were sealed to prevent moisture loss and refrigerated to limit bacterial growth. Prior to permeation, cores nominally 100 mm in length were cut from the larger intact samples taken from the Shelby tubes. The cores were trimmed to 51

mm diameter using a soil lathe. Fig. 3.1a shows a trimmed soil core prior to installation within the permeameter core holder. Many relict root holes were present and were cylindrical, generally free of root material, ranging up to 2 mm in diameter. Relict root holes were commonly visible in soil core (Fig. 3.1b). The dominant observed soil aggregate structure was micro-blocky, subangular, and 2–4 mm in size, with relict root holes cross cutting the micro-blocky structure. Relict root holes and inter-aggregate pore space represent the most conductive portion of the pore network, visible by X-ray tomography in Fig. 3.1c.

The salt-affected soil has an average saturated paste extract electrical conductivity (EC) of 8 dS m^{-1} (0–2.4 m depth, August 2008 sampling). Details of soil sample collection and analysis are given in section 2.2.1. In addition to high salinity, the soils are sodic, with an average saturated paste extract SAR of 9. Elevated salinity is highly correlated with sodicity, with a correlation coefficient of 0.86. The soil contains a minor fraction of sparingly soluble minerals with an average calcite content of 3.9 % and a gypsum content of 0.029 % (Table 3.1). Calcite is naturally occurring in the calcareous sediment, while gypsum was applied as a soil amendment. In the pre-remediation state, elevated levels of salinity are expected to mitigate potential decreases in soil hydraulic conductivity caused by sodium-induced clay swelling or soil structure breakdown. However, as salt leaching progresses and pore water salinity levels decrease, the potential for sodic effects on hydraulic conductivity is uncertain.

3.2.2 Permeameter Design and Operation

Soil cores were permeated upwards under load to simulate in situ soil effective stress conditions. A schematic of the custom-built apparatus is shown in Fig. 3.2. The samples were encased in a split sample holder, 52 mm inside diameter, composed of clear acrylic plastic, shown in Fig. 3.1a. To minimize sidewall leakage, soil cores were adhered to the inside of the sample holders using epoxy cement thickened with colloidal silica, similar to the method used by Kodikara et al. (2002). Prior to securing the cores in the permeameter end plates, the ends of the cores were scarified with a fine steel point then

covered with coarse filter paper, 25 μm opening size, and stainless steel screen, 152 μm opening size, for structural support of the soil core.

Due to the relatively low permeability of the soil under study, artificially high hydraulic gradients were required to increase the flow rate and thereby shorten the duration of the experiment. A pressure tank maintained an upstream pressure of 34.5 kPa (3.52 m of hydraulic head). Upstream pressure head was monitored at the permeameter inlet with a pressure transducer and datalogger. The tailwater end of the permeameter was connected to a graduated standpipe used to measure tailwater head ranging from 0–9.8 kPa (0–1 m of hydraulic head). The hydraulic gradient therefore varied from 25–35 m m^{-1}. Flow rate varied with soil hydraulic conductivity and ranged from 0.020–1.4 mL hr^{-1}, which corresponds to a specific discharge of 0.24–17 mm d^{-1}. This permeameter configuration is that of constant head with rising tailwater, for which the calculation of hydraulic conductivity is identical to the more common falling head with constant tailwater configuration (ASTM, 2007). To resist hydraulic uplift, a central shaft and perforated platen applied a vertical load downwards to the top of the soil core during permeation. The static vertical load was applied via an external frame loaded with steel plates producing an applied vertical stress of 22 kPa. The resulting average effective stress ranged from 5 kPa to 10 kPa, varying with tailwater level. For comparison, these levels of effective stress correspond to in situ field conditions.

The permeant solution was an aqueous mixture of NaCl and $CaCl_2$ salts. The permeant solution was de-aired by agitation under a partial vacuum, prior to filling the constant-head pressure tank. The pressure tank held approximately 2 L of permeant solution. Each permeant tank fed two permeameters and required periodic refilling during the experiment. Aqueous cupric sulphate was added to the permeant solution to a final concentration of 1×10^{-3} mmol L^{-1} to limit bacterial growth.

Two permeameter experiments were conducted over a two-and-a-half-year period. Due to the relatively low permeability of these soils, individual permeameter experiments extended up to 641 d elapsed permeation time. The first experiment was designed to study the effect of decreasing salinity on hydraulic conductivity, while maintaining a constant elevated level of sodicity in the permeameter influent water. The second experiment was conducted to examine remediation of elevated sodium levels

through the application of Ca-amendment water. For both experiments, hydraulic conductivity, effluent salinity, and effluent sodicity were the primary parameters of interest. To normalize the observed decreases in hydraulic conductivity induced during subsequent stages of the experiment, relative hydraulic conductivity (K_{rel}) was calculated as a percentage of the reference hydraulic conductivity, taken as the value determined at the end of the initial equilibration stage of permeation (Stage 1). This definition is consistent with that used in other studies to which our results are compared (McNeal and Coleman, 1966; Curtin et al., 1994). The standard deviation on replicate K_{rel} measurements was 4 % on average. Permeameter effluent samples were collected every one or two days depending on the rate of flow. On a subset of these samples, EC was measured using a calibrated handheld probe. A smaller subset of samples was analyzed for major cations (Ca, Mg, Na, and K) and anions (Cl and SO_4) by ion chromatography (IC) with EC detection. The magnitude of the charge balance error for the permeameter effluent samples error was 5% on average. Samples with charge balance error greater than 10 % were culled from the dataset. Carbonate alkalinity was determined on unfiltered samples by titration with dilute sulfuric acid to pH 4 and is reported as HCO_3 concentration. Effluent total electrolyte concentration (C) was determined from EC using a site-specific relationship determined by least squares regression between C (as the sum of major cations) and EC ($n = 50$, $r^2 = 1.00$, data not shown). Effluent SAR was calculated from cation concentrations determined by IC. Sodium, calcium and magnesium are assumed to be in equilibrium with cation exchange sites in the soil cores. Therefore sodium adsorption ratio (SAR) is used as a proxy for cation exchange site composition.

3.2.3 Leaching with Water of Constant Sodicity

Experiment 1 consisted of leaching intact soil cores with a permeant solution of constant elevated sodicity. Due to the long experiment duration and a limited number of custom-built apparatus, the number of replicates was limited to four, P1 to P4. Influent salinity was varied in four stages for which the first three stages had constant SAR of 14. The soil cores were equilibrated during Stage 1 with a solution of elevated salinity and sodicity that approximated the in situ salinity and sodicity levels of the area from

which the cores were collected (C = 230 $mmol_c\ L^{-1}$ for cores P1 and P2, and 270 $mmol_c\ L^{-1}$ for cores P3 and P4, both pairs with SAR = 14). For Stage 2, permeant salinity was decreased approximately an order-of-magnitude to C = 17 $mmol_c\ L^{-1}$, in an attempt to induce a reduction in hydraulic conductivity. As Stage 2 permeation progressed, it became obvious that the relatively low hydraulic conductivity of the soil cores necessitated permeameter testing of multiple cores in parallel and not in series as originally planned. Therefore, permeation was halted during the latter portion of Stage 2 for a duration of 322 and 261 days for P1 and P2, to construct additional permeameter apparatus. Permeation of cores P3 and P4 was initiated following the break from permeation. Addition of two cores doubled the number of replicates and allowed the hydraulic conductivity during Stage 2 for P3 and P4 to be monitored without hiatus. This resulted in better quantification of the time required for stabilization of hydraulic conductivity during Stage 2 permeation. For Stage 3, influent salinity was decreased by an additional order-of-magnitude to C = 1.5 $mmol_c\ L^{-1}$. Stage 4 was an attempt to recover hydraulic conductivity decreases induced in previous stages by applying an influent of high salinity and low sodicity (C = 500 $mmol_c\ L^{-1}$ and SAR = 0.1).

3.2.4 Leaching with Calcium-Amended Water

For permeameter Experiment 2, Ca-amended water (SAR = 0.1) was permeated through soil cores previously equilibrated with a solution of high sodicity (SAR = 60). This is analogous to the application of Ca-amended irrigation water to ameliorate elevated sodic conditions in the field. Two intact soil cores (P5 and P6) were initially equilibrated with a high salinity, high sodicity permeant (C = 520 $mmol_c\ L^{-1}$ and SAR = 60, Stage 1). An SAR of 60 corresponds to the approximate upper end of sodicity, on a pore water basis, measured in soil at the study site. Following Stage 1, Ca-amended permeant solution was added with C = 50 $mmol_c\ L^{-1}$ and SAR = 0.1 (Stage 2). Application of a permeant C = 50 $mmol_c\ L^{-1}$ proved to be insufficient to maintain a reasonable level of hydraulic conductivity. Therefore, the permeant C was increased to 150 $mmol_c\ L^{-1}$, while maintaining SAR = 0.1 (Stage 3). This was done in an attempt to

recover the prior induced hydraulic conductivity decrease and continue permeation with the Ca-amended solution.

3.3 Results

3.3.1 Leaching with Water of Constant Sodicity

Results for Experiment 1 are shown in Fig. 3.3, including effluent C, SAR, and K_{rel} during permeation Stages 2 to 4. Results from Stage 1 are not shown, as they represent the initial equilibration period prior to the leaching portion of the experiment. Hydraulic conductivity determined at the end of Stage 1 ranged from 1.6–6.4 × 10^{-9} m s^{-1}, with an arithmetic mean of 3.5 × 10^{-9} m s^{-1}. Between 19 and 85 pore volumes of effluent were collected over the duration of the experiment (Stages 1–4) due to variation in absolute hydraulic conductivity between cores. Pore volumes of effluent collected during each stage of the experiment and the duration of permeation are summarized in Table 3.2.

Upon application of the first leaching solution (C = 17 $mmol_c$ L^{-1}) at the start of Stage 2, hydraulic conductivity initially decreased jointly with the permeameter effluent C (Fig. 3.3). Effluent C stabilized at concentrations ranging from 20–24 $mmol_c$ L^{-1}, with an average of 22 $mmol_c$ L^{-1}, which is above the influent level of 17 $mmol_c$ L^{-1}. The higher level of effluent salinity is attributed to dissolution of calcite and to a lesser degree gypsum within the soil cores. This is corroborated by average HCO_3 and SO_4 levels of 3.3 and 0.26 $mmol_c$ L^{-1} in the effluent at the end of Stage 2a (data not shown). In comparison, concentrations of HCO_3 and SO_4 in the influent were negligible.

Following stabilization of effluent C, hydraulic conductivity continued to decrease. To aid discussion of the mechanism of hydraulic conductivity decrease, Stage 2 results have been subdivided into Stage 2a and b. Stage 2a represents the period during which effluent C reaches a constant value, while Stage 2b represents the remainder of Stage 2, during which constant hydraulic conductivity was achieved. The observed decrease in hydraulic conductivity during Stage 2a ranged from 11–52 %, with an average of 26 %. The hiatus in permeation for cores P1 (322 d) and P2 (261 d) resulted in a discontinuity in their K_{rel} curves (Fig. 3.3a and 3.3b). Prior to the hiatus, the hydraulic conductivity of both cores was

decreasing, while following the hiatus, the hydraulic conductivity maintained a lower but stable value. This apparent time dependency of the hydraulic conductivity decrease in cores P1 and P2 is the first indication that a diffusion-controlled process may be partly responsible for the observed hydraulic conductivity decline. The hiatus in permeation for cores P1 and P2 precludes accurate determination of the time required for stabilization of hydraulic conductivity. Cores P3 and P4 were run without interruption of permeation; therefore, an estimate of the duration of time required to reach stable hydraulic conductivity was determined as the duration of Stage 2b. For cores P3 and P4, the duration of Stage 2b was 125 and 138 d, respectively. By the end of Stage 2b, the total decrease in K_{rel} reached 19–81 %, with an average decrease of 49 %. Stabilized effluent salinity, sodicity, and hydraulic conductivity for each stage of the experiment are summarized in Table 3.2.

Following Stage 2 permeation, the influent C was further reduced to 1.5 $mmol_c\ L^{-1}$, while maintaining an SAR of 14. During Stage 3, further reduction in K_{rel} was experienced for all four cores ranging from 2–21%. At the end of Stage 3, the total decrease in K_{rel} ranged from 37–83 %, with an average decrease of 62 %. As in Stage 2, the decline in effluent C slowed after passage of a few pore volumes (Fig. 3.3). However, calcite and gypsum dissolution contributed a greater relative proportion to the effluent C during Stage 3 permeation. Effluent concentrations for HCO_3 and SO_4 averaged 3.8 $mmol_c\ L^{-1}$ and 0.19 $mmol_c\ L^{-1}$. The short duration fluctuations in observed effluent C, particularly for P1 and P2, are the result of kinetic effects related to calcite dissolution. Increases in effluent C correspond to increases in HCO_3 concentration, which are correlated with minor decreases in permeameter flow rate. Minor fluctuations in permeameter flow rate were associated with draining of the permeant storage tank. As the permeant level in the tank approached empty, upstream head decreased slightly causing a corresponding decrease in flow rate. Bicarbonate concentration is negatively correlated to the permeameter flow rate ($r = -0.81$), highlighting the dependency of calcite dissolution on pore water residence time within the soil cores. A higher residence time, associated with lower flow rate, corresponds to higher HCO_3 concentrations. Sulfate concentrations are relatively low compared to HCO_3 concentrations and did not show the same dependency on flow rate.

In addition to elevated effluent HCO_3 concentrations attributed to calcite dissolution, excess Ca is produced. Relative to the constant influent SAR of 14, a minor decrease in effluent SAR was observed during Stage 2 and a larger decrease during Stage 3 (Fig. 3.3). With the exception of P2 which maintained an elevated SAR of 17, Stage 2 effluent SAR decreased to an average of 11. The dissolution effect increases with decreasing C and decreasing flow rate such that by the end of Stage 3 the average effluent SAR decreased to 4.7. The slow rate of supply of Ca from mineral dissolution results in a relatively low rate of decrease in sodicity by cation exchange. Only P1, with an SAR of 1.6 at the end of Stage 3, can be considered to have reached equilibrium during Stage 3. This is a result of the much larger number of pore volumes passed through P1 during Stage 3 (50 pore volumes) relative to the other three soil cores (6.7–22.5 pore volumes). Approximately 32 pore volumes of effluent were required to flush excess Na from P1 to reach equilibrium conditions during Stage 3. This demonstrates that at low salinity levels, natural dissolution of calcite is capable of supplying sufficient Ca to remediate elevated sodicity. However, due to the low rate of Ca supply through calcite dissolution, the number of pore volumes required to complete the exchange of Ca for Na is high. Efficiency of Ca amendment addition is explored further in the results of Experiment 2.

In an attempt to reverse hydraulic conductivity decreases induced during Stage 2 and 3 permeation, Stage 4 was conducted using a permeant of high salinity (C = 500 $mmol_c\ L^{-1}$) and low sodicity (SAR = 0.1). Hydraulic conductivity of the soil cores was only partially recovered. The increase in K_{rel} during Stage 4 ranged from insignificant to 26 %, with an average increase of 11 %. With the exception of P4, which reached a final K_{rel} of 87 %, the remaining three cores reached an average K_{rel} of 35 %. This relatively low degree of recovery of hydraulic conductivity shows that a significant portion of the hydraulic conductivity decrease is not immediately recoverable upon application of high salinity, low sodicity water. This motivates prevention of decreases of hydraulic conductivity in field soils rather than trying to reverse the effect after it has occurred. Permeation for a longer duration or application of a drying period, as suggested by McNeal and Coleman (1966), may improve hydraulic conductivity recovery. These are two potential avenues for future research.

3.3.2 Leaching with Calcium-Amended Water

Results of leaching with Ca-amended water are shown in Fig. 3.4, for permeation Stages 2 and 3. Stage 1 represents the initial permeation conducted to equilibrate the cores with the high salinity (C = 500 $mmol_c\ L^{-1}$), high sodicity (SAR = 60) influent, and therefore, the results for Stage 1 are not presented. Upon application of the Stage 2 permeant (C = 50 $mmol_c\ L^{-1}$), the hydraulic conductivity of both cores dropped sharply in conjunction with decreasing effluent C. During Stage 2, K_{rel} of cores P5 and P6 decreased to lows of 18 and 37 %, respectively, which resulted in a corresponding decrease in average flow rate from 0.56 mL hr^{-1} to 0.16 mL hr^{-1}. This relatively large hydraulic conductivity decrease was induced while using a permeant of low sodicity (SAR = 0.1). This illustrates that high antecedent soil sodicity (SAR = 60), to a large degree, controlled the saline-sodic response of the soil. To mitigate the loss of hydraulic conductivity and recoup the permeameter flow rate, influent C was increased three-fold to 150 $mmol_c\ L^{-1}$ (Stage 3). Note that the hydraulic conductivity of core P6 increased marginally (<10 %) prior to the application of the higher salinity permeant at the start of Stage 3 (Fig. 3.4b). This early increase in hydraulic conductivity is assumed to be a response to slowly decreasing sodicity occurring during Stage 2.

The degree of decline in effluent C was much greater than effluent SAR during Stage 2. Effluent C for P5 and P6 decreased an average of 88 % to 63 $mmol_c\ L^{-1}$ after passage of 2.5 pore volumes. Effluent SAR decreased an average of 31 % to an average of 42 at its lowest level, after passage of 1.6 pore volumes. Near the start of Stage 3, after passage of 2.9 pore volumes, effluent SAR rebounded to an average value of 60. This rebound in SAR may reflect increased contribution of Stage 1 water through internal diffusion from soil aggregates. Upon application of the higher salinity permeant, K_{rel} recovered to levels of 59 and 95 % for P5 and P6, respectively. The K_{rel} of core P6 later declined to 90 %, without an evident cause. This fluctuation in hydraulic conductivity is relatively minor and does not affect interpretation. As the effluent C increased, the effluent SAR resumed its descent reaching the influent value of 0.1 after passage of 10 pore volumes total. Although a large portion of hydraulic conductivity

lost during Stage 2 was recovered, the results were mixed for the two cores. The final hydraulic conductivity of core P5 was substantially lower than that reached by P6. This demonstrates that even with relatively prompt increase in permeant salinity, the hydraulic conductivity decrease is not universally reversible. Following reclamation of field soils suffering from saline-sodic effects, heterogeneity in the spatial distribution of hydraulic conductivity may be a significant issue.

3.4 Discussion

3.4.1 Leaching with Water of Constant Sodicity

3.4.1.1. Mechanism of Hydraulic Conductivity Decrease

Two main mechanisms of saline-sodic hydraulic conductivity decrease are typically identified in clay-bearing soils: clay swelling, and/or clay dispersion (Quirk and Schofield, 1955; McNeal and Coleman, 1966; Frenkel et al., 1978; Alperovitch et al., 1985; Curtin et al., 1994; Suarez et al., 2006). These mechanisms are interrelated in that clay dispersion is an end result of diffuse double layer (DDL) swelling (Laird, 2006). In their review work, Shainberg and Singer (2011) summarize a number of studies demonstrating swelling and dispersion effects on soils containing smectite clay; while soils containing illite and kaolinite do not swell appreciably but are susceptible to dispersion. Soils containing vermiculite clay have also been demonstrated to be susceptible to swelling effects (Quirk and Schofield, 1955). The active swelling component of the soil under study can therefore be assumed to be its smectite clay component.

Absence of dispersed clay in the permeameter effluent during Experiment 1 is not sufficient to eliminate clay dispersion as the mechanism of hydraulic conductivity reduction. This is due to dispersed clay typically not being observed in effluent of fine-grained soils such as loams and clays due to the relatively small size of conducting pores (Shainberg and Singer, 2011). In a substantial summary of sodic effects on soils, Shainberg and Letey (1984) divided studies on the effects of hydraulic conductivity into those that used a minimum permeant C above 3 $mmol_c\ L^{-1}$, for which clay swelling was the dominant

mechanism of hydraulic conductivity reduction, and those studies that used a permeant C below 3 $mmol_c$ L^{-1}, for which clay dispersion was the dominant mechanism. Consequently, we assume a C of 3 $mmol_c$ L^{-1} can be used as a threshold value below which spontaneous clay dispersion may occur. An influent of C = 17 $mmol_c$ L^{-1} was used in Experiment 1, Stage 2, which is well above the dispersion threshold of 3 $mmol_c$ L^{-1}. Therefore clay swelling is assumed to be the dominant mechanism of hydraulic conductivity disruption during Stage 2 permeation. During Stage 3, calcite and gypsum dissolution was sufficient to maintain an effluent C of 4–6 $mmol_c$ L^{-1}, upon application of influent C = 1.5 $mmol_c$ L^{-1}. However, C at the influent end of the soil core was low enough to potentially induce clay dispersion.

Knowledge of the mechanism responsible for hydraulic conductivity reduction is useful from a land management perspective, in which recovery of degraded soil permeability is of interest. A greater degree of reversibility is generally assumed for swelling versus dispersion effects (Shainberg and Letey, 1984). The assumption that hydraulic conductivity reduction is reversible is an extrapolation from the observation that clay swelling is a reversible process. However, even though clay swelling is reversible, declines in hydraulic conductivity resulting from clay swelling have been observed to be substantially irreversible (McNeal and Coleman, 1966; Mitchell and Donovan, 1991; Mohan et al., 1993). The low degree of reversibility is attributed to pore network damage occurring due to swelling and repositioning of non-swelling minerals adjacent to swelling particles (Mohan et al., 1993). A contributing factor may be the partial destruction of soil aggregates due to internal swelling pressures resulting in clogging of inter-aggregate macropores (Quirk, 2001). Therefore, decreases in hydraulic conductivity due to pore network clogging caused by either clay swelling or clay dispersion should be considered only partially reversible.

3.4.1.2. Role of Diffusion in the Clay Swelling Process

Smectite quasicrystal break down (swelling process) occurs on the order of minutes (Shainberg and Kaiserman, 1969). Therefore, over the time period of permeation (e.g., days), clay swelling can be assumed to be locally in equilibrium with pore water salinity and sodicity. However, it was observed during Stage 2 permeation that hydraulic conductivity continued to decline for a duration >120 d

following stabilization of effluent C for cores P3 and P4. To understand this slow rate of hydraulic conductivity decline, we must examine the process by which salts are leached from a structured soil. The cores were collected from a soil that had >30 yrs to equilibrate with in situ salinity and sodicity conditions. Therefore, the cores are assumed to have been fully equilibrated prior to the initiation of the leaching experiment. Upon application of low salinity permeant, the flow through the conductive inter-aggregate macropores results in a decrease in solution concentration at the boundary of the soil aggregates. Salt transport out of the aggregates can be described macroscopically by Fickian diffusion driven by the concentration gradient between pore water within the soil aggregate and inter-aggregate pore water (Siyal et al., 2002). The rate of diffusion is therefore controlled to a large degree by the magnitude of the gradient between the intra-aggregate soil solution and the inter-aggregate pore space. However, diffusion from aggregates containing swelling clays is complicated by the presence of the DDL on clay particle surfaces. Diffusion of anions is limited within the DDL, which is enriched in cations (Appelo et al., 2010). As the DDL becomes more diffuse due to lower permeant C, overlap of the DDL between clay domains results in increased swelling. Diffusion of salt out of clay soils can be limited by this process of DDL overlap and the resulting anion exclusion effect (Blackmore, 1976). Thereby, diffusion of salt out of the smallest pores becomes more limited as swelling progresses. This effect has been termed “salt sieving” or “salt filtering” (Shackelford and Daniel, 1991).

Diffusion of the majority of the salt mass out of soil aggregates occurred during the early portion of leaching, after passage of approximately 4 pore volumes of effluent (Stage 2a). Given that the decrease in hydraulic conductivity is controlled by the swelling clay fraction, the lag between decreasing hydraulic conductivity and effluent salinity suggests that salinity in the clay-bound intra-aggregate pores is in physical disequilibrium with bulk salinity in the inter-aggregate pores. As salt slowly diffuses out of the clay-bound pores within the soil aggregates, swelling increases and hydraulic conductivity continues to decline. Clay swelling continues until equilibrium is reached between salinity inside and outside the clay-bound pores (end of Stage 2b). Contribution of salt diffusing out of soil aggregates does not produce a noticeable decline in effluent C, during Stage 2b. One possible explanation for this is that the contribution

of salt from diffusion is small enough that any decrease in salt concentration coming from diffusion is not detectable as a decrease in effluent C. A second possible explanation is that declining concentration of Cl from diffusion is balanced by an increase in HCO_3 sourced from calcite dissolution. Bicarbonate concentration was shown to be correlated with permeameter flow rate in the results section of this paper. Therefore, an increase in HCO_3 concentration is expected in response to declining hydraulic conductivity and flow rate.

The portion of the hydraulic conductivity decrease that occurred during Stage 2 following stabilization of the effluent C accounted for 46 % of the observed decline on average. Therefore, swelling-controlled diffusion plays a relatively large role in the observed decreases in hydraulic conductivity.

3.4.1.3. Relative Sensitivity to Saline-Sodic Swelling Effects

The relative sensitivity of a soil to clay swelling can be evaluated by examining the threshold concentration (TC) at which a significant decrease in hydraulic conductivity occurs at a specific sodicity level. The TC concept was introduced by Quirk and Schofield (1955) and was defined as the concentration at which a 10–15% reduction in hydraulic conductivity occurred for a given level of sodicity. Subsequently, other authors have defined the TC at a hydraulic conductivity decrease of 25% (McNeal and Coleman, 1966; Rhoades, 1982; Curtin et al., 1994). Literature-derived TC curves are used to evaluate the relative sensitivity of the soil under study to saline-sodic effects on hydraulic conductivity.

Four literature-derived threshold curves from McNeal and Coleman (1966) and Curtin et al. (1994), plotted in Fig. 3.5, were selected to illustrate a range in sensitivity to saline-sodic effects on hydraulic conductivity. For each threshold curve, salinity levels above the TC result in maintenance of K_{rel} >75 %. The principal variable between the curves presented is the swelling clay content (smectite + vermiculite). Sensitivity to saline-sodic effects increases from low to high TC. From least sensitive to most sensitive, the four soils are ordered: McNeal and Coleman (1966)-Pachappa with a whole soil swelling clay content of 5 %; McNeal and Coleman (1966)-Waukena with a whole soil swelling clay content of 16 %; Curtin et

al. (1994)-Sceptre with a 54 % clay fraction containing smectite, but with the smectite content unquantified; and, McNeal and Coleman (1966)-Gila, with 29 % whole soil smectite content. These four curves are hereafter referred to as the Pachappa, Waukena, Sceptre and Gila curves. The location of the Sceptre curve between the Waukena and Gila curves is consistent with a swelling clay content between 16 and 29 %. All four of these threshold curves were developed on dried, sieved, and repacked soil columns. Two additional threshold curves of Quirk (1971) and Rhoades (1982) have appeared widely in literature and are reproduced here after Quirk (2001) and Suarez (2011), respectively.

In Experiment 1, application of a permeant of C = 17 $mmol_c\ L^{-1}$ and SAR = 14 (Stage 2) resulted in an average decrease in hydraulic conductivity of 49 %. Plotted on Fig. 3.5, the Stage 2 SAR-C pairing plots below Gila and Sceptre curves, but above the remaining curves. The intact soil under study is more sensitive than the repacked Waukena soil with a swelling clay content of 16 %. Even though, the intact soil under study has a whole soil swelling clay content of 7 %, it behaves like a repacked soil of much higher swelling clay content.

Repacked soils can be expected to react differently to swelling compared to structured soils (Shainberg and Letey, 1984). Therefore, it is worth examining major factors that may control the relative sensitivity of a structured soil to saline-sodic effects on hydraulic conductivity. Pores >30 μm serve as the major water conducting porosity in structured soils (Gebhardt et al., 2009). Breakdown of soil macroaggregates (>250 μm) into microaggregates (20–250 μm) reduces the number of macropores and thereby reduces soil permeability (Oster and Shainberg, 2001). Studies of the effects of saline-sodic swelling on the hydraulic conductivity of intact soils (field or laboratory) are few. A number of studies have applied distilled or relatively fresh water to intact soils resulting in clay dispersion (Oster and Schroer, 1979; Scotter, 1985; Bagarello et al., 2006). However, application of distilled water to simulate rain is more applicable to studies of saline-sodic effects on surface soils as opposed to subsoils. Mitchell and Donovan (1991) found that soil aggregate size was the dominant factor controlling hydraulic conductivity during leaching of a saline-sodic field soil (topsoil and subsoil). Lower infiltration rates were attributed to smaller aggregate sizes caused by aggregate breakdown under conditions of low salinity and

high sodicity. In comparison, higher infiltration rates were attributed to larger aggregate sizes that were maintained by high salinity conditions. Additionally, Abu-Sharar et al. (1987) reported a larger relative decrease in hydraulic conductivity for repacked soils with larger aggregates as compared to those with smaller aggregates. Their conclusion was that a greater proportion of inter-aggregate macropores results in greater aggregate instability due to less restriction against aggregate breakdown into open inter-aggregate pore space.

The majority of the hydraulic conductivity of the structured soil cores under study is assumed to occur through inter-aggregate pores and relict rootholes (Fig. 3.1b and 3.1c). The observed decline in hydraulic conductivity induced by reduction in pore water salinity, while maintaining elevated sodicity, is attributed to a reduction in pore cross-sectional area, caused by swelling and breakdown of the soil aggregates. This reduction in pore size need not occur over the entire length of a conductive pore since hydraulic conductivity is controlled to a large degree by the narrowest pore throat constriction. Heterogeneity in the distribution of swelling clay within a structured soil could also result in higher sensitivity to swelling effects in localized regions of higher than average swelling clay content.

An additional factor that may serve to increase the sensitivity of the intact soil under study is the confined soil condition under which the permeameter testing was conducted. The intact soil cores were restricted from swelling vertically by application of an axial load. This is analogous to overburden loading of subsoil. The TC curves, presented in Fig. 3.5, were developed on repacked soils in open-top permeameters, allowing free vertical swelling. The confined soil condition used in our experiment serves to internalize swelling, resulting in a greater reduction in hydraulic conductivity for a given amount of clay swelling. The confined testing conditions used here are considered representative of subsoil field conditions. Therefore, structured subsoils are likely to be more sensitive to saline-sodic swelling effects than their unstructured, unconfined counterparts.

3.4.2 Leaching with Calcium-Amended Water

When leaching sodic soil with Ca-amended water, antecedent sodicity plays a large role even when applying a low sodicity permeant. This effect is due to the cation exchange front lagging behind the salt flushing front within the soil core. As illustrated by measured effluent salinity and sodicity shown in Fig. 3.4, the effluent C approached the influent C after a passage of approximately three pore volumes; however, the effluent SAR remained elevated. The expected magnitude of the lag between the cation exchange front and the freshening front can be explored using a simple plug flow model (i.e., assuming no solute dispersion or aggregate-macropore solute interaction). Under plug flow conditions, one pore volume of permeant would be required to fully flush the salt out of the soil core. Under the same plug flow conditions and assuming equilibrium cation exchange, with an influent C of 50 $mmol_c\ L^{-1}$ and SAR = 0.1, the exchange of Ca in the influent for Na in the soil would require 6 pore volumes, or 6 times that required to flush the soil cores of elevated salinity. This calculation was done using a soil-specific cation exchange capacity of 220 $mmol_c\ kg^{-1}$ and a Gapon Na-Ca selectivity coefficient of 0.0125 $(mmol_c\ L^{-1})^{-1/2}$ reported in Chapter 2.

An increase of the permeant salinity to 150 $mmol_c\ L^{-1}$ at the start of Stage 3, while maintaining an SAR of 0.1, resulted in an increase in the rate of cation exchange. Assuming the same plug flow condition as above, only 2 pore volumes of permeant would be required to lower the sodicity level from SAR = 60 to 0.1. This volume is one-third of the amount of permeant required using a solution of C = 50 $mmol_c\ L^{-1}$ and SAR = 0.1. The reduction in pore volumes required to complete Na exchange can therefore be calculated as the ratio between the lower and higher permeant C values. Dispersion adds to the number of pore volumes required to leach elevated salinity from soil relative to plug flow conditions. For example, the results of Experiment 1, Stage 2a, indicate that approximately four pore volumes of flow are required to leach elevated salinity from this soil, which represents the effect of dispersion but does not include cation exchange effects. If two pore volumes are required to complete cation exchange under plug flow

conditions, approximately eight pore volumes would be required in practice. This calculated number of pore volumes compares well with the duration of Stage 3 of Experiment 2, which required 6.8 and 7.8 pore volumes at an influent C of 150 $mmol_c\ L^{-1}$ to lower the SAR of cores P5 and P6 from 38 and 45 to 0.1, respectively (Table 3.3).

3.5 Conclusion

Permeameter testing on intact cores taken from a structured subsoil indicates that diffusion of salt out of low permeability soil aggregates is controlling the rate of saline-sodic swelling and thereby the rate of hydraulic conductivity decrease. The resultant decrease in hydraulic conductivity is greater than expected based on a comparison to threshold curves from a range of clay-bearing repacked soils from other studies. Potential causes of increased sensitivity to saline-sodic swelling include: localized loss in hydraulic conductivity in conductive pores causing a disproportionate decrease in bulk soil hydraulic conductivity; or subsoil confinement increasing the degree of internal swelling. Increased sensitivity observed for the intact cores used in this study, suggests that loss of hydraulic conductivity in structured field soils would be underpredicted by conducting similar permeameter tests on repacked soil columns.

Remediation of fine-grained soil via leaching is often limited by the maximum infiltration rate of these low permeability soils. Decreases in soil hydraulic conductivity due to saline sodic effects can adversely affect remediation timelines. Therefore, timely remediation relies on maintenance of maximum soil hydraulic conductivity. Decreases in hydraulic conductivity resulting from macropore disruption are not fully reversible. Uncertainty regarding the reversibility of pore network damage caused by clay swelling, motivates prevention of saline-sodic swelling in field soils before it occurs. Safe salinity and sodicity levels can be determined prior to initiation of salt leaching (e.g., via laboratory permeameter testing on intact soil cores). Subsequent monitoring of soil salinity and sodicity conditions during the leaching process can aid in the prevention of deleterious loss of soil permeability.

3.6 References

Abrol, I.P., J.S.P. Yadav and F.I. Massoud. 1988. Salt-affected soils and their management. FAO Soils Bulletin No. 39, Rome, Italy.

Abu-Sharar, T.M., F.T. Bingham and J.D. Rhoades. 1987. Reduction in hydraulic conductivity in relation to clay dispersion and disaggregation. Soil Sci. Soc. Am. J. 51: 342-346.

Alberta Environment. 2001. Salt contamination and remediation guidelines. Environmental Sciences Division, Environmental Service, Pub. No. T/606, Edmonton, AB.

Alperovitch, N., I. Shainberg, R. Keren and M.J. Singer. 1985. Effect of clay mineralogy and aluminum and iron-oxides on the hydraulic conductivity of clay-sand mixtures. Clay Clay Miner. 33: 443-450.

Appelo, C.A.J., L.R. Van Loon and P. Wersin. 2010. Multicomponent diffusion of a suite of tracers (HTO, Cl, Br, I, Na, Sr, Cs) in a single sample of Opalinus clay. Geochim. Cosmochim. Acta 74: 1201-1219.

ASTM. 2007. ASTM standard D5856-95(2007): Test method for measurement of hydraulic conductivity of porous material using a rigid-wall, compaction-mold permeameter. ASTM International, West Conshohocken, PA.

Bagarello, V., M. Iovino, E. Palazzolo, M. Panno and W.D. Reynolds. 2006. Field and laboratory approaches for determining sodicity effects on saturated soil hydraulic conductivity. Geoderma 130: 1-13.

Beven, K. and P. Germann. 1982. Macropores and water flow in soils. Water Resour. Res. 18: 1311-1325.

Blackmore, A.V. 1976. Salt sieving within clay soil aggregates. Aust. J. Soil Res. 14: 149-158.

Bowser, W.E., A.A. Kjearsgaard and T.W. Peters. 1962. Soil survey of Edmonton sheet (83-H). Canada Department of Agriculture. University of Alberta Bulletin No. SS-4. Alberta Soil Survey Report No. 21, Edmonton, AB.

Brown, P.L., A.D. Halvorson, Siddoway, H.F. Mayland and M.R. Miller. 1982. Saline-seep diagnosis, control, and reclamation. U.S. Department of Agriculture Conservation Research Report No. 30, U.S. Gov. Print. Office, Washington, DC.

Callaghan, M.V. 2014. Remediation of a salt-affected, macroporous soil in central Alberta, Canada. Ph.D. diss., University of Calgary, Calgary, AB.

Curtin, D., H. Steppuhn and F. Selles. 1994. Structural stability of Chernozemic soils as affected by exchangeable sodium and electrolyte concentration. Can. J. Soil Sci. 74: 157-164.

Frenkel, H., J.O. Goertzen and J.D. Rhoades. 1978. Effects of clay type and content, exchangeable sodium percentage, and electrolyte concentration on clay dispersion and soil hydraulic conductivity. Soil Sci. Soc. Am. J. 42: 32-39.

Gebhardt, S., H. Fleige and R. Horn. 2009. Effect of compaction on pore functions of soils in a Saalean moraine landscape in north Germany. J. Plant Nutr. Soil Sci. 172: 688-695.

Hanson, B.R., S.R. Grattan, and A. Fulton. 2006. Agricultural salinity and drainage. Division of Agriculture and Natural Resources Publication 3375. University of California, Davis, CA.

Jury, W.A. and L.V. Weeks. 1978. Solute travel-time estimates for tile-drained fields: III. Removal of a geothermal brine spill from soil by leaching. Soil Sci. Soc. Am. J. 42: 679-684.

Keren, R. and S. Miyamoto. 2011. Reclamation of saline, sodic, and boron-affected soils. In: W. W. Wallender and K. K. Tanji, editors, Agricultural salinity assessment and management, 2nd ed. ASCE Manuals and Reports on Engineering Practice No. 71. ASCE, Reston, VA. p. 655-686.

Kodikara, J.K., F. Rahman and S.L. Barbour. 2002. Towards a more rational approach to chemical compatibility testing of clay. Can. Geotech. J. 39: 597-607.

Laird, D.A. 2006. Influence of layer charge on swelling of smectites. Appl. Clay Sci. 34: 74-87.

Leskiw, L.A., R.B. Sedor, C.M. Welsh and T.B. Zeleke. 2012. Soil and vegetation recovery after a well blowout and salt water release in northeastern British Columbia. Can. J. Soil Sci. 92: 179-190.

McNeal, B.L. and N.T. Coleman. 1966. Effect of solution composition on soil hydraulic conductivity. Soil Sci. Soc. Am. Proc. 30: 308-&.

McNeal, B.L., D.A. Layfield, W.A. Norvell and J.D. Rhoades. 1968. Factors influencing hydraulic conductivity of soils in presence of mixed-salt solutions. Soil Sci. Soc. Am. Proc. 32: 187-&.

Merrill, S.D., K.J. Lang and E.C. Doll. 1990. Contamination of soil with oil-field brine and reclamation with calcium-chloride. Soil Sci. 150: 469-475.

Mitchell, A.R. and T.J. Donovan. 1991. Field infiltration of a salt-loaded soil: Evidence of a permeability hysteresis. Soil Sci. Soc. Am. J. 55: 706-710.

Mohan, K.K., R.N. Vaidya, M.G. Reed and H.S. Fogler. 1993. Water sensitivity of sandstones containing swelling and non-swelling clays. Colloid Surface A 73: 237-254.

Oster, J.D. and F.W. Schroer. 1979. Infiltration as influenced by irrigation water-quality. Soil Sci. Soc. Am. J. 43: 444-447.

Oster, J.D. and I. Shainberg. 2001. Soil responses to sodicity and salinity: Challenges and opportunities. Aust. J. Soil Res. 39: 1219-1224.

Quirk, J.P. 1971. Chemistry of saline soils and their physical properties. In: T. Talsma and J. R. Philip, editors, Salinity and water use. Macmillan Press, London. p. 79-91.

Quirk, J.P. 2001. The significance of the threshold and turbidity concentrations in relation to sodicity and microstructure. Aust. J. Soil Res. 39: 1185-1217.

Quirk, J.P. and R.K. Schofield. 1955. The effect of electrolyte concentration on soil permeability. J. Soil Sci. 6: 163-178.

Rhoades, J.D. 1982. Reclamation and management of salt-affected soils after drainage. First Annual Western Provincial Conference, Rationalionalization of Water and Soil Research and Management: Soil Salinity. Lethbridge, AB.

Scotter, D.R. 1985. The effect of electrolyte-solutions on the unsaturated hydraulic conductivity of a sodic clay soil. Aust. J. Soil Res. 23: 301-307.

Shackelford, C.D. and D.E. Daniel. 1991. Diffusion in saturated soil. I. Background. J. Geotech. Eng.-ASCE 117: 467-484.

Shainberg, I. and A. Kaiserman. 1969. Kinetics of formation and breakdown of Ca-montmorillonite tactoids. Soil Sci. Soc. Am. Proc. 33: 547-551.

Shainberg, I. and J. Letey. 1984. Response of soils to sodic and saline conditions. Hilgardia 52: 1-57.

Shainberg, I., J.D. Rhoades and R.J. Prather. 1981. Effect of low electrolyte concentration on clay dispersion and hydraulic conductivity of a sodic soil. Soil Sci. Soc. Am. J. 45: 273-277.

Shainberg, I. and M.J. Singer. 2011. Soil response to saline and sodic conditions. In: W. W. Wallender and K. K. Tanji, editors, Agricultural salinity assessment and management, 2nd ed. ASCE Manuals and Reports on Engineering Practice No. 71. ASCE, Reston, VA. p. 139-168.

Shaw, R.J., K.J. Coughlan and L.C. Bell. 1998. Root zone sodicity. In: M. E. Sumner and R. Naidu, editors, Sodic soils: Distribution, properties, management and environmental consequences. Oxford University Press, New York, NY. p. 95-106.

Siyal, A.A., A.G. Siyal and Z.A. Abro. 2002. Modelling of solute transport from a single soil aggregate. J. Appl. Sci. 2: 470-473.

Soil Classification Working Group. 1998. The Canadian system of soil classification, 3rd ed. Agric. and Agri-Food Can. Publ. 1646, NRC Research Press, Ottawa, ON.

Suarez, D.L. 2011. Irrigation water quality assessments. In: W. W. Wallender and K. K. Tanji, editors, Agricultural salinity assessment and management, 2nd ed. ASCE Manuals and Reports on Engineering Practice No. 71. ASCE, Reston, VA. p. 343-370.

Suarez, D.L., J.D. Rhoades, R. Lavado and C.M. Grieve. 1984. Effect of pH on saturated hydraulic conductivity and soil dispersion. Soil Sci. Soc. Am. J. 48: 50-55.

Suarez, D.L., J.D. Wood and S.M. Lesch. 2006. Effect of SAR on water infiltration under a sequential rain-irrigation management system. Agric. Water Manage. 86: 150-164.

3.7 Figures and Tables

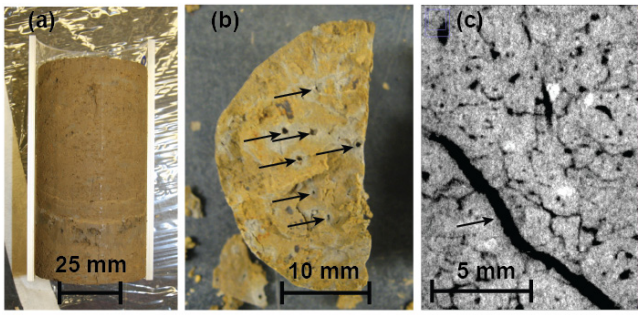

Fig. 3.1. Images of intact silt loam soil: (a) photograph of soil core (vertical profile) prior to adhesion within rigid wall permeameter core holder (b) photograph of relict root holes (indicated by arrows) in horizontal section of soil core, and (c) x-ray computed tomogram of relict root hole (indicated by arrow) and inter-aggregate macropores (black) in vertical cross section.

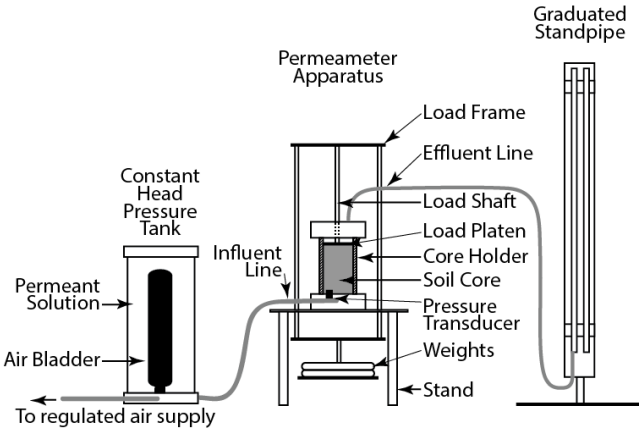

Fig. 3.2. Schematic of rigid wall permeameter apparatus including upstream pressure head influent tank and downstream graduated standpipe.

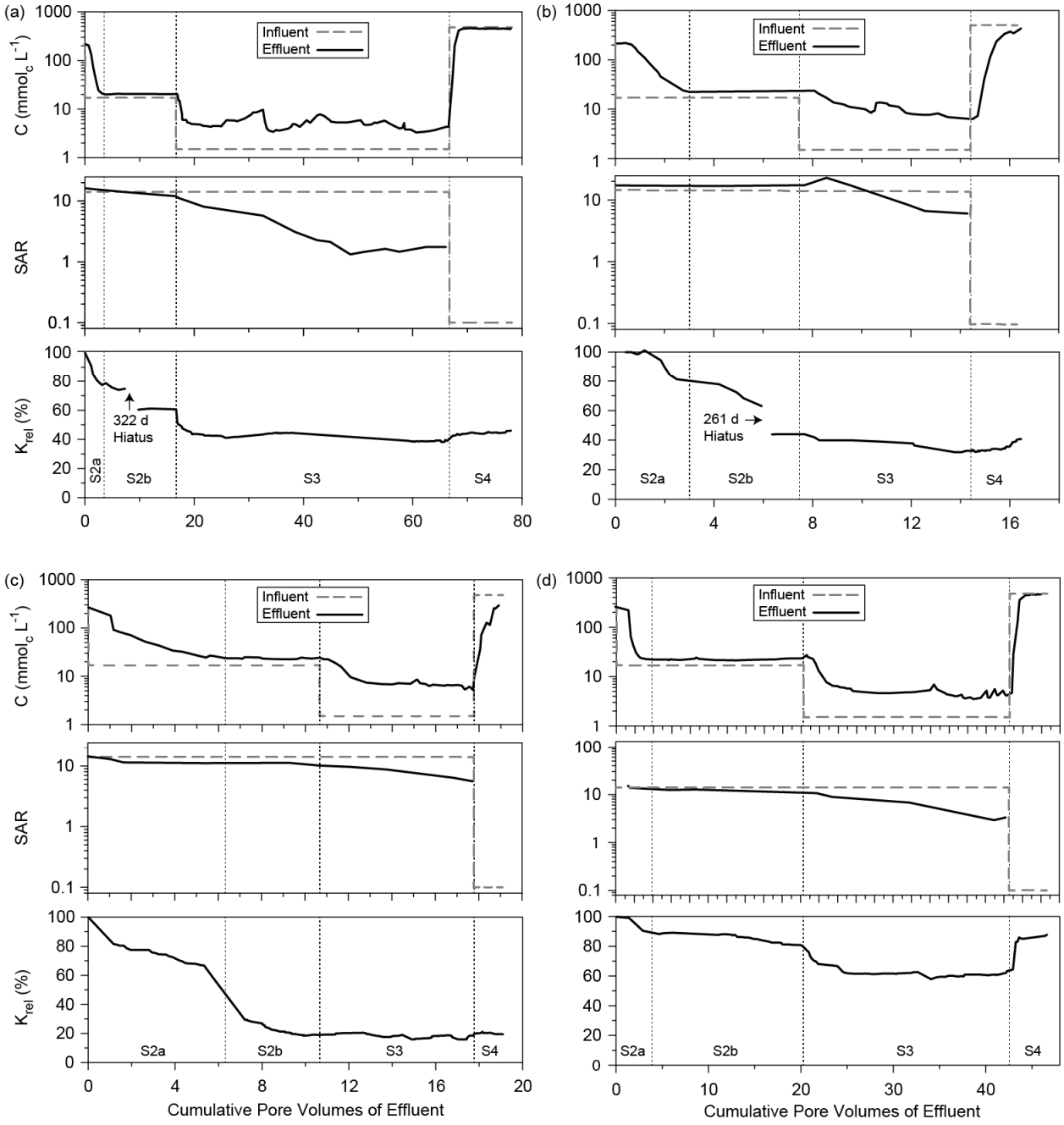

Fig. 3.3. Experiment 1 results: leaching of saline-sodic soil with constant influent sodicity. Permeameter influent and effluent concentrations (C) and sodium adsorption ratio (SAR) and relative hydraulic conductivity (K_{rel}) for four intact soil cores: (a) P1, (b) P2, (c) P3, and (d) P4. Results are shown for the three final stages of permeation (S2–S4), results for the initial equilibration stage (S1) are not included. Sub-stage 2a is the portion of S2 required for stabilization of the effluent C; while S2b is the remainder.

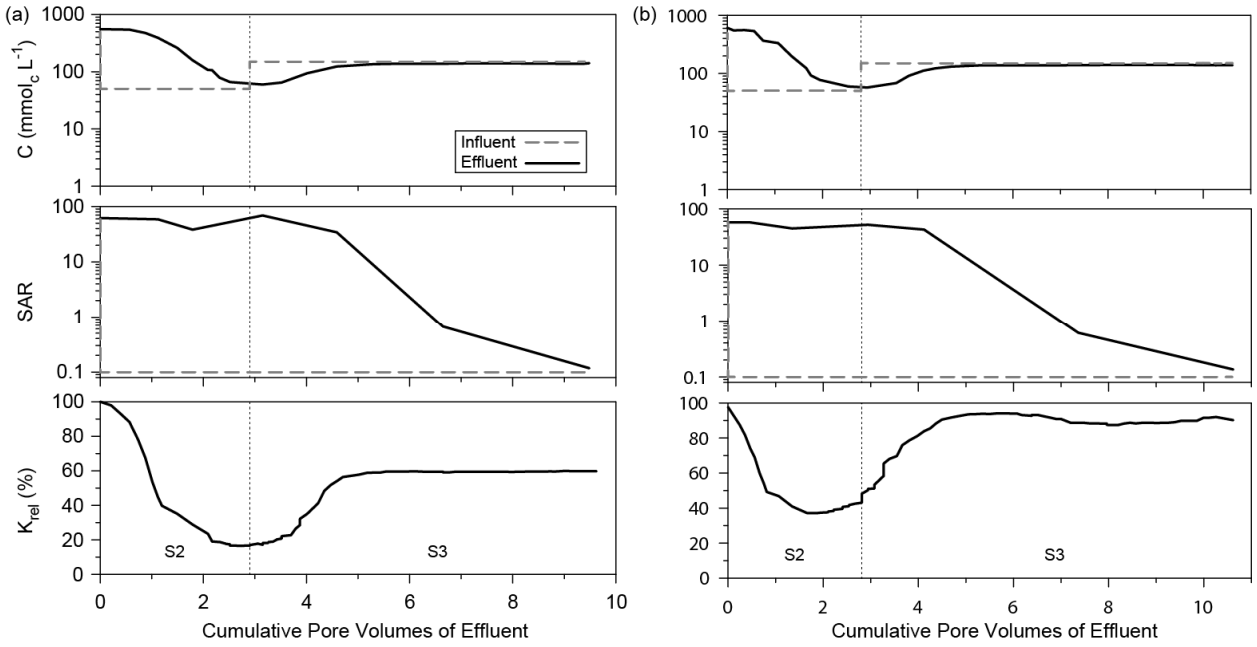

Fig. 3.4. Experiment 2 results: leaching of saline-sodic soil with Ca-amended water. Permeameter influent and effluent concentrations (C) and sodium adsorption ratio (SAR) and relative hydraulic conductivity (K_{rel}) for two intact soil cores: (a) P5, and (b) P6. Results are shown for the two final stages of permeation (S2–S3), results for the initial equilibration stage (S1) are not included.

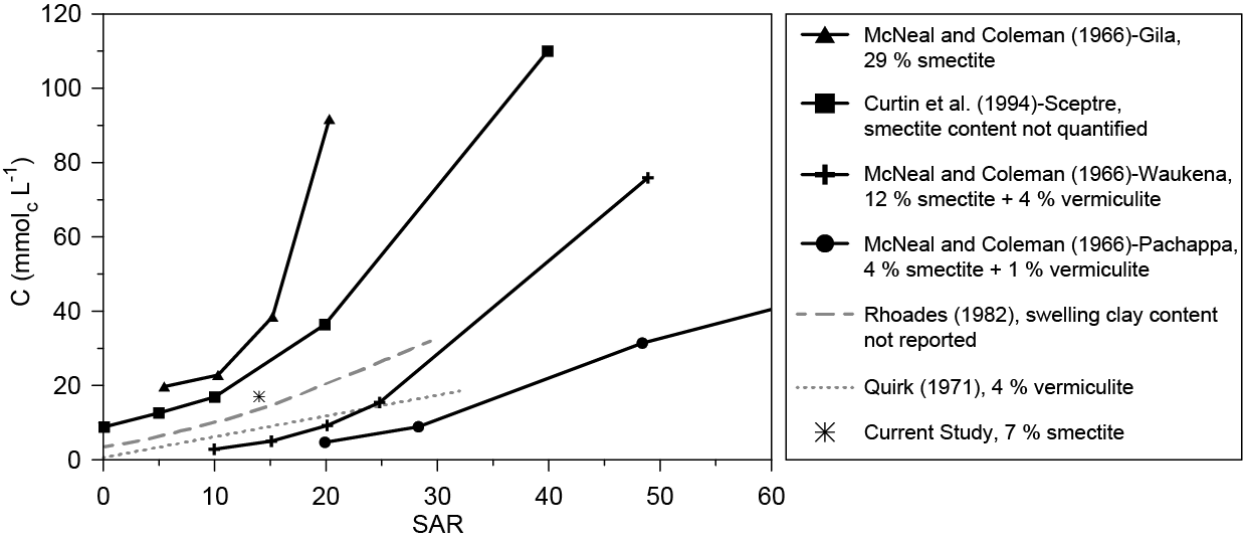

Fig. 3.5. Comparison of experiment 1, stage 2 influent to threshold concentration curves for soils containing varying fractions of swelling clay. The Quirk (1971) curve is reproduced after Quirk (2001), for a decrease in hydraulic conductivity (K) of 10–15 %. The other three authors used a 25 % K decrease. Rhoades (1982) is reproduced after Suarez (2011). For the current study, experiment 1, stage 2, the average K decrease for four intact soil cores was 49 %.

Table 3.1. Select subsoil (0.15–2.4 m depth) properties.

Property	Value
Physical	
Bulk Density, kg m^{-3}	1550
Hydraulic Conductivity†, m s^{-1}	3.5×10^{-9}
Soil texture‡, m^3 m^{-3}	
Sand	0.04
Silt	0.82
Clay	0.14
Chemical	
Soil pH ($CaCl_2$)	7.6
CEC $mmol_c$ kg^{-1}	220
K_G§ $(mmol_c\ L^{-1})^{-1/2}$	0.0125
Mineralogy of Clay Fraction¶, g kg^{-1}	
Smectite	480
Illite	230
Kaolinite	170
Chlorite	50
Quartz	60
Bulk Mineralogy, g kg^{-1}	
$CaCO_3$	39
$CaSO_4 \cdot 2H_20$	0.29

† Laboratory-determined hydraulic conductivity measured on 52 mm diameter soil cores.

‡ Measured by laser diffractometry on a Malvern Mastersizer 2000.

§ Gapon Na-Ca selectivity coefficient.

¶ Determined by X-ray diffraction analysis on <2 μm fraction.

Table 3.2. Summary of end-of-stage results for permeameter experiment 1: leaching of saline-sodic soil with constant influent sodicity.

Permeant Stage	Effluent Chemistry		Hydraulic Conductivity		Stage Duration	
	C†	SAR†	HC_{meas}†	HC_{rel}†	PV†	t†
	$mmol_c\ L^{-1}$	$(mmol_c\ L^{-1})^{1/2}$	$m \times 10^{-9}\ s^{-1}$	%	$m^3\ m^{-3}$	d
Stage 1, Influent C = 230 $mmol_c\ L^{-1}$, SAR = 14						
P1	229	16	6.4	100	6.7	22
P2	226	17	1.6	100	2.5	48
Stage 1, Influent C = 270 $mmol_c\ L^{-1}$, SAR = 14						
P3	268	14	3.1	100	7.7	39
P4	260	15	2.8	100	4.6	37
Stage 2a, Influent C = 17 $mmol_c\ L^{-1}$, SAR = 14						
P1	20	15	4.9	77	3.5	11
P2	22	17	1.3	81	3.0	45
P3	24	11	1.4	48	6.3	40
P4	22	12	2.5	89	3.9	17
Stage 2b, Influent C = 17 $mmol_c\ L^{-1}$, SAR = 14						
P1	20	12	3.9	61	13.2	377‡
P2	24	17	0.70	44	4.7	405‡
P3	24	11	0.59	19	4.4	125
P4	24	11	2.3	81	16.2	138
Stage 3, Influent C = 1.5 $mmol_c\ L^{-1}$, SAR = 14						
P1	4.3	1.7	2.6	40	50.0	394
P2	6.3	6.2	0.52	33	6.7	325
P3	5.2	5.6	0.50	17	7.1	190
P4	4.1	3.3	1.8	63	22.5	192
Stage 4, Influent C = 500 $mmol_c\ L^{-1}$, SAR = 0.1						
P1	456	NM †	2.9	46	11.3	68
P2	434	NM †	0.63	41	2.1	79
P3	296	NM †	0.58	19	1.3	39
P4	464	NM †	2.5	88	4.0	39

† Abbreviations: C, total electrolyte concentration; K_{meas}, measured hydraulic conductivity; K_{rel}, relative hydraulic conductivity; NM, not measured; PV, pore volumes elapsed from the start of each stage; SAR, sodium adsorption ratio; t, time elapsed from the start of each stage.

‡ Elapsed time includes 322 d hiatus from permeation for core P1 and a 261 d hiatus for core P2.

Table 3.3. Summary of end-of-stage results for permeameter experiment 2: leaching of saline-sodic soil with Ca-amended water.

Permeant Stage	Effluent Chemistry		Hydraulic Conductivity		Stage Duration	
	C†	SAR†	K_{meas}†	K_{rel}†	PV†	t†
	$mmol_c\ L^{-1}$	$(mmol_c\ L^{-1})^{1/2}$	$m \times 10^{-9}\ s^{-1}$	%	$m^3\ m^{-3}$	d
Stage 1, Influent C = 520 $mmol_c\ L^{-1}$, SAR = 60						
P5	523	62	3.2	100	10.3	48
P6	518	57	2.3	100	4.9	41
Stage 2, Influent C = 50 $mmol_c\ L^{-1}$, SAR = 0.1						
P5	66	38	0.55	17	2.9	46
P6	60	45‡	0.85‡	37‡	2.8	46
Stage 3, Influent C = 150 $mmol_c\ L^{-1}$, SAR = 0.1						
P5	141	0.11	1.9	59	6.8	73
P6	151	0.14	2.1	90	7.8	70

† Abbreviations: C, total electrolyte concentration; K_{meas}, measured hydraulic conductivity; K_{rel}, relative hydraulic conductivity; PV, pore volumes elapsed from the start of each stage; SAR, sodium adsorption ratio; t, time elapsed from the start of each stage.

‡ Values correspond to the minimum measured during stage 2 and not to the value at the end of the stage.

CHAPTER 4: HYDROLOGIC CONTROLS ON EFFECTIVE SALT LEACHING IN A FINE-GRAINED, MACROPOROUS SOIL WITH IRRIGATION AND TILE DRAINAGE

4.1 Introduction

Sources of salt in soil include: direct deposition from rainfall or irrigation; uptake from shallow groundwater; mineral weathering; and numerous anthropogenic sources (Tanji and Wallender, 2011). Salt-affected soils may require reclamation to improve plant growth, or for industrially related impacts, soil may require remediation to meet regulatory guidelines. Leaching of salts from the rooting zone in conjunction with leachate collection using tile drains is a common method used to reclaim or remediate salt-affected soils (Abrol et al., 1988). In dry climates such as a large portion of the Canadian prairies (CP), rainfall alone is often insufficient to leach salt from the soil profile in a reasonable amount of time. Therefore, the addition of irrigation water is used to accelerate the leaching process (Ayers and Westcot, 1994).

Conventional oil and gas production in the CP produces a variable fraction of saline wastewater. Accidental releases of saline water to the environment often require remediation to meet regulatory guidelines for soil salinity. The motivation for our study is the need to understand hydrologic controls on leaching and salt transport to optimize the design of remedial irrigation programs. Soils developed on fine-grained glacial sediments are typical in the CP region. While most of the salt is stored in the fine-grained soil matrix, most of the flow occurs in macropores. Relatively little research has focused on improving leaching effectiveness in macroporous soils. Of the few existing studies, they have typically been performed on well-aggregated soils. In well-aggregated soils, leaching of salt from soil aggregates is controlled to a large extent by diffusion from the aggregates into the inter-aggregate pore space (Siyal et al., 2002). Leaching efficiency is therefore strongly related to the aggregate size (Armstrong et al., 1998) and the residence time of water within the inter-aggregate pores (Cote et al., 2000). In contrast, the soil under study is weakly aggregated and macroporosity is dominated by vertically continuous structures

such as root holes, wormholes and fractures. Well-aggregated soils tend to have more uniformly distributed preferential flow zones than do weakly aggregated soils (Wuest, 2009). Therefore, water flow and salt transport in a macroporous, weakly-aggregated soil can reasonably be expected to exhibit different leaching behavior than observed in well-aggregated soils. Having a well-connected macropore network with a weakly aggregated matrix is a distinct feature of the soil in our study.

Two criteria are generally used to evaluate leaching effectiveness. The first is leaching efficiency, and the second is the time required to achieve successful soil remediation. Leaching efficiency can be defined as the mass of salt leached from a soil profile per unit volume of water applied (Keren and Miyamoto, 2011). Improved leaching efficiency is not only beneficial in terms of water conservation, but can also result in a reduction of time required to meet a specific soil salinity endpoint (Oster et al., 1972). Both conservation of water and time can result in cost savings for a soil reclamation or remediation project. Variation in leaching efficiency is attributed to differences in soil texture, soil structure, irrigation method, and degree of soil water saturation (van Hoorn and van Alphen, 1994). Fine-textured soils generally exhibit a lower leaching efficiency than do coarser soils, caused by a lower degree of soil water mixing due to preferential flow in fine-grained soils. Leaching efficiency in fine-grained soils is improved by maintaining partially saturated conditions through the use of intermittent ponding or sprinkler irrigation (Miller et al., 1965). This improvement in leaching efficiency is attributed to a disconnection of fast flow paths (larger pores) under slightly unsaturated conditions. Thereby, a greater proportion of infiltrating water passes through the smaller pore spaces of the matrix that contain the majority of the salt mass. When soil water content approaches saturation, macropore flow may be initiated and a large fraction of infiltrating water will bypass the saline soil matrix, resulting in reduced leaching efficiency (Thomas and Phillips, 1979; White, 1985).

The objective of this study is to understand the hydrologic processes that control salt leaching in fine-grained macroporous soil. Irrigation with tile drainage is used in an attempt to improve leaching effectiveness in dry climate conditions. The experiment was conducted on a fine-grained, macroporous soil susceptible to preferential flow. In the following, we present results of two years of field experiments.

The results are then analyzed with respect to flow and transport processes and used to make recommendation for improving irrigation effectiveness.

4.2 Materials and Methods

4.2.1 Study Site

A field study was conducted at a former oil and gas production facility in central Alberta, Canada, approximately 35 km southwest of the city of Edmonton. During petroleum production, a fraction of NaCl brine was co-produced, and accidental release of the brine to the environment resulted in salt-affected soil and shallow groundwater. Facilities associated with oil and gas production were removed from the site by 1976. The areal extent of salt-affected soils is shown in Fig. 4.1a, as a region of elevated apparent electrical conductivity (EC). In 2003, prior to initiation of the current study, a tile drain system was installed within the most highly salt-affected area, approximately 2 ha in size. The tile drain system collects saline leachate and routes it for disposal. Tile drains were installed in an east-west direction spaced 10 m apart at a nominal depth of 2 m. The tile drains were laid within excavated trenches with sidewalls cut at a 45 º angle. The tile drains, composed of slotted, 100 mm diameter, PVC pipe, were buried within a clean gravel pack and backfilled with previously excavated soil.

The land use in the area is primarily agricultural with livestock farming and cereal/legume cropping being dominant. The study site is planted with a mix of forage species, mainly perennial grasses. The regional climate is classified as Continental Humid according to the Köppen Climate Classification. Average daily temperature at the nearby Edmonton International Airport meteorological station for the period 1981–2010 is 15 ºC in summer (Jun.–Aug.) and −11 ºC in winter (Dec.–Feb.) (Environment Canada, 2014a). The average annual precipitation is 446 mm, with 50 % of precipitation falling in summer (Jun.–Aug.), 21 % in spring (Mar.–May), 18 % in fall (Sep.–Nov.), and 11 % in winter (Dec.–Feb.). On average 26 % of the annual precipitation falls as snow. Average annual potential evapotranspiration (PET) for the period 1971–2000 is estimated to be in the range 476–500 mm by the Thornthwaite method (Barker et al., 2011). High average annual PET, in relation to precipitation, limits

leaching under natural precipitation conditions and motivates the use of irrigation to increase leaching rates. A previous modeling study conducted at the same site estimated it would take >100 yrs to leach the salts from the rooting zone under natural precipitation conditions (Smith, 2008).

Soil at the study site is classified as an Orthic Black Chernozem (Navarre series) in the Canadian System of Soil Classification (Soil Classification Working Group, 1998) and is developed on slightly saline glaciolacustrine sediment of silt loam texture (Bowser et al., 1962). The glaciolacustrine layer (B and C horizons) comprising the upper 2.4 m of the soil profile, is shown in cross-section in Fig. 4.2. This layer comprises the plant rooting zone and is the target interval for salt remediation. The glaciolacustrine layer is of silt loam texture, with an average clay-sized (<2 μm) fraction of 14 %. The sand fraction is relatively small, <5 %, with the remainder composed of silt-sized material. The tile drains are located at a nominal depth of 2 m, near the base of the glaciolacustrine silt loam layer. Excavation and backfilling of the tile drains produced a disturbed soil zone above each tile drain. Macropores are present as relict root holes ranging up to 2 mm in diameter within the undisturbed glaciolacustrine material (Fig 4.3a), and additionally as inter-pedal fractures in disturbed soils (Fig. 4.3b). In the disturbed soil zones the dominant soil structure is coarse, angular, weakly prismatic to blocky, and 20–50 mm in size. Within the undisturbed glaciolacustrine material, the dominant structure was micro-blocky, subangular, and 2–4 mm in size. The glaciolacustrine layer overlies a dense glacial till of sandy loam texture. The glacial till material is highly oxidized and fractured near its top (Fig. 4.3c), with degree of oxidation and fracturing decreasing with depth. Fractures were noted within soil core to a depth of at least 5 m. Oxidation halos on the fractures are attributed to downward percolation of oxic water, indicating that the fractures serve as active flow paths (Fig. 4.3d). Two laterally extensive sand lenses are found within the glacial till at nominally depths of 4 and 6 m (Fig. 4.2). Due to the presence of fractures within the glacial till, the uppermost sand lens at 4 m depth is considered to be hydraulically well connected to the glaciolacustrine layer.

4.2.2 Irrigation Experiment

The goal of the irrigation experiment was to improve understanding of the hydrologic controls on salt leaching and to make recommendations for irrigation to maximize the rate of leaching. In August 2008, two test plots, 20 m by 20 m in size, were constructed over an area of elevated salinity in the northwest corner of the site (Fig. 4.1a and 4.1b). In the test plot area, the average EC of soil saturated paste extracts (SPE) was 8.8 dS m^{-1} in the rooting zone (0–2.4 m depth), with a Cl concentration of 1560 mg kg^{-1}. Details of the soil sampling methodology and analysis are given in section 2.2.1. Each test plot was centered over two tile drains and was surrounded with a soil berm to limit runoff and runon. Both test plots were vegetated with a forage grass mix. The purpose of vegetating the test plots was to have a surface cover similar to remainder of the field site. Grass was periodically cut to limit transpiration, both within the test plots and on the remainder of the site.

The irrigation experiment was conducted over two field seasons, with irrigation applied from July–October 2009 in the first year and June–October 2010 in the second year. To simplify comparison of water balance and soil salinity results from the 2009 and 2010 field seasons, the two years are referred to hereafter as Year 1 and Year 2, respectively. Year 1 spanned November 2008 to October 2009, while Year 2 spanned November 2009 to October 2010.

Drip irrigation lines (Model XFD, Rain Bird) were placed on the soil surface at a spacing of 1.2 m. Pressure compensating emitters in the drip irrigation lines were spaced at 0.46 m. The source of irrigation water was the local domestic water supply taken from the nearby North Saskatchewan River, which is of low salinity (EC = 0.3 mS cm^{-1}, Cl = 2 mg L^{-1}) and of low sodicity (SAR = 0.4). Water was stored on site in a 10 m^3 plastic tank, which was refilled every few days. The duration of irrigation and thereby the depth of water applied was set to avoiding contiguous ponding of water on the soil surface. Isolated ponding occurred on small portions of the test plot; however, the duration of ponding was limited to a few hours following the end of irrigation.

4.2.3 Characterization of Soil Hydraulic Conductivity

Both laboratory and field methods were used to characterize soil hydraulic conductivity. Laboratory determination of saturated hydraulic conductivity, $K_{s,}$ was made on 51-mm diameter, 100-mm length intact soil cores collected from the glaciolacustrine layer. Due to the presence of swelling smectite clay and elevated sodicity in these soils, the cores were permeated with an aqueous solution of high salinity, 230–500 $mmol_c\ L^{-1}$. Further details of the permeameter methodology and results are contained in Chapter 3.

Field measurements of in situ, saturated hydraulic conductivity, K_{fs}, were made at depths of 0.2 m and 0.5 m using a Guelph Permeameter (GP). Constant head infiltration tests were conducted in 51 mm diameter boreholes, as per the procedure of Reynolds and Elrick (2002). The tests conducted at 0.2 m depth were performed using a constant head of 0.05 m, while tests conducted at 0.5 m depth used a constant head ranging from 0.1–0.25 m. Higher heads were used in wetter soil conditions to increase the flow rate to enable accurate determination of the volume of water infiltrated. Single-head analysis was conducted using a fixed capillary length factor, α^*, of 0.12 cm^{-1}, typical for structured soils (Soilmoisture Equipment Corp., 2012), and the shape factor for the measurement wells, C, was calculated by the empirical formula of Zhang et al. (1998).

Unsaturated $K_f(\Psi)$ measurements were made on the soil surface using a tension infiltrometer (TI) (20 cm Model, Soil Measurement Systems). Prior to making measurements with the TI, the ground surface was prepared by manually trimming the grass level with the soil surface. Any loose stones or topographic irregularities were trimmed to provide a near level measurement surface. Care was taken not to disturb the soil structure or smear the soil surface. A 3-mm thick layer of nominally 100–200 μm diameter glass beads was used to ensure good hydraulic contact between the TI disc and the soil surface. Infiltration rates were determined by manual reading of the water level in the water reservoir. For each measurement location, infiltration measurements were made for three to five tension settings, ranging

from 0.1–24 cm of H_2O (hereafter soil water tension will be given in units of cm). Tension infiltrometer measurements were made at eight locations within the test plot area. Analysis of the TI measurement data was performed as per the methodology of Reynolds and Elrick (1991).

4.2.4 Soil Moisture Monitoring

High soil water retention in the glaciolacustrine silt loam results in relatively little change in soil moisture content near saturation. Soil water characteristic curves developed for the soil under study is contained in Appendix B. Under regular irrigation, the soil was near saturation for the majority of the irrigation season. To increase measurement resolution under near-saturated conditions, measurement of soil water tension was selected as the method for soil moisture monitoring. Tensiometers were installed at two locations, each at the center of the two test plots at depths of 0.1, 0.3, 0.6, and 1.0 m in the irrigated test plot and at depths of 0.3, 0.6, 1.0 and 1.5 m in the unirrigated control plot. The tensiometers, 0 to 820 cm tension range, (Model Irrolis Sense TX-80-WL, Hortau) were connected via a wireless receiver (Model Irrolis Com WR, Hortau) to a laptop computer. Data was recorded on a 20 min time interval. The tensiometers were removed for the period from late fall to late spring to avoid potential damage caused by frozen ground.

4.2.5 Soil Sampling

To evaluate temporal changes in soil salinity, soil samples were collected at five locations along a north-south transect in each of the two test plots (10 locations total). Sampling locations were located alternately above and between the tile drains, shown in Fig. 4.1b for the irrigated test plot. Soil samples, 0.15–0.20 m in length, were taken from 32 mm diameter soil cores collected using a direct-push drilling rig at the following depths: 0 m, 0.15 m, 0.4 m, 0.9 m, 1.5 m, 1.9 m, 2.4 m, 3.0 m, 4.0 m, 5.0 m, 6.0 m, and 7.0 m. In boreholes located above the tile drains, the maximum depth of drilling was limited to 1.5 m, to protect the drains from drilling damage. Soil samples were sent for saturated paste extract (SPE) analysis at a commercial laboratory (Maxxam) in Calgary, AB. Boreholes were backfilled with hydrated

bentonite granules following the completion of drilling to minimize preferential infiltration. Soil coring locations were re-sampled in October 2008, November 2009, and October 2010. Each subsequent borehole was offset 0.15 m from the previous location to avoid drilling through the bentonite backfill. Saturated paste extracts (SPE) were analyzed for EC, major ion concentrations, and carbonate alkalinity. Electrical conductivity of the SPE was measured by EC electrode. Major ion concentrations (Na, Ca, Mg, K, SO_4) were determined using inductively couple plasma (ICP)-atomic emmission spectroscopy (AES). Chloride was determined by ion chromatography (IC) with EC detection, and carbonate alkalinity was determined by strong acid titration. The average magnitude of the charge balance error for each of the three sampling events did not exceed 3 %. Samples with charge balance error greater than 10 % were culled from the dataset.

4.2.6 Electrical Resistivity Tomography

Electrical resistivity tomography (ERT) was used to quantify soil salinity in the irrigated test plot and to provide greater coverage than that provided by borehole sampling alone. Apparent resistivity measurements were made with a 10-channel DC resistivity system with 72 electrodes (Model SYSCAL Pro, IRIS Instruments). Each survey consisted of 14 parallel north-south lines spaced 2 m apart, with a 1 m electrode spacing for a total line length of 72 m. The ERT surveys were conducted using a dipole-dipole array with a measurement electrode spacing from 1–5 m and a dipole spacing from 1–30 m. The measurement and dipole spacing was chosen to provide high resolution imaging of the rooting zone. The ERT survey lines were centered north-south over the irrigated test plot to maximize the resolution and depth of measurement in that area. Three dimensional resistivity inversion was performed using the RES3DINV code (Loke and Barker, 1996). Data were converted to a standard temperature of 6 ºC, which is equal to the annual average soil temperature at the study site (Hayley et al., 2007). To conduct the temperature normalization, soil temperature was measured using copper-constantan (type-T) thermocouples installed near the center of the irrigated test plot at depths of 0.25 m, 0.5 m, 1 m, 1.5 m, 2.0 m, and 3.0 m. ERT data was corrected to a standard temperature equivalent using the methodology for

time-lapse ERT inversion of Hayley et al. (2010), which was incorporated into a custom version of the RES3DINV code.

The Cl anion was selected as the most suitable parameter for monitoring the progress of remediation. Chloride is the dominant anion in the oilfield brine that is the source of elevated soil salinity at the site. Additionally, natural Cl concentrations in soil samples from the study site are relatively low, below 20 mg kg^{-1} on a dry soil basis. Inverted EC results were transformed to soil Cl concentration using a site-specific relationship, determined through least squares linear regression:

$$Cl_s = 8.83\ EC_b - 553,\ R^2=0.81 \qquad [4.1]$$

where Cl_s is the soil Cl concentration on a dry mass basis (mg kg^{-1}) calculated from the soil saturated paste extract results, and EC_b is the bulk soil EC (mS m^{-1}) resulting from inversion of the ERT apparent resistivity measurements.

ERT surveys were performed in June 2009 and again in June 2010. The timing of the two surveys spans the Year 1 irrigation period, plus the intervening winter prior to the start of irrigation in Year 2. The ERT surveys were scheduled for the late spring, to take advantage of moist soil conditions following melt of the winter snowpack. Moist soil conditions improve soil-electrode contact, and thereby, reduce noise in the apparent resistivity measurements. The difference in timing between soil sample collection in the fall and the ERT surveys in the spring is a source of uncertainty in applying the EC-Cl regression model, Eq. [4.1]. The assumption is made that there was negligible salt redistribution in soil over winter, when the upper portions of the soil profile were frozen, and therefore negligible salt redistribution occurred over the winter period. A third ERT survey scheduled for spring 2011, following Year 2 of the irrigation experiment, was cancelled due to excessive flooding of the study site by meltwater from a large winter snowpack. Time lapse interpretation of the ERT survey data is therefore only performed for Year 1 of the irrigation experiment.

4.2.7 Tile Drain Effluent Monitoring

During construction of the irrigated test plot, the two tile drains passing underneath the plot were disconnected from the site-wide tile drainage system and routed to a dedicated sump for monitoring of flow and effluent chemistry (Fig. 4.1b). Flow from each of the two tile drains was measured using tipping bucket gauges (Model TB1L, Hydrological Services), nominally 0.7 L per tip, and recorded on a 20 min time interval. Samples for salinity analysis were collected from the two tile drains using automated water samplers (Model 6712, Teledyne ISCO) during the period of flow. The sampling interval was every three hours in Year 1 and every six hours in Year 2.

4.2.8 Soil Water Sampling

To monitor temporal variations in pore water salinity in the soil profile, two nests of soil suction lysimeters (Model SW-071, Soil Measurement Systems) were installed in the irrigated test plot in June of Year 2. The suction lysimeters are 50 mm in diameter with a porous stainless steel sampling interval, 100 mm in length. The samplers were installed at four depths, spanning 0.15–0.90 m, in two locations within the irrigated test plot: above the north tile drain; and, between the two tile drains (Fig. 4.1b). For sampling, a partial vacuum of approximately 500–600 cm was applied to the lysimeters with a hand pump. Due to the relatively low hydraulic conductivity of the soil, leachate was allowed to collect overnight before sampling. The suction lysimeters were sampled monthly during the irrigation period in Year 2. Therefore, soil water salinity data is available only for Year 2 of the irrigation experiment.

4.2.9 Shallow Groundwater Sampling and Water Level Measurement

Shallow PVC wells, 25 and 51 mm diameter, were installed to measure groundwater elevation and salinity within and surrounding the irrigated test plot (Fig. 4.1b). In Year 1, eight monitoring wells were installed within the drained glaciolacustrine layer. Well depth was 2.5 m in locations adjacent to tile drains and 2 m for wells distal to the tile drains. Monitoring wells were screened over the bottom 0.5 m . In Year 2, 13 additional wells were installed in six locations to monitor groundwater chemistry and water

levels in the two sand lenses interlayered with the glacial till at nominal depths of 4 and 6 m. Groundwater levels for the three nominal monitoring depths of 2, 4, and 6 m were measured using pressure transducers (Model Levelogger Gold, Solinst; or Model Level Troll 500, InSitu). Water levels were recorded at a 20 min time interval. Barometric compensation for the unvented Levelogger pressure transducers was calculated using using data from an on-site barometer (Model Barologger Gold, Solinst).

4.2.10 Water Chemistry

Chloride concentration was used as the principal parameter for monitoring soil water and tile drain effluent salinity. A strong relationship between water sample EC and Cl concentration motivated use of EC as a surrogate for Cl concentration. Chemical analyses on select water samples from the tile drains and suction lysimeters was used to build an EC-Cl relationship. Electrical conductivity of the water samples was measured by EC electrode. Major ion concentrations (Na, Ca, Mg, K, Cl, SO_4) were determined using IC with EC detection, and carbonate alkalinity was determined by strong acid titration. The average magnitude of the charge balance error on individual sample results was 3 %. Samples with charge balance error greater than 10 % were culled from the dataset. The following relationship between EC and Cl concentration in the water samples was developed using least squares linear regression:

$$Cl_w = 392EC_w - 923,\ R^2 = 0.98 \qquad [4.2]$$

Where Cl_w is the Cl concentration in the water sample (mg L^{-1}), and EC_w is the EC of the water sample (mS cm^{-1}). The formula given in Eq. [4.2] was used to calculate Cl concentration in tile drain effluent and suction lysimeter samples reported in the results section.

4.2.11 Monitoring of Meteorological Parameters

To calculate water balance components within the irrigated test plot, precipitation and meteorological parameters related to evapotranspiration were recorded at the site during the irrigation

season. Rainfall, wind speed at 2 m height, air temperature, and relative humidity were measured using a compact meteorological station (Model Watchdog 2900ET, Spectrum Technologies). Additional parameters were measured in the irrigated test plot to calculate the reference evapotranspiration (ET_0) including: net solar radiation by radiometer (Model NR-Lite, Kipp & Zonen); ground surface temperature by infrared radiometer (Model SI-111, Apogee Intruments); and, ground heat flux by heat flux plate (Model HFT3, Radiation Energy Balance Systems) with shallow soil heat storage determined using a four point averaging thermocouple (Model TCAV-L, Campbell Scientific). Meteorological parameters were recorded on a 15–20 min time interval.

Daily ET_0 was estimated using the FAO Penman-Monteith method for a reference surface of well watered grass, 0.12 m in height, and fully shading the ground (Allen et al., 1998). The dual crop coefficient approach of the FAO method was used to calculate separate soil surface evaporation (E) and plant transpiration (T). The calculation of E includes time-variable soil surface wetness, which was maintained relatively wet throughout the irrigation season. The calculation of T includes variation in transpiration with plant growth by applying empirical crop coefficients for each growth stage. Crop coefficients for pasture were used, which varied from 0.3 at the start of the growing season to 0.8 in the mid and late growing season.

4.3 Results

4.3.1 Characterization of Soil Hydraulic Conductivity

Saturated hydraulic conductivity was determined for six intact soil cores collected from the glaciolacustrine layer, 0.7 to 1.6-m depth The arithmetic mean K_s for the six cores is 3.5×10^{-9} m s^{-1} (0.30 mm d^{-1}). Details of K_s determination are given in section 3.3.2. Hydraulic conductivity determined from GP infiltration tests were two to three orders of magnitude higher than the K_s determined on the soil cores. The geometric mean K_{fs} determined from 57 GP measurements at a depth of 0.15–0.2 m is 3.1×10^{-6} m s^{-1} (270 mm d^{-1}). For 18 GP measurements made deeper in the soil profile, at 0.5 m depth, the geometric mean K_{fs} is 4.3×10^{-7} m s^{-1} (37 mm d^{-1}). The relatively small volume of the 51 mm diameter

soil cores and their relatively low hydraulic conductivity suggests that the K_s of the soil cores is representative of the fine-grained soil matrix. The larger sample volume and large number of measurements made in the field using the GP increases the likelihood that any individual measurement will include macropores in its sample volume. High K_{fs}, in relation to K_s, is therefore attributed to the influence of macropore flow on the field GP measurements. The results of the saturated hydraulic conductivity testing highlight the important role that macropores play in conducting water through the soil under study.

Unsaturated hydraulic conductivity determined from TI measurements is useful for characterizing the hydraulic properties of surface soil. Results for $K(\Psi)$ exhibit a log-linear relationship, shown in Fig. 4.4. Over the range of applied tension, measured hydraulic conductivity ranges from $K(0.4) = 3.4 \times 10^{-6}$ m s^{-1} (290 mm d^{-1}) to $K(24.3) = 1.9 \times 10^{-8}$ m s^{-1} (1.6 mm d^{-1}). At low tension, the $K(\Psi)$ measurements agree well with the mean $K_{fs} = 3.1 \times 10^{-6}$ m s^{-1} (270 mm d^{-1}) measured in shallow soil, 0.15–0.2 m depth, with the GP tests. The large increase in hydraulic conductivity as soil approaches saturation is indicative of the initiation of macropore flow.

4.3.2 Water Applied to the Irrigated Test Plot

Irrigation was used in an attempt to increase the salt leaching rate beyond that under natural precipitation conditions. Irrigation was applied such that a similar total depth of water (irrigation + rainfall) was applied in both years of the experiment. Total annual precipitation was 268 mm in Year 1 and 515 mm in Year 2. This is a 92 % increase in precipitation between Years 1 and 2. For comparison, the 30-year (1981-2010) average annual precipitation for the nearby Edmonton International Airport meteorological station is 446 mm. The majority of the difference in total precipitation between the two years occurred from April to September, when totals for the period were 160 mm for Year 1 and 443 mm for Year 2. Monthly precipitation totals are given in Table 4.1.

A relatively large portion of applied water evaporated from the soil surface or was transpired by the grass cover. Calculation of the water balance for the irrigated test plot gives insight into the fate of the

applied water. Irrigation and rainfall were inputs to the irrigated test plot, while evapotranspiration, tile drainage, and deep drainage that bypassed the tile drains represent outputs from the system. Soil profile wet-up at the start of the irrigation season is assigned to soil water storage. Following the initial wet up, soil water storage is assumed to be in dynamic equilibrium for the duration of the monitoring period (i.e., negligible change in long term average soil water storage occurred). Water balance components were calculated for a duration starting from the first irrigation event to the final tile drain outflow, for each of the two years of the irrigation experiment, shown in Table 4.2. For Year 1, the water balance was calculated for the period from 7 July–2 Nov. (119 d), and for Year 2 from 2 June–19 Oct. (140 d). Water balance components are reported as equivalent depths of water, applied to or removed from the irrigated test plot.

During the water balance period in Year 1, 607 mm of irrigation was applied plus 115 mm of rainfall for total water applied of 722 mm. As calculated using the FAO dual crop coefficient method, evaporation from the soil surface was 134 mm and transpiration by the grass cover was 218 mm for a total ET of 352 mm. The fraction of applied water lost to ET in year 1 was 0.49, or half of the water applied. The resulting net applied water was 370 mm, calculated as the difference between total water applied and total ET. This is the amount of water that is available to drain through the soil profile, prior to accounting for changes in soil water storage. During the monitoring period in Year 2, 379 mm of irrigation was applied with 305 mm of rainfall for total water applied of 684 mm. Evaporation from the soil surface was calculated to be 114 mm and transpiration by the grass cover was 239 mm for a total ET of 353 mm giving net applied water of 331 mm. The amounts of total water applied, total ET and net applied water were very similar between Years 1 and 2 of the experiment. The difference in net applied water between the two years was within 11 % of the two-year average.

4.3.3 Salt Leaching in Irrigated and Unirrigated Test Plots

Time-lapse analysis of salt concentrations is used to interpret salt leaching effectiveness. Soil Cl concentrations within the test plot area were calculated from ERT survey results using Eq. [4.1]. Soil Cl

concentration at the start of Year 1 is shown in Fig. 4.5a. The total Cl mass within the irrigated test plot, to a depth of 2.4 m, at the start of Year 1 was calculated to be 2800 kg +/− 4 % (Head, 2013). However, as noted by Hayley et al. (2009) in their interpretation of inverted ERT images of soil salinity distribution, smoothing of high and low concentrations is an issue and direct interpretation of inverted ERT results should be made with caution.

Soil Cl concentrations in the vicinity of the irrigated test plot show a relatively high degree of spatial variability; therefore, the concentrations at the end of Year 1, C, are normalized by the concentration at the start of the year, C_0. This normalization highlights relative changes in Cl concentration. Normalized concentration, C/C_0 values, for each electrode location is shown in Fig. 4.5b. Appreciable Cl leaching within the irrigated test plot is shown as C/C_0 values < 1 (blue). No change in concentration results in C/C_0 values of 1 (green), and increases concentration results in C/C_0 values > 1 (yellow to red). In the shallowest depth interval within the test plot, 0–0.35 m, C/C_0 values show a high degree of variability, but generally indicate decreased concentration within the bounds of the irrigated test plot. The next four depth intervals, spanning 0.35–2.4 m, show a pattern of greater decrease in Cl concentration in the southern half of the plot and adjacent to the northern boundary. The largest Cl concentration decrease occurred in the interval 0.35–0.76 m. In general, the ERT results indicate less salt leaching occurred between the tile drains. Within the irrigated test plot, from the ERT results the residual Cl mass at the end of Year 1 to 2.4 m depth was calculated to be 1900 kg +/− 5 % (Head, 2013). The ERT results yield a decrease in mass of 25 % for Year 1 of the irrigation experiment.

The general decrease in soil Cl concentrations within the irrigated test plot is consistent with the soil sample SPE results collected across the plot in Year 1. When averaged over the five borehole locations along the north-south transect (Fig. 4.1b), soil Cl concentrations in soil samples decreased throughout the glaciolacustrine layer during Year 1 (Fig. 4.6a). The C/C_0 values ranged from 0.12 at 0.23 m depth to 0.66 at 0.08 m depth. The depth-averaged Cl concentration in the irrigated test plot at the start of Year 1 was 1930 mg kg^{-1} for the upper 2 m of the soil profile. At the end of Year 1, the depth-averaged Cl concentration decreased to 1120 mg kg^{-1}, a 42 % decrease (p-value = 0.010 by paired t-test).

Outside of the irrigated test plot, ERT results for C/C_0 show negligible leaching occurred over the majority of the unirrigated area, except for local decreases in the northwest and northeast corners (Fig. 4.5b). Within the upper two depth intervals, red areas indicating increases in Cl concentration may be artifacts associated with lower soil moisture content outside of the irrigated test plot and should be interpreted with caution. Consistent with the ERT survey results, soil sample results from the unirrigated test plot show negligible leaching occurred during Year 1 (Fig. 4.6b). Chloride concentrations show minor increases from the start of the year at four of the six sample depths; however, none of the increases are statistically significant ($p > 0.1$). The observation of negligible leaching within the unirrigated test plot is consistent with our hypothesis that during dry years, substantive salt leaching is unlikely to occur under natural precipitation conditions.

In Year 2, an ERT survey was not performed due to unfavorably wet site conditions (see Methods and Materials section). Monitoring of Cl concentrations included both soil sampling and soil water sampling. Within the irrigated test plot, soil chloride concentrations did not decrease appreciably following the irrigation period. Relative Cl concentration (C/C_0) show little change in the Year 2 sample results from that measured in Year 1 (Fig. 4.6a). There is a slight increase in concentrations at 0.075-, 0.225- and 1.0-m depth, although not statistically significant ($p > 0.1$). The depth-averaged Cl concentration at the start of Year 2 was 1120 mg kg^{-1} for the upper 2 m of the soil profile. At the end of Year 2, the depth-averaged Cl concentration was relatively unchanged at 1250 mg kg^{-1} (p-value = 0.13 by paired t-test). Soil water samples were collected from suction lysimeter nests located above the northern tile drain and between the tile drains in the irrigated test plot (Fig. 4.1b). The maximum depth of the installed soil suction lysimeters was 1.5 m. Two monitoring wells adjacent to the suction lysimeter nests were also sampled, extending the depth of monitoring to 2 m at the location adjacent to the northern tile drain and to 1.8 m bgs at the location between the drains. Chloride concentrations from both nests of lysimeters, included in Fig. 4.7, show a distinct absence of leaching during the irrigation season. For the lysimeter nest located above the northern tile drain, Cl concentrations show an increase from July–Oct. at depths 0.56, 0.72 and 1.46 m (Fig. 4.7a). The cause of the increase in Cl concentrations above the

northern tile drain is not readily evident from the data available. The increase in soil water Cl concentration coincides with a contemporaneous increase in soil sample Cl concentration at the same location (data not shown). Therefore, it is assumed that the observed increase is a result of local, lateral redistribution of Cl mass. The lack of leaching evident in the soil water sample results confirms the same observation made on soil sample results.

Chloride concentrations in soil samples collected within the unirrigated test plot decreased in Year 2 (Fig. 4.6b). Relative Cl values, C/C_0, at depths 0.075–2.0 m ranged from 0.58–0.97. The observation of leaching in the unirrigated test plot in Year 2 demonstrates that leaching can be achieved under natural precipitation during a wetter than average year; however, the degree of leaching achieved was more modest than that achieved in Year 1 using irrigation.

In contrast, observation of negligible leaching within the irrigated test plot during Year 2 is inconsistent with improved leaching through application of irrigation water (331 mm net applied water). To support discussion into the cause of the poor leaching observed during Year 2 of the irrigation experiment, details of the hydrologic response within the irrigated test plot are presented.

4.3.4 Hydrologic Conditions within the Irrigated Test Plot

Measured irrigation, rainfall and calculated ET are shown daily for the irrigation periods in Years 1 and 2 in Fig. 4.8a. Soil moisture conditions within the irrigated test plot were monitored using soil water tension measurements. In Year 1, soil water tension measured at 1.0-m and 0.1-m (installed later on 23 July) depths is presented in Fig. 4.8b. Soil water tension at 0.1 m depth fluctuated between zero and a maximum of 125 cm between water applications. During the period from 23 July–16 Sep., the near surface soil (0.1 m depth) was saturated for 5 % of the time, with an average soil water tension of 29 cm. After 16 Sep., the tensiometer signal quality declined, resulting in lower measurement resolution. Therefore, the calculation of the duration of saturated conditions was limited to prior to that date. Following initial wet up of the soil profile, soil at 0.3- and 0.6-m depth was saturated 99 % and 98 % of the time, respectively (data not shown). At the 1.0-m monitoring depth (Fig. 4.8b), soil water tension

showed similar cycles of wetting and drying as at the 0.1-m depth, but of lower magnitude, ranging from zero to 42.8 cm. Outside the irrigated test plot, soil moisture conditions were dry due to low rainfall. During the monitoring period soil water tension at the two shallowest monitoring depths, 0.3 and 0.6 m, was > 820 cm, the tension limit of the tensiometers used. At 1.0 m depth, soil water tension increased from 29 cm in late May to 785 cm by mid-September, before declining to 530 cm by mid-October.

In Year 2, within the irrigated test plot, the proportion of time during the irrigation period that the soil matrix was saturated at 0.1 m depth was greater than in Year 1. For the period in Year 2 with recorded data, soil at 0.1 m had an average of soil water tension of 10 cm and was fully saturated 61 % of the time. After the large rainfall event on 22 June, soil at 0.1 m depth soil water tension was zero on average, and the proportion of time under saturated conditions increased to 70 %. Outside the irrigated test plot, the soil moisture conditions were wetter in Year 2 than in Year 1. Soil water tension at 0.3-m depth was zero from early June until late Aug., while at 0.6-m depth, soil water tension was initially 100–150 cm, but became saturated during the heavy rainfall in mid-July and remained saturated until mid-Sep.

From the soil water tension and water table elevation results, it is clear that the irrigated test plot was wetter in Year 2 than in Year 1. Water balance results give additional insight into the fate of drainage water and the source of salt collected in the tile drains. In Year 1, prior to the start of irrigation, soil water tension reflected relatively dry soil conditions. A large rainfall event of 35 mm later on 7 July followed by two irrigation events of 25 mm each on 9 and 10 July resulted in saturation of the soil profile. Therefore, 85 mm of water is attributed to soil water storage required to wet up the soil at the start of the Year 1 (Table 4.2). Tile drain flow from the irrigated test plot is shown for the south tile drain in Fig. 4.8d. Flow was similar in the north tile drain (data not shown). Peak flow rate reached 14 L hr^{-1} in the south tile drain, with an average flow rate of 5.3 L hr^{-1} for both tile drains combined. From a net applied water of 370 mm (calculated previously), 85 mm of water entering soil water storage, and 36 mm of water collected in the tile drains, 249 mm of water is assigned to deep drainage. Deep drainage represents the net amount of water that is bypassing the tile drains and draining to depth. Therefore 87 % of the total drainage water became deep drainage and 13 % was collected in the tile drains.

Based on the relatively wet month of May in Year 2 (Table 4.1), it was assumed that the soil was relatively close to saturation at the start of irrigation. Therefore, a negligible amount of water entered soil water storage at the start of the irrigation period. The maximum flow rate in the north and south tile was 70 and 200 L hr^{-1} (Fig. 4.8d), respectively, with an average flow rate for both tiles of 19 L hr^{-1}. For comparison, the average flow rate in Year 2 was almost four times that in Year 1. Total tile drainage in Year 2 of 334 mm is approximately 10-fold of that in Year 1. Given a net applied water of 331 mm, the tile drainage is approximately equal, resulting in negligible calculated deep drainage (Table 4.2). It is important to note that the calculated value for deep drainage is net of downward drainage and upward seepage across the test plot (perpendicular to the tile drains). To gain further insight into variation in drainage across the plot, vertical hydraulic gradients beneath the plot are discussed below.

4.3.5 Drainage Conditions under the Irrigated Test Plot

Drainage above the water table is assumed to be dominantly vertical. When drainage water reaches the water table, vertical and lateral hydraulic gradients control the flow to either the tile drains or to deep drainage. In a soil profile where the tile-drained layer overlies a practically impermeable material, the flow to the drains can be assumed to be quasi-horizontal from the centerline between drains. In contrast, the fractured nature of the glacial till underlying the tile-drained glaciolacustrine layer (Fig. 4.1c and 4.1d) results in deeper flow paths than would be expected, if the glacial till had been unfractured. This deep flow below the tile-drained layer includes both deep drainage and upward seepage depending on the direction of vertical hydraulic gradients, which can vary both temporally and spatially.

In Year 1, due to relatively low precipitation two years in a row, the regional water table was not present within the glaciolacustrine layer across the site except in the region of the irrigated test plot. Groundwater levels measured in the uppermost sand lens below the tile-drained layer ranged from 2.8 m below ground surface (bgs) on 21 May to 3.4 m bgs on 24 Sep. Upon application of irrigation to the test plot, a water table was formed within the glaciolacustrine layer. Between the tile drains the water table reached a peak of 0.9 m bgs, 6 d after the onset of irrigation, shown in Fig. 4.8c. At the tile drain

locations, the water table was maintained at a level near that of the tile drains, at 2.0 m depth (data not shown). The water table within the irrigated test plot remained elevated relative to natural conditions for the duration of the irrigation period, at an average depth of 1.7 m bgs. Groundwater levels measured in monitoring wells in late-May in Year 1 are shown in cross-section in Fig. 4.9a. The difference in hydraulic head between the tile-drained glaciolacustrine layer and the uppermost sand lens resulted in downward flow across the entire test plot. Consequently, in Year 1, the flow regime was dominantly one of deep drainage.

Due to the increase in precipitation from 268 mm in Year 1 to 516 mm in Year 2 (Table 4.1), the regional water table rose in response as did the hydraulic head in the sand lenses below the irrigated test plot. This resulted in a change in the drainage regime within the plot. The groundwater level within the uppermost sand lens rose from 2.6 m bgs at the start of June to 0.9 m bgs by late July. Following the peak, the water level decreased gradually to 1.8 m bgs by late October.

Within the irrigated test plot, the water table rose in response to irrigation. In Year 2, the average water table depth was 1.1 m bgs between 2 June and 19 Oct. (Fig. 4.8c). This compares to an average water table depth in Year 1 of 1.8 m bgs between 15 July and 2 Nov. Not only was the water table higher on average in the irrigated test plot in Year 2 than in Year 1, but it also maintained a more stable level. Groundwater levels measured in monitoring wells in late-July in Year 2 are shown in cross-section in Fig. 4.9b. In Year 2, the higher hydraulic head in the sand lens below the irrigated test plot resulted in a lower downward hydraulic gradient between the tile drains, as compared to Year 1. At the tile drain locations, upward seepage was induced from below, shown schematically in Fig. 4.9b.

The higher hydraulic head in the sand lens beneath the test plot, coupled with similar water application in Year 2, resulted in wetter conditions even though the daily average drainage rate was similar during both years. The drainage rate is calculated as the total tile of tile drainage and net deep drainage given in Table 4.2, divided by the duration of the water balance period. In Year 1, total drainage was 285 mm over a period of 119 d, which results in an average drainage rate of 2.4 mm d^{-1}. In Year 2, total drainage was 331 mm over a duration of 140 d, which results in an average drainage rate of 2.4 mm

d^{-1}, identical to that in Year 1. In Year 2, the higher water table between tile drains in the irrigated test plot is a response to higher head in the sand lens below. The rise in the water table in the irrigated plot in Year 2 resulted in a similar net drainage rate as compared to Year 1. Therefore the cause of wetter soil moisture conditions in the irrigated test plot in Year 2 is attributed to the higher regional water table.

4.3.6 Irrigated Test Plot Tile Drain Effluent Concentrations

In Year 1, the vertical hydraulic gradient below the tile drains results in downward vertical flow (Fig. 4.9a). Therefore tile drain effluent concentrations are a good measure of the salinity of the water leaching downwards through the soil column from above. During Year 1, the tile drain effluent Cl concentration was relatively stable through the monitoring period, ranging 5040–6630 mg L^{-1}, with an average of 5800 mg L^{-1} in the south tile drain (Fig. 4.8e). Concentrations in the north tile drain were similar (data not shown). The total mass of Cl removed by the tile drains during Year 1 was 83 kg, which represents 9 % of the 900 kg calculated to have leached from upper 2.4 m of the soil profile based on the ERT results given in section 4.3.3. In comparison 13 % of total drainage water was collected in the tile drains. Given spatial variability in the initial soil Cl distribution (Fig 4.5a), the mass of chloride collected appears reasonable.

In Year 2, the vertical hydraulic gradient below the tile drains reversed resulting in upward seepage into the tile drains. Due to upward seepage, Cl in the tile drain effluent (Fig. 4.8e) is at least partially sourced from below the tile drains. For comparison, the chloride concentration in the sand lens below the tile-drained layer is relatively high, with an average concentration of 8770 mg L^{-1}. In addition to the evidence for upward seepage into the tile drains, both soil sample and soil water sample Cl concentrations (Fig. 4.6a and Fig. 4.7, respectively) show that negligible leaching occurred within 0–2.0 m depth interval during Year 2. The tile drain effluent concentration ranged 2260–7130 mg L^{-1} for the south tile drain, with a total chloride mass removed by both tile drains of 340 kg. We can reasonably conclude that the salt within the tile drain effluent in Year 2 was sourced from below the tile drains. This demonstrates the

source depth for salinity in tile drain effluent cannot be reliably interpreted without corresponding local hydraulic gradient information.

4.4 Discussion

Under drier than average precipitation conditions, such as occurred during Year 1 of the irrigation experiment, results from the unirrigated test plot confirm that negligible leaching can be expected. Addition of irrigation improves the rate of salt leaching resulting in mass removal ranging from 38-46 % of the initial mass based on soil sampling and ERT survey results, respectively. Under wetter than average precipitation conditions in Year 2, leaching within the unirrigated test plot was appreciable, but it was substantially less than that achieved the previous year under irrigation (Fig. 4.6a and 4.6b). The negligible leaching observed within the irrigated test plot in Year 2 stands out as anomalous. A similar amount of net water was applied as in the previous year, when substantial leaching occurred. The net water balance was similar between years, but the difference in soil moisture condition may provide a possible explanation.

The concept of leaching efficiency provides a useful metric with which to evaluate our leaching results relative to others. Leaching efficiency was previously defined as the mass of salt removed per unit volume of water applied. To enable comparison between soils of differing initial salt mass, a normalized method of defining leaching efficiency is adopted here, after Hoffman (1980) as reported in Keren and Miyamoto (2011), termed salt transport efficiency. The salt transport efficiency coefficient is given as:

$$k = \frac{C}{C_0}\frac{D_{\mathrm{W}}}{D_{\mathrm{S}}} \qquad [4.3]$$

Where C_0 and C are as defined previously (mg L^{-1}), D_s is the depth of soil leached (m), and D_w is the depth of water applied (m). A larger decrease in salt concentration for a given amount of water applied results in a lower k coefficient. Likewise, a lower amount of water required to leach a depth of

soil to a given concentration results in a lower k coefficient. Therefore, a lower k coefficient corresponds to higher leaching efficiency.

Within the irrigated test plot, at the end of Year 1, the average soil Cl concentration in the irrigated test plot decreased through the depth of the rooting zone (Fig. 4.8a). From soil sample results reported in section 4.3.3, the 0-2.0 m depth-weighted average chloride concentration at the start of Year 1 was 1930 mg kg^{-1} and at the end was 1120 mg kg^{-1}, resulting in a C/C_0 of 0.58. For the water balance period in Year 1, 607 mm of irrigation water was applied, in addition to 115 mm of rainfall for a total of 722 mm of water applied (Table 4.2). As per other authors, ET was subtracted from the amount of water added to provide a net water applied of 370 mm for the water balance period (Table 4.2). The depth of the soil profile, Ds, was taken to be 2.0 m, which results in a D_w/D_s of 0.185. The resulting k coefficient calculated using Eq. [4.3] is 0.11. In a study on the effects of different methods of water application on leaching efficiency, Oster et al. (1972) reported C/C_0 and D_w/D_s results for leaching of a silty clay soil using intermittent ponding. For a D_w/D_s ratio of 0.3 and a profile depth of 0.9 m, their calculated k value was 0.18. Keren and Miyamoto (2011) using the results of Hoffman (1980) report a k value of 0.1 as being representative of a variety of soil textures from silty clay to sand under intermittent ponding or sprinkler irrigation. The level of leaching efficiency attained in year 1 in the irrigated test plot (k = 0.13) is therefore comparable to what others have reported for efficient leaching. However, under continuously ponded irrigation of a clayey soil, Keren and Miyamoto (2011) give a higher k value of 0.3 (i.e., lower leaching efficiency). Therefore, there is some precedence for lower leaching efficiency under wetter soil conditions as would be induced under continuously ponded irrigation.

A parallel investigation conducted at our study site showed rapid breakthrough of surface applied 2,6-Difluorobenzoic acid tracer to the tile drains after 2 d (Bishop, 2012). Additionally, tracer was detected in wells screened within the sand lenses at 4 and 6 m depth, after a few weeks. Rapid breakthrough of surface applied tracers to depth is interpreted as being indicative of preferential flow in macropores (Kladivko et al., 1991; Kohne and Gerke, 2005). Given the low matrix hydraulic conductivity measured on soil cores from our study site of 3.5×10^{-9} m s^{-1} (0.30 mm d^{-1}), the relatively

rapid breakthrough observed is considered indicative of preferential flow and transport, likely along vertical macropores.

Conceptually, drainage water can be separated into fractions of fresh inflow from the soil surface and water sourced from within the soil matrix, which in our case is saline. In addition to rapid breakthrough, preferential flow in macropores can result in varying proportions of flow that bypasses the soil matrix during drainage to depth. Stone and Wilson (2006) studied preferential flow and transport to tile drains using a Cl tracer. For two rainfall events, the direct infiltration through macropores ranged from 11-51 % of total storm flow and 40-81 % of peak flow. The range in proportion of direct macropore flow was attributed to varying rainfall intensity between the two storm events. A lower degree of macropore flow was associated with lower intensity rainfall. In another study, Klaus et al. (2013) calculated the proportion of tile drain flow attributed to direct infiltration through macropores using Br as a tracer. The peak contributions for two sprinkler-applied irrigation events were relatively similar at 19.5 % and 18 %, even though antecedent soil moisture conditions were much wetter for the first of their two experiments. Therefore a range of direct macropore infiltration from surface can result in varying degrees of bypass of the saline soil matrix. We hypothesize that this is the mechanism that produced low leaching efficiency in Year 2. Excessively wet soil conditions should be avoided during leaching of fine-grained macroporous soils in order to improve salt leaching efficiency. Control of soil moisture conditions through soil moisture monitoring and triggered irrigation is the subject of a subsequent manuscript.

4.5 Conclusion

Leaching of salt-affected, fine-grained macroporous soil is complicated by the low hydraulic conductivity of the soil matrix. Results of our plot-scale irrigation experiment demonstrate that efficient leaching is possible in fine-grained, macroporous soil, if water application is appropriate for the soil moisture conditions. Excessive water application and/or poor drainage can result in excessively wet soil moisture conditions that promote preferential flow in macropores. Direct infiltration through macropores may result in inefficient leaching of the soil matrix. Avoidance of excessively wet soil conditions by

adjusting water application in response to soil water tension may serve to limit bypass flow and promote efficient leaching of the soil matrix. By improving leaching effectiveness, both soil remediation timelines and the amount of applied irrigation water will be reduced. Benefits of efficient leaching include reduced soil remediation costs and improved irrigation water conservation.

4.6 References

Abrol, I.P., J.S.P. Yadav and F.I. Massoud. 1988. Salt-affected soils and their management. FAO Soils Bulletin No. 39, Rome, Italy.

Alberta Agriculture and Rural Development. 2006. Alberta municipality profile 2006 census of agriculture, northwest region. Government of Alberta., Edmonton, AB.

Alberta Agriculture and Rural Development. 2013. Salinity classification, mapping and management in Alberta. Government of Alberta. http://www1.agric.gov.ab.ca/$department/deptdocs.nsf/all/sag3267. (accessed 1 Aug. 2013).

Alberta Environment. 2001. Salt contamination and remediation guidelines. Environmental Sciences Division, Environmental Service, Pub. No. T/606, Edmonton, AB.

Allen, R.G., L.S. Pereira, D. Raes and M. Smith. 1998. Crop evapotranspiration - guidelines for computing crop water requirements. FAO Irrigation and Drainage Paper No. 56, Rome, Italy.

Armstrong, A.S.B., T.W. Tanton and D.W. Rycroft. 1998. The effect of ped size, simulated rainfall duration and frequency on the leaching of salts from clay topsoils. Agric. Water Manage. 37: 133-143.

Ashworth, J., D. Keyes and J.L. Crepin. 1999. A comparison of methods for gypsum requirement of brine-contaminated soils. Can. J. Soil Sci. 79: 449-455.

Ayers, R.S. and D.W. Westcot. 1994. Water quality for agriculture. FAO Irrigation and Drainage Paper No. 29 Rev. 1, Rome, Italy.

Barker, A.A., J.T.F. Riddell, S.R. Slattery, L.D. Andriashek, H. Moktan, S. Wallace, et al. 2011. Edmonton-Calgary corridor groundwater atlas. ERCB/AGS Information Series No. 140, Edmonton, AB.

Beven, K. and P. Germann. 1982. Macropores and water flow in soils. Water Resour. Res. 18: 1311-1325.

Bishop, J.M. 2012. The influence of macropores on flow and transport to subsurface drains in low permeability, salt affected soils. M.Sc. diss., University of Calgary, Calgary, AB.

Bowser, W.E., A.A. Kjearsgaard and T.W. Peters. 1962. Soil survey of Edmonton sheet (83-h). Canada Department of Agriculture. University of Alberta Bulletin No. SS-4. Alberta Soil Survey Report No. 21, Edmonton, AB.

Cey, E.E. and D.L. Rudolph. 2009. Field study of macropore flow processes using tension infiltration of a dye tracer in partially saturated soils. Hydrological Processes 23: 1768-1779.

Chang, C., S. Dubetz, T.G. Sommerfeldt and D.C. Mackay. 1982. Leaching fractions and salt status of two irrigated gypsum-rich soils in southern Alberta. Can. J. Soil Sci. 62: 97-103.

Cote, C.M., K.L. Bristow and P.J. Ross. 2000. Increasing the efficiency of solute leaching: Impacts of flow interruption with drainage of the "preferential flow paths". J. Contam. Hydrol. 43: 191-209.

Curtin, D. and H.P.W. Rostad. 1997. Cation exchange and buffer potential of Saskatchewan soil estimated from texture, organic matter and pH. Can. J. Soil Sci. 77: 621-626.

Curtin, D., H. Steppuhn and F. Selles. 1994. Structural stability of chernozemic soils as affected by exchangeable sodium and electrolyte concentration. Can. J. Soil Sci. 74: 157-164.

Environment Canada. 2014a. Canadian climate normals (1981-2010) – Edmonton International Airport, Alberta, Government of Canada. http://climate.weather.gc.ca/climate_normals/index_e.html (accessed 1 Aug. 2013).

Environment Canada. 2014b. Historical climate data – Edmonton International Airport, Alberta, Government of Canada. http://climate.weather.gc.ca/ (accessed 1 Aug. 2013).

Flury, M., H. Fluhler, W.A. Jury and J. Leuenberger. 1994. Susceptibility of soils to preferential flow of water - a field-study. Water Resour. Res. 30: 1945-1954.

Hanson, B.R., S.R. Grattan and A. Fulton. 2006. Agricultural salinity and drainage. Division of Agriculture and Natural Resources Publ. 3375, University of California, Davis, CA.

Hayley, K. 2010. Time lapse electrical imaging of salt affected soil and groundwater. Ph.D. diss., University of Calgary, Calgary, AB.

Hayley, K., L.R. Bentley and M. Gharibi. 2009. Time-lapse electrical resistivity monitoring of salt-affected soil and groundwater. Water Resour. Res. 45. W07425.

Hayley, K., L.R. Bentley, M. Gharibi and M. Nightingale. 2007. Low temperature dependence of electrical resistivity: Implications for near surface geophysical monitoring. Geophysical Research Letters 34: L18402

Hayley, K., L.R. Bentley and A. Pidlisecky. 2010. Compensating for temperature variations in time-lapse electrical resistivity difference imaging. Geophysics 75: WA51-WA59.

Head, F. 2013. Geophysical monitoring of salt remediation. M.Sc. diss., University of Calgary, Calgary, AB.

Hendry, M.J. 1982. Hydraulic conductivity of a glacial till in Alberta. Ground Water 20: 162-169.

Hendry, M.J., J.A. Cherry and E.I. Wallick. 1986. Origin and distribution of sulfate in a fractured till in southern Alberta, Canada. Water Resour. Res. 22: 45-61.

Hoffman, G.J. 1980. Guidelines for the reclamation of salt-affected soils. In: G. A. O'Connor, editor 2nd Inter-American Conf. on Salinity and Water Management Technology, Juarez, Mexico, 11-12 Dec. 1980. p. 49-64.

Keller, C.K., G. van der Kamp and J.A. Cherry. 1991. Hydrogeochemistry of a clayey till .1. Spatial variability. Water Resour. Res. 27: 2543-2554.

Keren, R. and S. Miyamoto. 2011. Reclamation of saline, sodic, and boron-affected soils. In: W. W. Wallender and K. K. Tanji, editors, Agricultural salinity assessment and management, 2nd ed. ASCE Manuals and Reports on Engineering Practice No. 71. ASCE, Reston, VA. p. 655-686.

Kladivko, E.J., G.E. Vanscoyoc, E.J. Monke, K.M. Oates and W. Pask. 1991. Pesticide and nutrient movement into subsurface tile drains on a silt loam soil in Indiana. J. Environ. Qual. 20: 264-270.

Klaus, J., E. Zehe, M. Elsner, C. Kuells and J.J. McDonnell. 2013. Macropore flow of old water revisited: Experimental insights from a tile-drained hillslope. Hydrol. Earth Syst. Sci. 17: 103-118.

Kohne, J.M. and H.H. Gerke. 2005. Spatial and temporal dynamics of preferential bromide movement towards a tile drain. Vadose Zone J. 4: 79-88.

Kohut, C.K. and M.J. Dudas. 1995. Layer charge characteristics of smectites in salt-affected soils in Alberta, Canada. Clay Clay Miner. 43: 78-84.

Lauchli, A. and S.R. Grattan. 2011. Plant responses to saline and sodic conditions. In: W. W. Wallender and K. K. Tanji, editors, Agricultural salinity assessment and management, 2nd ed. ASCE Manuals and Reports on Engineering Practice No. 71. ASCE, Reston, VA. p. 169-205.

Leskiw, L.A., R.B. Sedor, C.M. Welsh and T.B. Zeleke. 2012. Soil and vegetation recovery after a well blowout and salt water release in northeastern British Columbia. Can. J. Soil Sci. 92: 179-190.

Loke, M.H. and R.D. Barker. 1996. Practical techniques for 3d resistivity surveys and data inversion. Geophys. Prospect. 44: 499-523.

McNeal, B.L. and N.T. Coleman. 1966. Effect of solution composition on soil hydraulic conductivity. Soil Sci. Soc. Am. Proc. 30: 308-312.

Merrill, S.D., K.J. Lang and E.C. Doll. 1990. Contamination of soil with oil-field brine and reclamation with calcium-chloride. Soil Sci. 150: 469-475.

Miller, R.J., J.W. Biggar and D.R. Nielsen. 1965. Chloride displacement in panoche clay loam in relation to water movement and distribution. Water Resour. Res. 1: 63-&.

Natural Resources Canada. 2013. Prairies - Canada in a changing climate. Climate Change Publications. Government of Canada. http://www.nrcan.gc.ca/environment/resources/publications/impacts-adaptation/reports/backgrounder/10065. (accessed 1 Aug. 2013).

Oster, J.D., Willards.Ls and G.J. Hoffman. 1972. Sprinkling and ponding techniques for reclaiming saline soils. T.ASAE 15: 1115-1117.

Quirk, J.P. 2001. The significance of the threshold and turbidity concentrations in relation to sodicity and microstructure. Aust. J. Soil Res. 39: 1185-1217.

Quirk, J.P. and R.K. Schofield. 1955. The effect of electrolyte concentration on soil permeability. J. Soil Sci. 6: 163-178.

Rapp, E. and G.E. Laliberte. 1968. Performance of tile drains under irrigation in southern Alberta. Can. Agr. Eng. 10: 64-69.

Reynolds, W.D. and D.E. Elrick. 1991. Determination of hydraulic conductivity using a tension infiltrometer. Soil Sci. Soc. Am. J. 55: 633-639.

Reynolds, W.D. and D.E. Elrick. 2002. Constant head well permeameter (vadose zone). In: J. H. Dane and C. Topp, editors, Methods of soil analysis. Part 4. Physical methods. SSSA Book Series No. 5, Madison, WI. p. 844-858.

Rhoades, J.D. 1982. Reclamation and management of salt-affected soils after drainage. First Annual Western Provincial Conference, Rationalionalization of Water and Soil Research and Management: Soil Salinity. Lethbridge, AB.

Rhoades, J.D. 1982. Soluble salts. In: A.L Page, R.H. Miller, and D.R. Keeney, editors, Methods of soil analysis, Part 2, Chemical and Microbiological Properties, 2nd ed. Agron. Monogr. 9. ASA and SSSA, Madison, WI. p. 167–179.

Robbins, C.W. and C.L. Wiegand. 1990. Field and laboratory measurements. In: K. K. Tanji, editor Agricultural salinity assessment and management. ASCE Manuals and Reports on Engineering Practice No. 71. ASCE, New York, NY. p. 201-219.

Shainberg, I. and M.J. Singer. 2011. Soil response to saline and sodic conditions. In: W. W. Wallender and K. K. Tanji, editors, Agricultural salinity assessment and management, 2nd ed. ASCE Manuals and Reports on Engineering Practice No. 71. ASCE, Reston, VA. p. 139-168.

Siyal, A.A., A.G. Siyal and Z.A. Abro. 2002. Modelling of solute transport from a single soil aggregate. J. Appl. Sci. 2: 470-473.

Smith, A.D. 2008. Evaluating tile drainage systems as a method of salt remediation in Alberta. M.Sc. diss., University of Calgary, Calgary, AB.

Soil Classification Working Group. 1998. The Canadian system of soil classification, 3rd ed. Agric. and Agri-Food Can. Publ. 1646, Ottawa, ON.

Soilmoisture Equipment Corp. 2012. Model 2800 Guelph permeameter operating instructions, Santa Barbara, CA.

Stone, W.W. and J.T. Wilson. 2006. Preferential flow estimates to an agricultural tile drain with implications for glyphosate transport. J. Environ. Qual. 35: 1825-1835.

Tanji, K.K. and W.W. Wallender. 2011. Nature and extent of agricultural salinity and sodicity. In: W. W. Wallender and K. K. Tanji, editors, Agricultural salinity assessment and management, 2nd ed. ASCE Manuals and Reports on Engineering Practice No. 71. ASCE, Reston, VA. p. 1-25.

Thomas, G.W. and R.E. Phillips. 1979. Consequences of water-movement in macropores. J. Environ.Qual. 8: 149-152.

United States Salinity Laboratory (USSL) Staff. 1954. Diagnosis and improvement of saline and alkali soils. U.S. Gov. Print. Office, Washington, DC.

van Hoorn, J.W. and J.G. van Alphen. 1994. Salinity control. In: H. P. Ritzema, editor Drainage principles and applications, 2nd ed. ILRI Publication No. 16, Wageningen, The Netherlands. p. 533-600.

van Schaik, J.C. and R.A. Milne. 1962. Reclamation of a saline-sodic soil with shallow tile drainage. Can. J. Soil Sci. 42: 43-48.

White, R.E. 1985. The influence of macropores on the transport of dissolved and suspended matter through soil. In: B. A. Stewart, editor. Advances in soil science. Springer New York, NY. p. 95-120.

Wuest, S.B. 2009. Comparison of preferential flow paths to bulk soil in a weakly aggregated silt loam soil. Vadose Zone J. 8: 623-627.

Zhang, Z.F.F., P.H. Groenevelt and G.W. Parkin. 1998. The well-shape factor for the measurement of soil hydraulic properties using the guelph permeameter. Soil Till. Res. 49: 219-221.

4.7 Figures and Tables

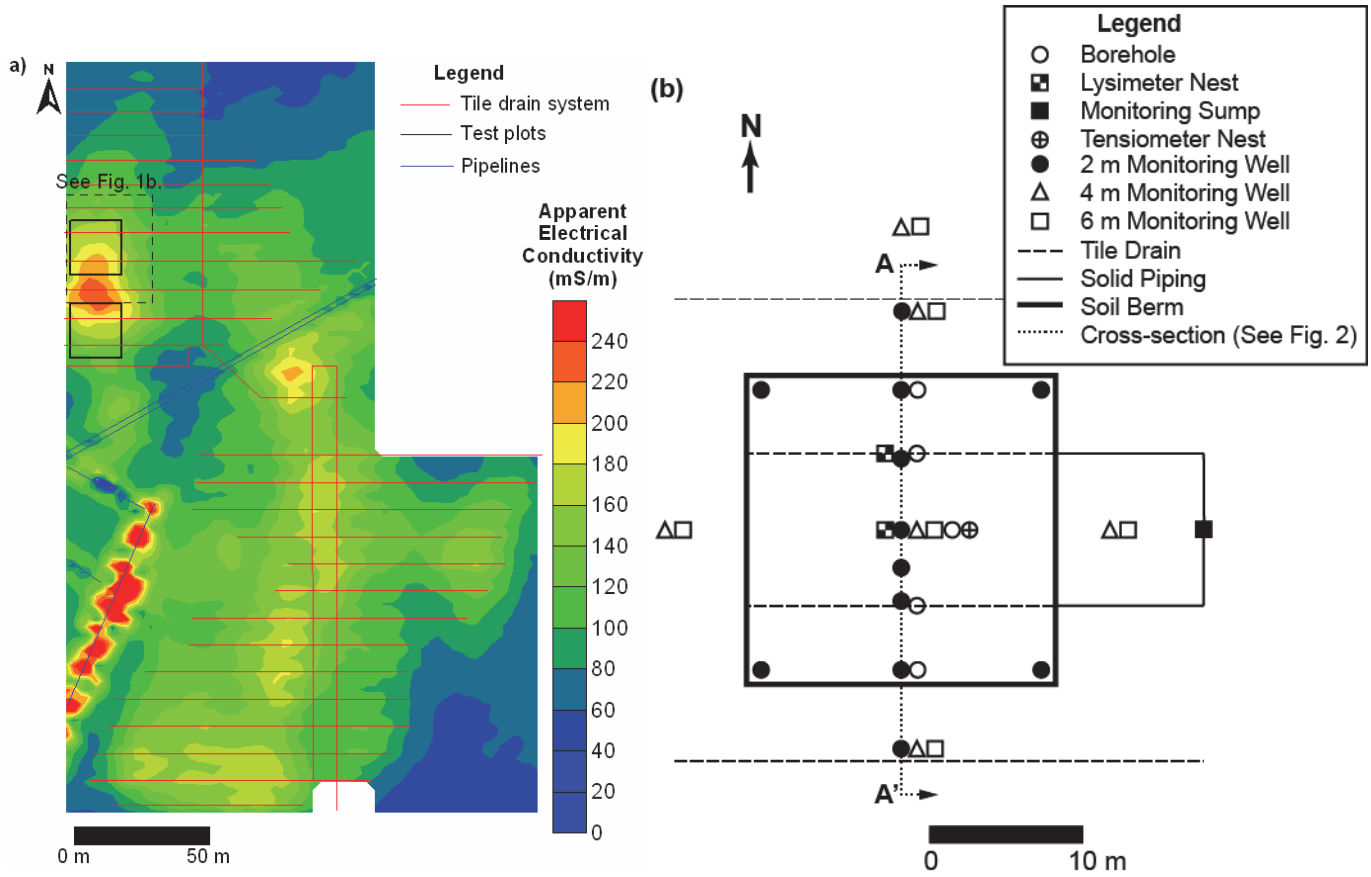

Fig. 4.1. Plan view of the study site. (a) Tile-drainage system showing distribution of apparent electrical conductivity. Warm colors indicate elevated salinity (modified after Head, 2013). Location of test plots is in the northwest corner: irrigated plot, north; unirrigated plot, south. (b) Soil, groundwater and tile drain monitoring locations in the vicinity of the irrigated test plot.

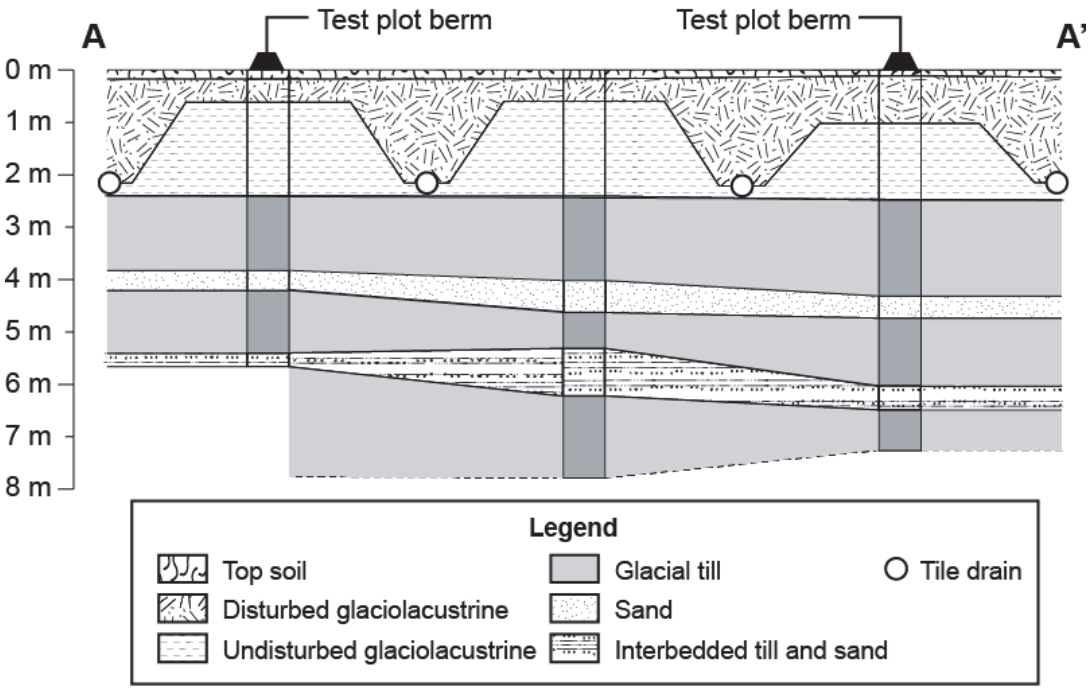

Fig. 4.2. Vertical cross section through the irrigated test plot showing the distribution of unconsolidated geologic materials. Vertical scale is approximate. Horizontal not to scale.

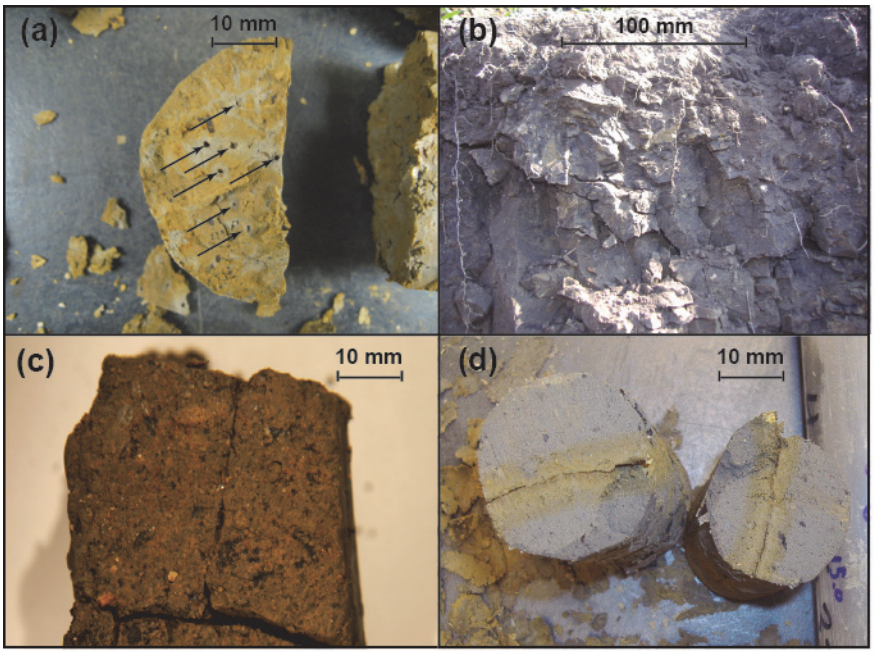

Fig. 4.3. Photographs of: (a) relict root holes (arrows) in soil core collected from the undisturbed glaciolacustrine silt loam; (b) weakly prismatic to blocky soil structure in the disturbed glaciolacustrine material; (c) heavily oxidized and fractured glacial till, depth of 2.4 m; and, (d) an oxidized vertical fracture in soil core collected from glacial till at a depth of 5.0 m.

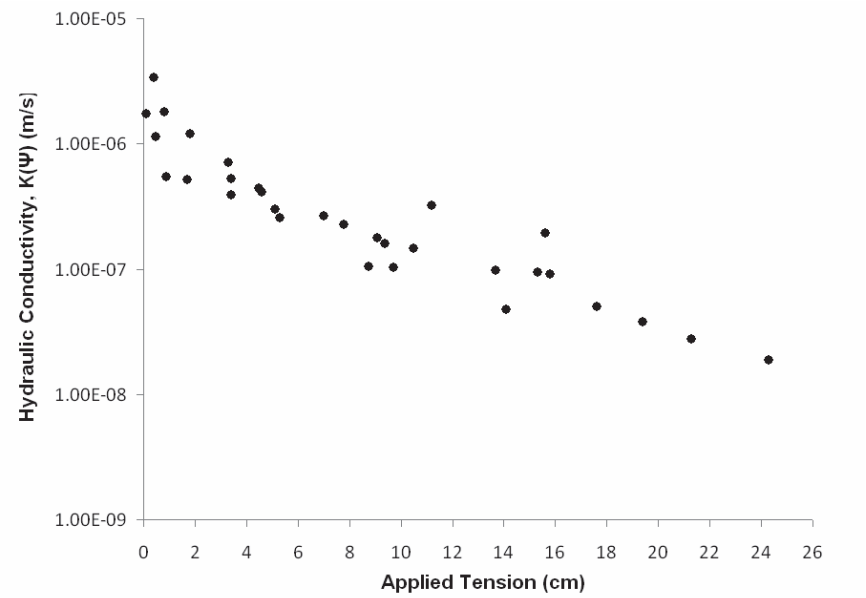

Fig. 4.4. Tension infiltrometer measurements of hydraulic conductivity as a function of soil tension at the soil surface.

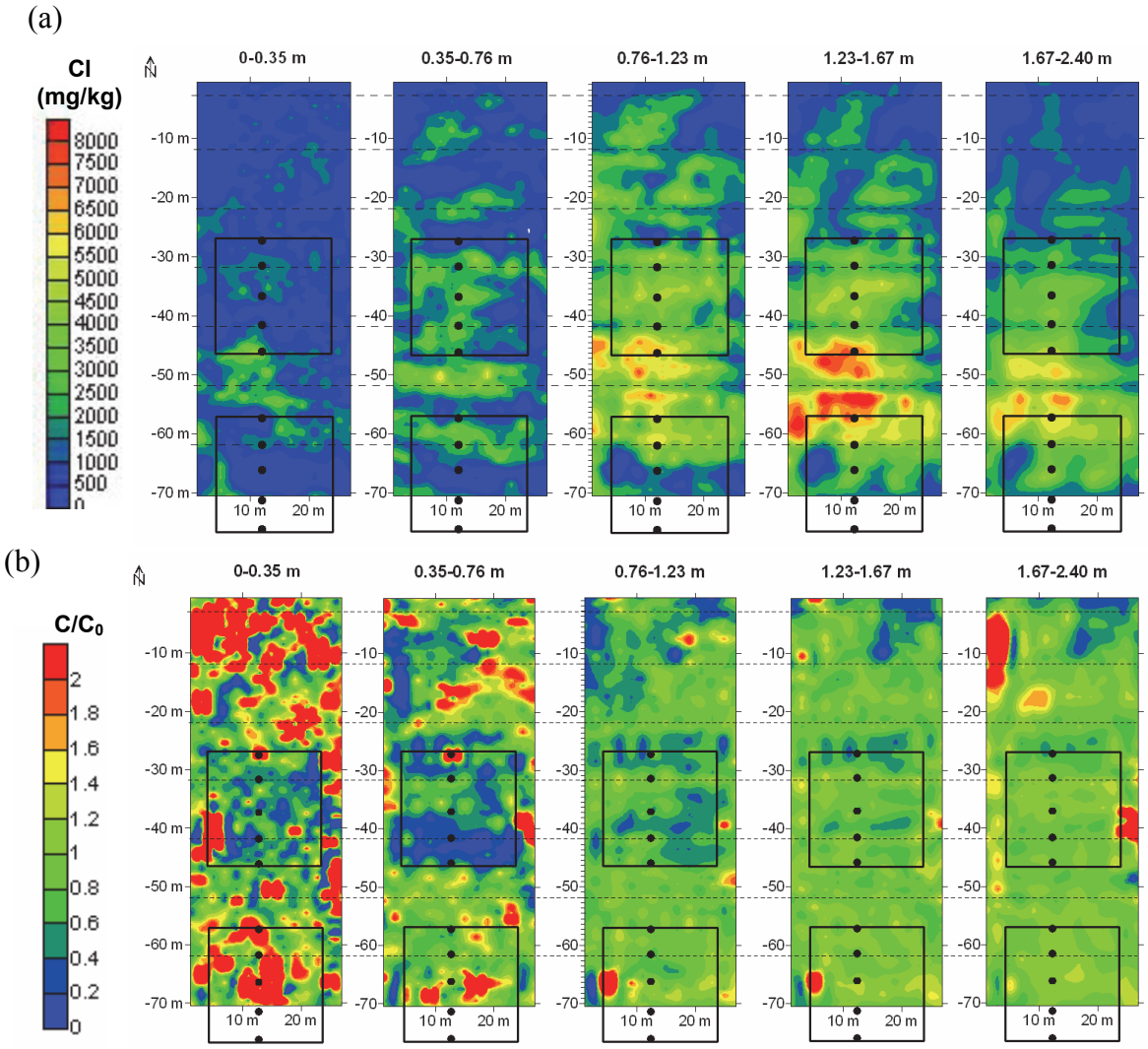

Fig. 4.5. Electrical resistivity tomography results for the irrigated test plot for Year 1 (a) initial chloride concentration prior to Year 1 irrigation, and (b) relative chloride concentration C/C_0 following irrigation in Year 1. Solid line indicates test plots (irrigated = north, unirrigated = south). Dashed line indicates tile drain locations. ● indicates borehole locations (modified after Head, 2013).

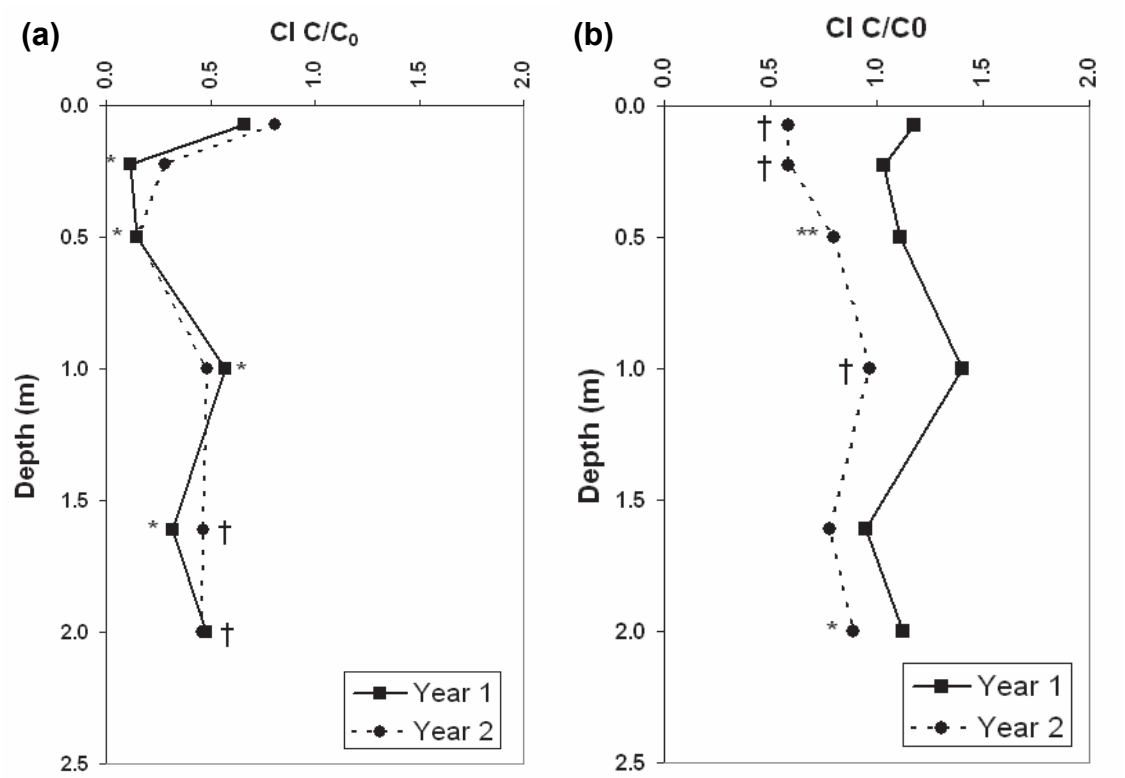

Fig. 4.6. Normalized soil chloride concentrations, C/C_0, for soil samples collected at the end of Years 1 and 2 of the irrigation experiment, in: (a) the irrigated test plot, and (b) the unirrigated control plot. The reference concentration used for normalization was that measured at the start of Year 1. Statistical significance of the difference in absolute Cl concentrations is denoted by: † for α = 0.1, * for α = 0.05, and ** for α = 0.01 levels by paired T-test. Absence of a symbol indicates that the p-value at that depth is >0.1.

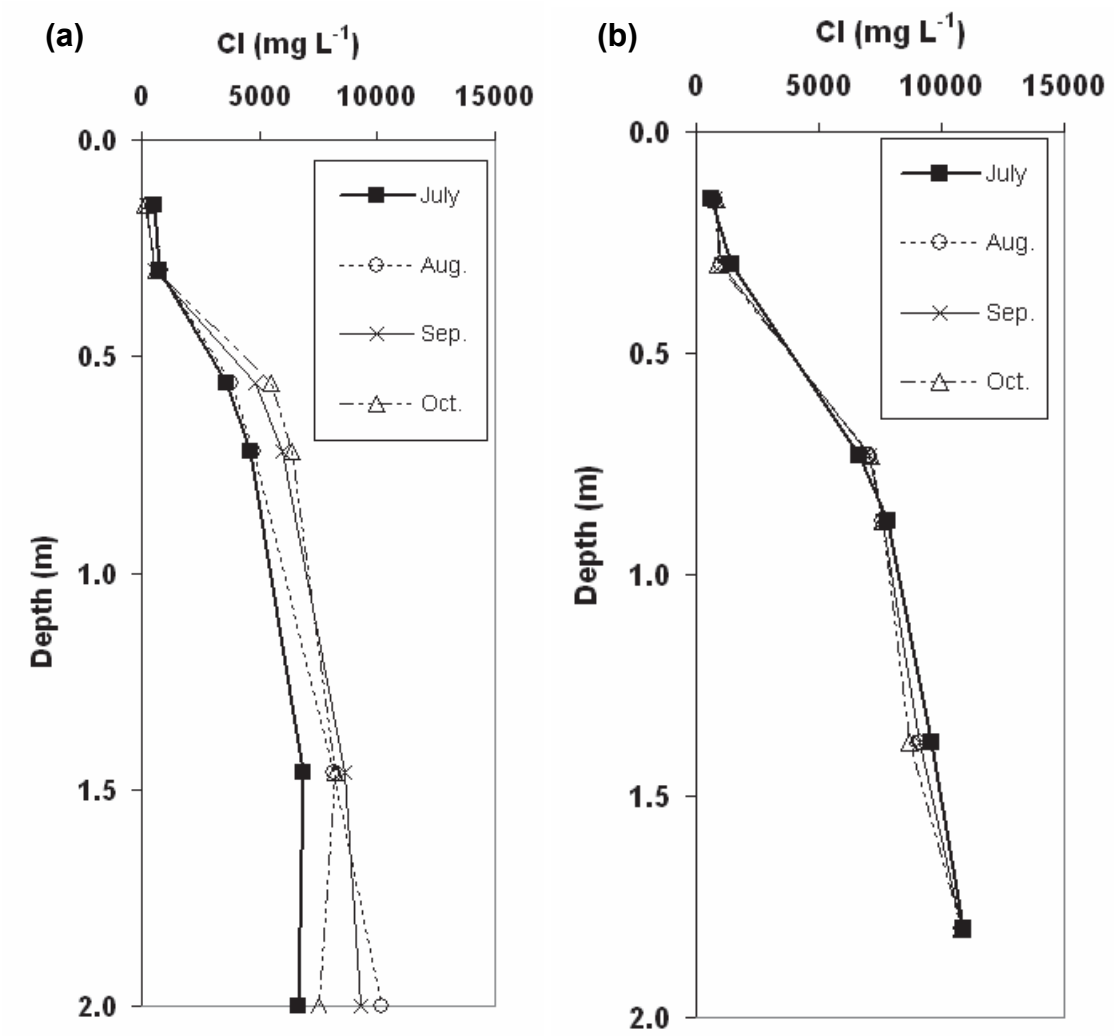

Fig. 4.7. Monthly (July–October) soil water Cl concentrations in the irrigated test plot during the year 2 irrigation season (a) above the north tile drain, and (b) between the two tile drains. Samples above 1.5 m collected from suction lysimeters and samples below 1.5 m were collected from shallow monitoring wells.

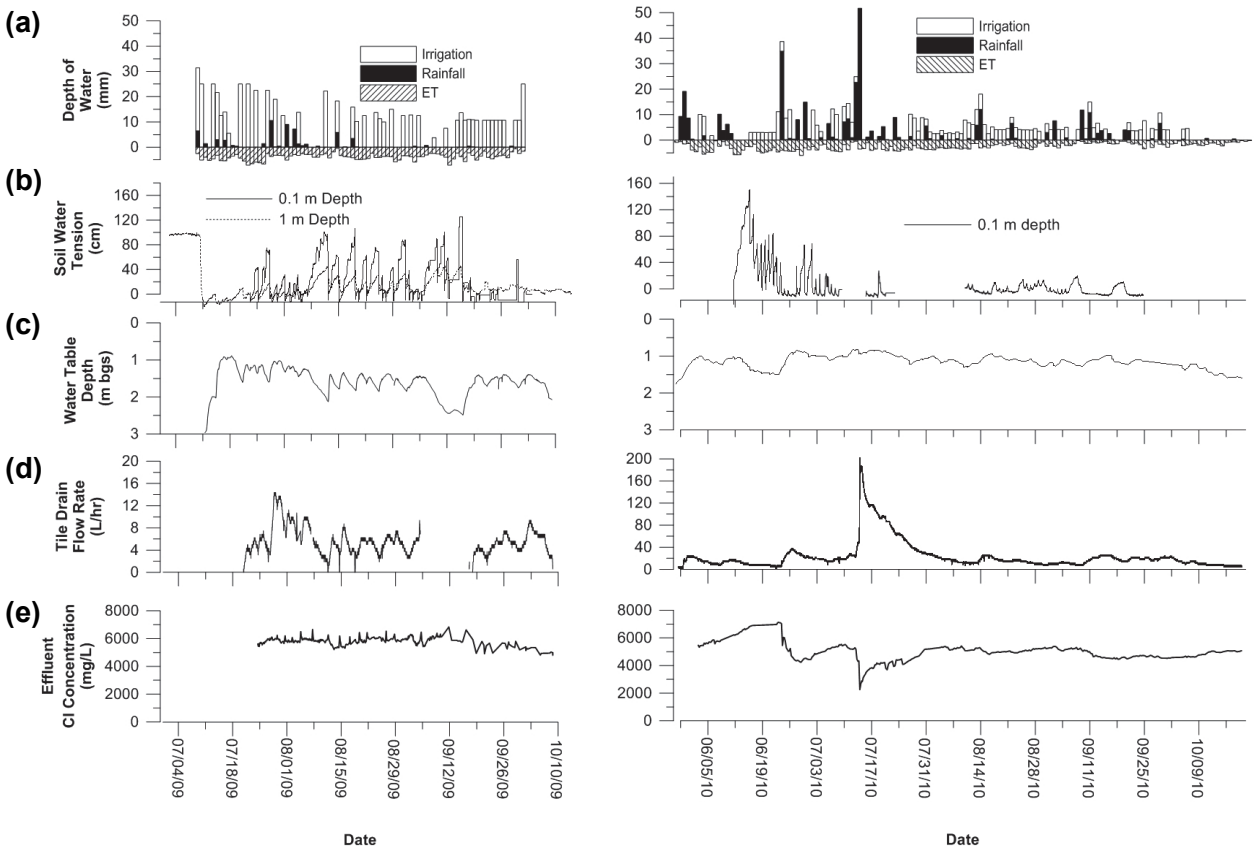

Fig. 4.8. Time-series results for the south tile drain within irrigated test plot during Year 1 (left) and Year 2 (right): (a) water applied to the test plot, with evapotranspiration (ET) shown as negative; (b) soil tension in shallow soil; (c) water table depth; (d) tile drain flow rate, and (e) tile drain effluent Cl concentration.

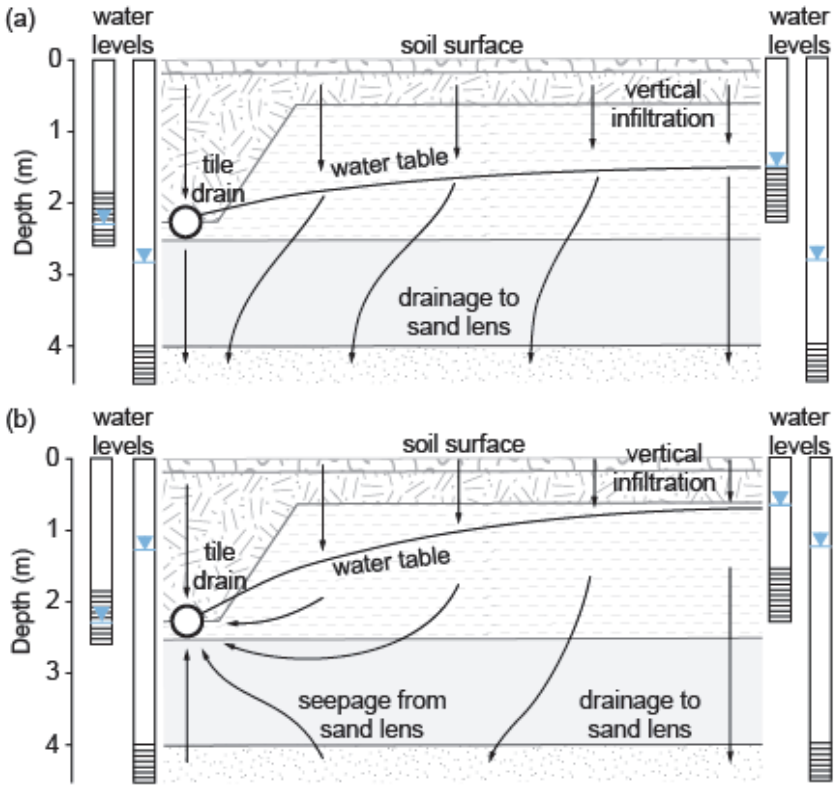

Fig. 4.9. Groundwater flow to tile drains, showing (a) dominantly deep drainage flow condition, with water levels in monitoring wells are shown for late-May in Year 1, and (b) combined deep drainage with upward seepage, with water levels in monitoring wells shown for late-July in Year 2. Vertical scale is approximate, horizontal not to scale. Refer to Fig. 4.2 for definition of soil lithologies.

Table 4.1. Monthly precipitation for Years 1 and 2 of the field study.

Year	Nov.	Dec.	Jan.	Feb.	Mar.	Apr.	May	Jun.	Jul.	Aug.	Sep.	Oct.	Total
	mm												
1[x]	2.6[z]	24.2[z]	18.8[z]	15.3[z]	26.8[z]	18.7[z]	16.4[z]	19.2[y]	74.1[y]	29.5[y]	2.2[y]	20.5[y]	268.3
2[w]	12.0[z]	38.9[z]	8.6[z]	1.2[z]	4.2[z]	41.0[z]	98.4[y]	84.2[y]	129.7[y]	33.1[y]	56.6[y]	7.8[z]	515.7

[z]Precipitation data from the Edmonton International Airport meteorological station (Environment Canada, 2014b)

[y]Precipitation data from on site meteorological station.

[x]Year 1 ran from Nov. 2008 to Oct. 2009.

[w]Year 2 ran from Nov. 2009 to Oct. 2010.

Table 4.2. Water balance results for the irrigated test plot.

Water Balance Period	Irrigation	Rainfall	Total Water Applied [x]	ET	Net Applied Water [w]	Soil Water Storage [v]	Tile Drainage	Net Deep Drainage [u]
	mm							
Year 1[z]	607	115	722	352	370	85	36	249
Year 2[y]	379	305	684	353	331	0	334	-3

[z]Year 1 water balance period is from 7 July–2 Nov. 2009, 119 d.

[y]Year 2 water balance period is from 2 June–19 Oct, 2010, 140 d.

[x]Total applied water is calculated as irrigation + rainfall.

[w]Net applied water is calculated as irrigation + rainfall – ET.

[v]Soil water storage is the amount of water required to wet up the soil profile at the start of the water balance period.

[u]Net deep drainage is calculated as net applied water – soil water storage – tile drainage and is positive downwards.

ET, evapotranspiration.

CHAPTER 5: A CONCEPTUAL FRAMEWORK FOR OPTIMIZING SALT LEACHING IN FINE-GRAINED, MACROPOROUS SOILS USING IRRIGATION TO CONTROL PREFERENTIAL FLOW

5.1 Introduction

Salt-affected soils and the associated decreases in crop yield are a global issue (Rengasamy, 2006). Leaching of salts from the rooting zone in conjunction with leachate collection using tile drains is a common method used to reclaim or remediate salt-affected soils (Abrol et al., 1988). In dry climates such as in the Canadian prairies (CP), rainfall alone is often insufficient to leach salt from the soil profile in a reasonable amount of time. Therefore, the addition of irrigation water is used to accelerate the leaching process (Ayers and Westcot, 1994). Agricultural water supply shortages are currently a constraint to food production in arid and semi-arid areas (Wallace and Batchelor, 1997). Therefore, improved water use efficiency for management of salinity levels in agricultural soils has wide application.

Water use efficiency may be incorporated into the leaching process through the concept of leaching efficiency. Leaching efficiency is defined as the mass of salt leached from the soil profile per unit volume of water applied (Keren and Miyamoto, 2011). Since the 1960's, it has been known that leaching efficiency is improved in fine-grained soils through the use of intermittent ponding or sprinkling, in comparison to the use of continuous ponding (Oster et al., 1972). The observed improvement in leaching efficiency under intermittent irrigation is attributed to improved drainage through smaller pores under partially saturated soil conditions. Poorer leaching efficiency under continuous ponding is attributed to fast flow through large pores bypassing salt stored in the smaller pore spaces (Nielsen et al., 1966).

Water flow and solute transport in fine-grained soils can be characterized as distinctly different from that in coarse-grained (e.g., sandy) soils. Soils with clay fractions in the range of 15–20 % typically develop an aggregated soil structure (Horn et al., 1994). Soil structure is hierarchical in nature and spans a range of scales from floccules of clay particles at smaller scale, to aggregates of soil particles, and aggregated clods at larger scale (Dexter, 1988). Additional components of soil structure, such as root

holes, wormholes, fractures, and cracks give rise to preferential flow, termed macropore flow (Hendrickx and Flury, 2001). Water within soil aggregates is considerably less mobile than water within interaggregate pore space and macropores. This variation in flow rates between pores of differing size gives rise to physical non-equilibrium in pressure heads between smaller and larger pores that controls the flow of water transport of solutes in structured soils (Nielsen et al., 1986). The role of macropore flow on water and solute movement in soil is increasingly recognized, to such a degree that the occurrence of macropore flow is likely the rule rather than the exception (Flury et al., 1994).

The objective of this study was to present a conceptual model for efficient and timely salt leaching in fine-grained, macroporous soil by incorporating concepts of soil moisture control on macropore flow and solute transport. The goal is to increase leaching rates while maintaining high leaching efficiency, thereby decreasing the time required to successfully leach salts from soil while conserving irrigation water.

5.2 Problem Formulation

5.2.1 Irrigation Experiment Results

An irrigation experiment was conducted to study the hydrologic controls on leaching in a salt-affected, fine-grained, macroporous soil. Details of the methodology of the experiment and comprehensive results are presented in Chapter 4. The study site is the location of a former oil and gas production facility in central Alberta, Canada. Salt-affected soil and shallow groundwater at the site resulted from accidental release of brine during oil and gas production, so-called “produced water”. Chloride is the dominant anion in the produced water (120 g L^{-1}). Given relatively low Cl concentrations occurring naturally in groundwater at the site (<10 mg L^{-1}), Cl serves as the primary parameter for tracing salt movement and monitoring the soil remediation effort. Production facilities were removed from the site by 1976, and in 2003 a tile drain system was installed at 2-m depth with 10-m drain spacing under the most highly salt-affected area (2-ha in size). The tile drain system collects saline leachate and routes it for disposal. Soil in the rooting zone comprises topsoil, 0 to 0.15-m depth, over a glaciolacustrine layer of silt

loam texture to 2.4-m depth, shown in cross-section in Fig. 5.1. Underlying the glaciolacustrine silt loam is a dense but fractured glacial till layer. The fractured nature of the glacial till allows vertical fluid migration to and from the overlying glaciolacustrine silt layer. The rooting zone is comprised of disturbed and undisturbed soil zones, the distribution of which is related to tile drain installation. Undisturbed soil is located between the tile drains, and contains abundant macropores as relict root holes and wormholes. Above the tile drains, disturbed soil zones are characterized by columnar to blocky structure. The subsoil matrix is characterized as weakly aggregated with small 2-4 mm aggregates, closely spaced so that the interaggregate pores are of limited continuity, shown in Fig. 5.2.

The irrigation experiment was conducted over two years on a 20 m by 20 m test plot. During each growing season, irrigation water of low Cl concentration, 2 mg L^{-1}, was applied to ground surface using drip irrigation. The depth of water applied per irrigation event was adjusted so that applied water was infiltrated within a few hours following irrigation and produced minimal surface ponding. The irrigated plot was vegetated with a typical pasture blend of mostly grasses, and therefore, evapotranspiration (ET) comprised a major component of the water balance. During the Year 1 irrigation period from 7 July to 1 Oct., 2009, 115 mm of rainfall plus 607 mm of irrigation was applied to the irrigated test plot for a total of 722 mm. During the same period, ET was calculated to be 352 mm, resulting in a net depth of water applied of 370 mm. During the Year 2 irrigation period from 3 June to 6 Oct., 2010, 305 mm of rainfall plus 379 mm of irrigation was applied to the irrigated test plot for a total of 684 mm. During the same period, ET was calculated to be 353 mm, resulting in a net depth of water applied of 331 mm. The depth of net water applied was therefore similar for the two years, within 11 % of the two-year average.

Average soil Cl concentration profiles for the irrigated test plot are shown in Fig. 5.3a: at the start of Year 1; at the end of Year 1; and, at the end of Year 2. Details of sample collection and analytical methods are contained in section 4.2.5. Chloride concentrations were measured using the soil saturated paste extract methodology and are converted to equivalent pore water concentrations for ease of comparison to tile drain effluent concentrations. Soil Cl concentration at the start of Year 1 was lowest near the soil surface and increased with depth, from 790 mg L^{-1} at 0.075-m depth to 8760 mg L^{-1} at 1-m

depth. From 1- to 2-m depth, Cl concentration was approximately constant. During Year 1 of the irrigation experiment, Cl concentrations decreased throughout the soil profile. Soil chloride concentrations at the end of Year 1 ranged from 490 mg L^{-1} at 0.075-m depth to 6840 mg L^{-1} at 2-m depth. Using the formulation of Hoffman (1980), a salt transport efficiency coefficient, k, of 0.11 was calculated for the leaching observed in Year 1 (section 4.4). This value of k is consistent with the value of 0.1 indicative of good leaching efficiency achieved under intermittent and sprinkler irrigation for a wide range of soil textures from silty clay to sand (Keren and Miyamoto, 2011). The leaching rate achieved in Year 1 is calculated here as: LR = $(1\text{-}C/C_0)$ in units of yr^{-1}, where C_0 is the depth-averaged soil Cl concentration at the start of the year, and C is the depth-averaged soil Cl concentration at the end of the year. The C/C_0 ratio calculated for Year 1 over the depth interval of 0–2.4 m is 0.62 (section 4.4), resulting in a LR of 0.38 yr^{-1}. Therefore, 38 % of the initial salt mass was leached from the 0- to 2.4-m depth interval in one year. To put this leaching rate into perspective, a previous modeling study conducted on the same site predicted >100 yrs would be required to fully leach the salt from the soil profile under natural precipitation conditions (Smith, 2008). Therefore the leaching rate achieved in Year 1 of the irrigation experiment is substantially greater than that expected under average natural precipitation conditions. In contrast to the large decrease in Cl concentrations observed during Year 1, Cl concentrations in Year 2 showed negligible leaching in the upper 2 m of the soil profile (Fig. 5.3a). Therefore, leaching efficiency and rate in Year 2 were negligible. Details of the leaching efficiency calculation are given in section 4.4.

5.2.2 Macropore Flow and Transport

The large contrast in leaching efficiency and rate observed between the two years of the irrigation experiment is inconsistent with equilibrium flow and transport theory. If equilibrium flow and transport were the operable mechanism of salt leaching in this soil, a similar amount of water applied to the soil profile would be expected to produce a similar degree of leaching of the salt mass. Macropore flow and transport is described as being in physical non-equilibrium due to lateral differences in water pressure or

solute concentration during vertical flow (Jarvis, 2007). The slow rate of equilibration of water pressure or solute concentration between the macropore and the soil matrix may result in a large contrast in water chemistry between that in the macropores and that in the soil matrix. The relative importance of macropore flow in the soil under study is illustrated by a number of additional observations. Field-saturated hydraulic conductivity, K_{fs}, (37–270 mm d^{-1}) is approximately two to three orders of magnitude greater than the saturated hydraulic conductivity, K_s, of intact 51-mm diameter soil cores (0.30 mm d^{-1}) (section 4.3.1). This contrast in hydraulic conductivity between the field scale and core scale is attributed to the presence of root holes, wormholes, and fractures that form a network of relatively continuous macropores in the field soil. The presence of macropores contributes a large fraction to the bulk soil hydraulic conductivity, measured as K_{fs}. In contrast, at the core scale, the relatively low K_s is indicative of the hydraulic conductivity of the soil matrix in the absence of macroporosity. Additional evidence of macropore flow and transport comes from observations made as part of a non-reactive tracer study conducted at the plot scale. For the test plot under study, Bishop (2012) and Bishop et al. (in submission) reported breakthrough of surface-applied tracer (2,6-Difluorobenzoic acid) to the tile drains within 47 h. Rapid breakthrough of surface applied tracers to tile drains is a commonly-used indicator for macropore flow and transport (Villholth et al., 1998; Kung et al., 2000). Given, the low hydraulic conductivity of the soil matrix the rapid transport of tracer to the tile drains is attributed to macropore flow.

Studies have found varying degrees of direct surface influx contributing to tile drain flow. Klaus et al. (2013) used sprinkler application of Br-traced water and hydrograph separation to estimate the proportion of surface-generated macropore flow to be 12-13% of total tile drain flow. Stone and Wilson (2006) used in situ soil chloride concentrations to quantify the surface-generated macropore contribution to tile drain flow. Their results show a range of macropore flow contribution ranging from 11–51 % of total tile drain flow and 40–81 % at peak flow. Higher macropore inflow contributions corresponded to higher intensity rainfall resulting in saturated soil conditions and localized surface ponding. These results demonstrate a wide range of macropore flow contribution to tile drain flow and illustrate a dependence on soil moisture conditions. In the current study, the net applied water for the two years of the experiment

were similar, yet a higher degree of leaching was observed in Year 1 compared to negligible leaching observed in Year 2 (Fig. 5.3). By inference, the water draining to depth in Year 2 can be inferred to have been relatively fresh in comparison to that of Year 1. The source of that fresh water was macropore flow that essentially bypassed the saline soil matrix. In the context of improving salt leaching, the proportion of flow passing through the soil matrix is of primary importance. Matrix flow contribution is simply the remainder of the total flow once macropore flow is accounted for.

5.3 Conceptual Model

5.3.1 Background on Soil Structure

Structured soils contain a range of pore sizes relevant to soil water transport from: micropores <10 μm in equivalent cylindrical pore diameter; to mesopores or capillary pores, 10 μm to 1 mm in diameter; up to macropores, > 1 mm in diameter (Luxmoore, 1981). Alternately, Jarvis (2007) classified macropores as having equivalent cylindrical diameters of 0.3–0.5 mm. Pore size divisions vary slightly between authors, but the given divisions are sufficient for illustrative purposes. A size-based classification of soil pores is useful, in that the different size ranges exhibit characteristic hydraulic behavior. Micropores hold water most strongly, sometimes termed adsorbed water, which is relatively less mobile than water in larger pores. Flow within capillary pores is considered to be laminar and is the scale of Darcian flow. Macropore flow is generally turbulent, and its physical characterization is a current topic of research. A number of models have been developed for describing macropore flow, such as: the equivalent porous medium model using Richard's equation (Gerke and vanGenuchten, 1996); the kinematic wave model (Jarvis, 1994); the thin film flow model (Tuller and Or, 2001); the infiltration-initiation-interaction model (Weiler, 2005); the rivulet flow model (Germann et al., 2007); and, the source-responsive model (Nimmo, 2010), to name a few. It is within this paradigm of advancing the understanding of macropore flow and transport that the current study fits. To aid in the development of the conceptual model a morphological description of the pore continuum is adopted here, whereby the pore space is divided into three domains from smallest pore size to largest: intra-aggregate pores,

interaggregate pores; and macropores, defined graphically in Fig. 5.2. Intra-aggregate pores may span the size range from micropores to capillary pores, while interaggregate pores may span the size range from capillary pores to macropores. Additionally, the term soil matrix is used here to describe the combined domain of aggregates and interaggregate pores.

Previous research on improving salt leaching efficiency in structured soils has primarily focused leaching of well-aggregated soils in laboratory soil columns (Al-Sibai et al., 1997; Armstrong et al., 1998; Cote et al., 1999). The term "well-aggregated" is used here to describe soil in which the aggregates are relatively distinct and have well-developed and relatively continuous interaggregate pore space. Therefore, in a well-aggregated soil, the interaggregate pores are of high hydraulic conductivity and represent the major flow paths within such a soil. In contrast, the term "weakly-aggregated" soil is used here to describe soil in which the interaggregate pore space is of limited continuity and of low hydraulic conductivity due to close aggregate spacing.

5.3.2 Initial Salt Distribution and the Role of Diffusion

Due to the relatively long exposure of the soil under study to saline pore water, >30 y, salt is assumed to have fully diffused into the soil aggregates. Macropores themselves do not represent a large volume fraction in soil and their rapid drainage results in very little residual water storage within the macropores. Through calibration of a dual permeability partially saturated flow and transport model, Bishop (2012) estimated volumetric fraction of macropores in the soil under study to be 0.25 %. In other studies on fine-grained macroporous soils, macropore fraction ranged from 0.4–5 % (Gerke and Kohne, 2004; Gardenas et al., 2006; Frey and Rudolph, 2011). Given the low volume fraction of macropores and their well-drained character under partially saturated moisture conditions, the majority of salt is assumed to be stored within the soil matrix. This is shown schematically in Fig. 5.4a, with salt stored within the soil aggregates and in water films within the interaggregate pores, shown in red.

In the soil under study, the low hydraulic conductivity of the soil matrix limits direct drainage of water and leaching of salt to depth. This is best evidenced by the negligible downward movement of Cl in

the soil profile during Year 2 of the irrigation experiment (Fig. 5.3). Therefore, it is hypothesized that leaching observed during Year 1, is the result of salt transfer from the matrix to the macropores, which rapidly conduct the saline water to depth. Diffusion of salt out of soil aggregates and leaching efficiency has been previously studied in well-aggregated soil. Armstrong et al. (1998) demonstrated higher leaching efficiency with smaller aggregate diameter. Higher leaching efficiency was attributed to a shorter radial diffusion path length for smaller aggregate sizes. Salt leaching efficiency was increased by Cote et al. (1999) using periodic filling and emptying of fresh water in the interaggregate pores, in comparison to using continuous flow. Their observed improvement in leaching efficiency was attributed to solute redistribution within the soil aggregates during drainage periods that resulted in a higher diffusion rate upon re-application of freshwater. Therefore, the process of salt diffusion into the interaggregate pore space is well established. However, due to the weakly aggregated nature of the soil under study, an additional transport mechanism is required to transfer salt from the relatively low hydraulic conductivity interaggregate pores to the more conductive macropores.

The lack of rooting zone leaching observed in Year 2 of the irrigation experiment (Fig. 5.3), in the presence of wet soil conditions, suggests that direct diffusion of salt from the soil matrix to the macropores was negligible. Potential explanations for low direct diffusion rates into macropores include: low effective diffusion coefficients caused by coatings on macropore walls (Kohne et al., 2002); and, smaller surface area per volume in larger pores (Luxmoore et al., 1990). Therefore, direct diffusion of salt from the interaggregate pores to the macropores is discounted as the dominant mechanism of salt transfer. This leads to exploring an advective mechanism of salt transfer from the matrix to the macropores.

5.3.3 Near-Surface Macropore Flow Generation

The two main mechanisms for macropore flow generation are: direct inflow of water at the soil surface; and, subsurface lateral flow from the soil matrix. Macropore flow may be initiated at the soil surface when the water application intensity exceeds the infiltration capacity of the soil matrix (Hendrickx

and Flury, 2001). Inflow to macropores may be initiated under small scale ponding or soil moisture near saturation. Results of tension infiltrometer measurements made on the soil surface at the study site show a sharp increase in hydraulic conductivity as SWT decreases to within a range of 2-4 cm (section 4.3.1). Cey and Rudolph (2009) used a combination of dye infiltration and unsaturated hydraulic conductivity measurements using a tension infiltrometer to determine the onset of preferential flow in a fine-grained macroporous soil to lie between a SWT of 2-5 cm.

Subsurface macropore flow generation is attributed to increased degree of saturation above a layer of lower matrix hydraulic conductivity in the shallow subsurface (Weiler, 2005). As with surface-generated macropore flow, the subsurface need not be fully saturated to initiate macropore flow. The implication of surface vs. subsurface macropore flow generation for salt leaching is that during subsurface macropore flow generation water passes through the soil matrix. Thereby, it has the opportunity to mix with and leach salts directly out of the matrix. In constrast, macropore flow generated at the soil surface, has limited potential to mix with saline water in the soil matrix, thus reducing its leaching potential.

Monitoring results for a representative 20-d period during Year 1, 7 Aug. to 27 Aug., 2009 are shown in Fig. 5.5. The irrigation + rainfall time series is shown in Fig. 5.5a. Soil water tension at 0.1 m depth shows rapid wetting in response to applied water (<30 min), highlighted in gray in Fig. 5.5b. Soil tensiometer readings are interpreted to be indicative of matrix soil water tension (SWT) (McDonnell, 1990). Applying a threshold water entry tension for macropore flow generation of 4 cm, SWT at 0.1 m depth reaches values low enough to initiate macropore flow following each water application. Furthermore, soil water tension is maintained <4 cm for approximately 6–9, hrs following the termination of water application, if additional water is not applied. Soil water tension measured at 0.3 and 0.6 m was effectively zero for the duration of the irrigation season following initial wet up (data not shown). The continually saturated matrix at 0.3- and 0.6-m depth resulted in persistent conditions conducive to macropore flow generation at those depths. Sub-surface macropore flow generation is shown schematically in Fig. 5.4b. As water drains from the matrix into the macropores, it transports salts from the interaggregate pores into the macropores. This is a relatively efficient salt leaching mechanism,

evidenced by the high degree of salt leaching observed during Year 1 over the depth interval of 0.3–0.5 m. Shown in Fig. 5.3b, are normalized C/C_0 concentrations; note the higher relative degree of decrease in Cl concentrations in samples collected at 0.3- and 0.5-m depth, in comparison to other sample depths.

Monitoring results for a representative 20-d period during Year 2, 20 Aug. to 9 Sep., 2010 are shown in Fig. 5.6. The irrigation + rainfall time series is shown in Fig. 5.6a. Soil water tension at 0.1-m depth, shown in Fig. 5.6b, is lower on average than in Year 1. A water entry tension of 4 cm for macropore flow initiation was determined from the tension infiltrometer results. Soil water tension was below the water entry tension for macropore flow initiation of 4 cm for 70 % of the irrigation period following initial wet up. At 0.3- and 0.6-m monitoring depths, SWT was essentially zero for the duration of the irrigation period following initial wet up. The SWT conditions during Year 2 were conducive to near continual macropore flow generation. Inconsistent with our model of macropore flow and leaching (Fig. 5.4b), soil Cl concentrations measured at 0.15-, 0.3- and 0.5-m depths at the end of Year 2 did not show appreciable salt leaching, shown in Fig. 5.3b. However, during the same monitoring period, tracer concentrations in soil water samples at 0.15- and 0.3-m depths did show persistent decrease throughout the Year 2 irrigation period (Bishop, 2012). One possible explanation for this discrepancy between the rate of Cl and tracer leaching in the 0- to 0.5-m depth interval is that the low soil chloride concentrations within this depth interval represent residual chloride trapped in micropores within the soil aggregates. Thereby the effective diffusion coefficient for residual Cl in Year 2 may be lower than that of the tracer. This hypothesis is consistent with observations made in a companion study on salt leaching from soil cores that hypothesized a decrease in salt diffusion coefficient as leaching progressed due to a “salt sieving” effect within the smallest clay-lined pores (section 3.4).

5.3.4 Lateral Macropore Infiltration and Drainage

Lateral infiltration through the walls of macropores into the soil matrix is commonly observed in dye infiltration studies (Weiler and Naef, 2003; Cey and Rudolph, 2009). Lateral infiltration from the macropore is observed as development of a halo of increased moisture content in the matrix adjacent to

the macropore (Beven and Germann, 1982; Booltink and Bouma, 1991; Greve et al., 2010). The degree of lateral infiltration is dependent on the antecedent soil moisture condition prior to infiltration. A lower degree of lateral infiltration occurs during infiltration in wet soil compared to dry soil (Weiler and Naef, 2003). Lateral infiltration is a key process that is exploited within our conceptual model.

Infiltration produces a decrease in SWT within the soil matrix at 1.0-m depth, shown in Fig. 5.5c, highlighted in gray. The SWT at 1.0-m depth responds 100–150 min following the start of water application. Again, due to the low hydraulic conductivity of the soil matrix, this rapid response is attributed to macropore flow. The water table depth at the center of the plot and the tile drain flow are shown in Fig. 5.5d and 5.5e, respectively. Similar to the SWT response at 1.0 m, the water table and tile drain flow rapidly respond to infiltration following the onset of water application.

The depth of the water table is interpreted as indicative of saturated water level within the macorpores (van Schaik et al., 2008). Currently no method exists for accurately measuring unsaturated pressure head within a macropore. Additionally, the physical description of flow within macropores is somewhat uncertain, as evidenced by the proliferation of models for the description of macropore flow, given earlier. However if the matrix below the depth of macropore flow generation is only partially saturated, then lateral infiltration from macropore to matrix will occur due to capillary suction exerted by the interaggregate pores on water within the macropores. The lateral infiltration process is shown schematically in Fig. 5.4c. Lateral infiltration essentially stops when the interaggregate pores are filled. Once lateral infiltration has stopped, flow within the macropores bypasses the soil matrix and drains to depth. A decrease in leaching efficiency occurs, if macropore flow persists, as shown in Fig. 5.4f.

Drainage is the key process in leaching salt from the matrix in this zone below the depth of macropore flow generation. If the macropores are unsaturated, they drain relatively rapidly. Gravity drainage of the interaggregate pores then follows. Drainage of the intra-aggregate pores is limited by the relatively high air entry tension of fine-textured sediments. Using the SWT measurements at 1.0 m depth from Year 1 as an example (Fig. 5.4c), a period of soil drying follows the infiltration period. The drying effect is a combination of the effects of soil drainage and plant transpiration. For a period of 119 d in Year

1, from total ET and drainage values in Table 4.2, a daily average ET rate of 3.0 mm d^{-1} and a daily net drainage rate of 2.4 mm d^{-1} were calculated. Therefore on an average daily basis, ET and drainage are of a similar magnitude. However, on a time scale of an individual wetting and drying cycle, the drainage rate is highest early in the drying cycle and decreases with time, while plant transpiration contributes throughout the cycle (Nachabe, 1998). This decrease in drainage rate with time is a result of the largest soil pores draining first, followed by drainage of progressively smaller pores. This concept is broadly known as field capacity, which is defined qualitatively as the soil water content reached when drainage has become very slow, typically after a few days (Nachabe, 1998). In irrigation management, field capacity is commonly invoked as an upper limit for soil moisture content to prevent deep drainage and undesirable leaching of nutrients (Fazackerley and Lawrence, 2012). However in the context of remediation of salt-affected soil, this concept can be exploited to promote deep drainage and leaching. Within the drying portion of the SWT curves at both 0.1 and 1.0 m (non-highlighted portions of Fig. 5.5b and 5.5c), smaller scale cycles of drainage and drainage + ET are visible. Drying due to ET is superimposed on the drainage effect, and results in steep portions of the daily drying curve from approximately 11:30 a.m. to 6:30 p.m. During the evening, night, and early morning, between periods of strong ET drainage is dominantly responsible for the drying effect. In Fig. 5.5b and 5.5c, the first two drainage periods are highlighted in a black box. The steepness of the drainage-only curve decreases with time as drainage slows. Therefore, drainage on the first day is greater than drainage on the second day. By the third day, at 0.1-m depth, a distinct drainage curve is no longer visible, and at 1.0-m depth, the drainage portion is flat, indicating drainage has slowed appreciably.

5.3.5 Salt Leaching Mechanisms

A persistent downward hydraulic gradient existed beneath the tile drains during Year 1 of the irrigation experiment (section 4.3.5). Thus the tile drain effluent concentrations, shown in Fig. 5.5f, reflect the salinity of water draining downwards through the soil column. Given the preferential nature of macropore flow one might expect a decrease in Cl concentrations as indicative of fresh water

breakthrough from the soil surface to depth. However, the observed tile drain Cl concentrations generally exhibit a sharp increase coincident with the start of the tile drain infiltration response. This observation of elevated Cl concentrations during infiltration indicates that very little fresh water is breaking through directly to the tile drains. The exact mechanism responsible for this increase has not been identified. One possibility is that the variation in Cl concentrations in the tile drain effluent reflects the depth distribution of soil Cl concentration. Soil chloride concentrations increased with depth in the soil profile, up to 8760 mg/L in the 1.0- to 2.0-m depth interval at the start of Year 1 (Fig. 5.3a). Thus, high concentration water arriving at the tile drain at the start of infiltration may reflect a source deeper within the soil profile.

The process of salt diffusion from the soil aggregates to the interaggregate pores was described earlier and is believed to be the primary mechanism of salt transfer from the soil aggregates to the interaggregate pore space. Depending on the depth within the soil profile, the mechanism of transfer of water and salt from the interaggregate pores to the macropores varies. In the shallow soil, where interaggregate porosity is higher than deeper in the soil profile, the primary mechanism of salt transfer to the macropores is by subsurface macropore flow generation (Fig. 5.4b). Based on SWT monitoring results and tracer test results of Bishop (2012), the depth of subsurface flow generation is <0.6 m. Below the depth of subsurface macropore flow generation, the process of salt transfer from the interaggregate pores to the macropores is by lateral macropore infiltration and drainage. As water infiltrates laterally from the macropores it mixes with residual saline water within the interaggregate pores. Subsequent diffusion of salts from the soil aggregates into the interaggregate pore space occurs. Diffusion is driven by the concentration gradient between the saline water in the intra-aggregate pores and the diluted pore water within the interaggregate pores (Fig. 5.4c). The diffusive transfer of salt from the aggregates may be limited by the concentration gradient between the intra-aggregate pore water and that in the inter-aggregate pores. It was determined using laboratory column experiments and numerical modeling that leaching efficiency can be improved up to 30 % using a rest period of 12 hrs between infiltration cycles (Cote et al., 2000). Inclusion of a drainage period between infiltration cycles allows for salt redistribution within the soil aggregates that improves the efficiency of diffusion.

In Year 2, the hydraulic gradient below the tile drains reversed and was upward for the majority of the irrigation period (section 4.3.4). Chloride concentrations in the tile drain are therefore not indicative of water draining solely from above but are a mixture of water from above and below the tile drains. Therefore, direct interpretation of the tile drain Cl concentration is not possible. However, from the soil sampling results (Fig. 5.3), negligible salt leaching occurred above the tile drains during Year 2. Therefore the majority of Cl in the tile drains is assumed to be sourced from below. Persistent saturation of the soil matrix during the Year 2 irrigation period suppressed drainage of the interaggregate pores; thereby, negligible salt leaching occurred, shown in Fig. 5.4f.

5.3.6 Optimization of Leaching in Macroporous Soil

Results from the irrigation experiment in the current study demonstrate not only the dependence of leaching efficiency on macropore flow and transport but leaching rate as well. Leaching efficiency and leaching rate are separate and sometimes competing measures. From the irrigation experiment results and some basic assumptions on leaching efficiency in macroporous soils, hypothetical relationships may be developed between the proportion of flow that passes through the saline soil matrix, leaching efficiency, and leaching rate.

Leaching efficiency is relatively well defined at the two extremes of macropore flow contribution, with leaching efficiency being high, when macropore flow is negligible with the majority of flow occurring through the saline soil matrix. Hypothetically, if no macropore flow occurs, then all of the flow passes through the soil matrix effectively leaching salts. This is shown in Fig. 5.7 as high leaching efficiency with 100 % of flow passing through the soil matrix. Correspondingly, elimination of macropore flow is likely to result in very low leaching rates resulting from low matrix hydraulic conductivity. Therefore a low leaching rate occurs when 100 % of flow passes through the soil matrix. At the other end of the spectrum, persistent macropore flow results in negligible leaching efficiency due to flow bypassing the salt stored in the soil matrix. This results in low leaching efficiency and slow leaching rates, as observed in Year 2 of the irrigation experiment.

Between the two end bounds of flow passing through the saline soil matrix, the relationships for leaching efficiency and leaching rate are uncertain. From the leaching results attained in Year 1, relatively good leaching efficiency was achieved simultaneously with a high leaching rate. Therefore, it is hypothesized that a peak leaching rate exists that is attributable to an optimal combination of macropore-matrix flow, shown in Fig. 5.7. Whether leaching efficiency or leaching rate is targeted for optimization may vary based on individual irrigation project objectives. The currently hypothetical relationships between leaching efficiency, leaching rate, and matrix flow condition have the potential to be refined through further experimentation or numerical simulation. The subsequent discussion on optimal use of irrigation for salt leaching is framed in a context of improving leaching rates.

5.4 Irrigation to Optimize Leaching Rate

Irrigation scheduling in response to soil moisture conditions has potential as a method to control cycles of infiltration and drainage that are integral to our proposed method of improving leaching rate and leaching efficiency. Irrigation for soil moisture control is a method commonly applied to optimize crop growth. For example, Shock and Wang (2011) summarize optimal soil water tensions for growth of more than 20 crops, for differing soil conditions and irrigation methods. Automated irrigation systems can be used to trigger water application in response to measured soil moisture conditions (Rekika et al., 2014). Advances in soil moisture control are not only limited to improving agricultural crop production. Wang et al. (2012) demonstrated greater salt leaching with a decrease in the SWT threshold used to trigger irrigation. Mori et al. (2013) controlled soil water tension in partially saturated macroporous soil columns to increase the efficiency of delivery of an aqueous nutrient solution for improved bioremediation of petroleum contaminated soils.

The contrast in leaching observed between Year 1 and Year 2 of the irrigation experiment demonstrates that application of similar amounts of irrigation water can produce a wide range of leaching rate and efficiency. To mitigate this problem, soil moisture monitoring can be incorporated into the irrigation strategy. Thereby, verification of drainage can be made prior to initiating subsequent irrigation.

A principle advantage of irrigation control based on soil moisture conditions is that it implicitly incorporates variations in soil moisture caused by additional factors such as rainfall, ET, and drainage conditions.

5.4.1 Determination of Irrigation Setpoint

Irrigation control based on soil moisture measurement is often implemented using a dry-end set point, whereby irrigation is turned on when the soil dries to a threshold limit. As demonstrated by Year 1 SWT results at 0.1- and 1.0-m depth of the irrigation experiment (Fig. 5.5b and 5.5c), soil drainage slows with time following an infiltration event. As soil drainage slows to negligible, further drying signifies water lost to ET. This water lost to ET does not contribute to leaching and represents a decrease in water use efficiency. In our file experiment soil drainage slowed appreciably after 2–3 d, which corresponded to a SWT of 50–60 cm at 0.1 m depth and a SWT of 30–40 cm at 1.0 m depth. The monitoring depth for triggering irrigation could be set on soil-specific basis. For example, if the target zone for leaching is the upper 0.3 m of the soil profile, then use of SWT monitoring in that depth is logical. In the current study, following successful leaching of the 0- to 0.5-m depth interval during Year 1, the target interval for leaching could have been increased to 0.5- to 2.0-m depth in Year 2. As remediation progresses, different depth intervals may be targeted for optimum leaching. Thereby, the depth of SWT monitoring for triggering irrigation may change over time. The optimal irrigation setpoint and depth of monitoring is soil-specific and should be determined through field trials.

5.4.2 Determination of Irrigation Rate and Depth

When using a dry end setpoint to trigger irrigation, the duration of irrigation is determined by the irrigation rate and the target depth of water to be applied. For timely remediation, effectiveness of each infiltration event should be maximized. Maximum salt leaching will occur when the soil matrix is filled to saturation prior to allowing it to drain. Therefore filling of the soil moisture deficit between the dry end setpoint and saturation should be the goal of each irrigation application.

When applying irrigation to fine-grained, macroporous soil, the irrigation rate should be set in excess of the maximum infiltration rate of the soil matrix, thereby generating macropore flow as per the conceptual model, Fig. 5.4b. The upper limit for irrigation rate is determined by the bulk maximum infiltration rate of the soil. If the bulk maximum infiltration rate is exceeded by irrigation, ponding will occur. Given that intermittent ponding has been shown to produce efficient leaching in fine-grained soils (Miller et al., 1965; Oster et al., 1972), short term ponding is likely not detrimental to either leaching rate or leaching efficiency. It is critical that sufficient drainage of the soil profile is allowed to occur following irrigation. As an example, irrigation was applied in Year 1 at rates up to 8 mm hr^{-1}, minor ponding did occur, but good leaching efficiency and rate were achieved. In contrast, in Year 2 irrigation was applied in a similar manner to Year 1; however the frequency of irrigation was too high for the wetter soil conditions in Year 2. Therefore, the frequency of irrigation should have been decreased to allow for sufficient soil drainage to occur.

The duration of irrigation application can be determined from the total depth of application desired. This value is best determined through field trials following soil wet up. The depth of irrigation water applied should be initially set low and then increased in subsequent irrigations until the desired SWT of 0 cm is achieved. If more water is applied than required to wet the soil matrix to saturation, a decrease in leaching efficiency will result, but it should not adversely affect the leaching rate.

5.5 Conclusion

Results from a field irrigation experiment were used to develop a conceptual model for timely and efficient salt leaching in fine-grained, macroporous soil. The key to effective leaching is cycles of irrigation and drainage that transfer saline water from the soil matrix to the macropores. If persistent macropore flow is generated in the absence of matrix drainage then negligible leaching may result. The optimum duration between irrigation events occurs when matrix drainage has decreased to a negligible rate a few days following infiltration. The SWT value corresponding to the slowing of drainage can be exploited as a setpoint to trigger irrigation. Soil moisture content is therefore cycled through an optimal

range for timely leaching. Field irrigation experiment results indicate that leaching may be both timely and efficient in terms of water use.

5.6 References

Abrol, I.P., J.S.P. Yadav and F.I. Massoud. 1988. Salt-affected soils and their management. FAO Soils Bulletin No. 39, Rome, Italy.

Al-Sibai, M., M.A. Adey and D.A. Rose. 1997. Movement of solute through a porous medium under intermittent leaching. Eur. J. Soil Sci. 48: 711-725.

Armstrong, A.S.B., T.W. Tanton and D.W. Rycroft. 1998. The effect of ped size, simulated rainfall duration and frequency on the leaching of salts from clay topsoils. Agric. Water Manage. 37: 133-143.

Ayers, R.S. and D.W. Westcot. 1994. Water quality for agriculture. FAO Irrigation and Drainage Paper No. 29 Rev. 1, Rome, Italy.

Beven, K. and P. Germann. 1982. Macropores and water flow in soils. Water Resour. Res. 18: 1311-1325.

Bishop, J.M. 2012. The influence of macropores on flow and transport to subsurface drains in low permeability, salt affected soils. M.Sc. diss., University of Calgary, Calgary, AB.

Bishop, J.M., M.V. Callaghan, E.E. Cey, and L.R. Bentley. In submission. Measurement and simulation of subsurface tracer migration to tile drains in low permeability, macroporous soil. Water Resour. Res.

Booltink, H.W.G. and J. Bouma. 1991. Physical and morphological characterization of bypass flow in a well-structured clay soil. Soil Sci. Soc. Am. J. 55: 1249-1254.

Cey, E.E. and D.L. Rudolph. 2009. Field study of macropore flow processes using tension infiltration of a dye tracer in partially saturated soils. Hydrol. Process. 23: 1768-1779.

Cote, C.M., K.L. Bristow and P.J. Ross. 1999. Quantifying the influence of intra-aggregate concentration gradients on solute transport. Soil Sci. Soc. Am. J. 63: 759-767.

Cote, C.M., K.L. Bristow and P.J. Ross. 2000. Increasing the efficiency of solute leaching: Impacts of flow interruption with drainage of the "preferential flow paths". J. Contam. Hydrol. 43: 191-209.

Dexter, A.R. 1988. Advances in characterization of soil structure. Soil Till. Res. 11: 199-238.

Fazackerley, S. and R. Lawrence. 2012. Automatic in situ determination of field capacity using soil moisture sensors. J. Irrig. Drain. 61: 416-424.

Flury, M., H. Fluhler, W.A. Jury and J. Leuenberger. 1994. Susceptibility of soils to preferential flow of water - a field-study. Water Resour. Res. 30: 1945-1954.

Frey, S.K. and D.L. Rudolph. 2011. Multiscale characterization of vadose zone macroporosity in relation to hydraulic conductivity and subsurface drainage. Soil Sci. Soc. Am. J. 75: 1253-1264.

Gardenas, A.I., J. Simunek, N. Jarvis and M.T. van Genuchten. 2006. Two-dimensional modelling of preferential water flow and pesticide transport from a tile-drained field. J. Hydrol. 329: 647-660.

Gerke, H.H. and J.M. Kohne. 2004. Dual-permeability modeling of preferential bromide leaching from a tile-drained glacial till agricultural field. J. Hydrol. 289: 239-257.

Gerke, H.H. and M.T. vanGenuchten. 1996. Macroscopic representation of structural geometry for simulating water and solute movement in dual-porosity media. Adv. Water Res. 19: 343-357.

Germann, P., A. Helbling and T. Vadilonga. 2007. Rivulet approach to rates of preferential infiltration. Vadose Zone J. 6: 207-220.

Greve, A., M.S. Andersen and R.I. Acworth. 2010. Investigations of soil cracking and preferential flow in a weighing lysimeter filled with cracking clay soil. J. Hydrol. 393: 105-113.

Hendrickx, J.M.H. and M. Flury. 2001. Uniform and preferential flow mechanisms in the vadose zone. Conceptual model of flow and transport in the vadose zone. The National Academies Press, Washington, DC. p. 149-187.

Horn, R., H. Taubner, M. Wuttke and T. Baumgartl. 1994. Soil physical-properties related to soil-structure. Soil Till. Res. 30: 187-216.

Jarvis, N.J. 1994. The macro model (version 3.1). Technical description and sample simulations. Reports and Dissertations 19. Department of Soil Science, Swedish University of Agricultural Science, Uppsala, Sweden.

Jarvis, N.J. 2007. A review of non-equilibrium water flow and solute transport in soil macropores: Principles, controlling factors and consequences for water quality. Eur. J. Soil Sci. 58: 523-546.

Keren, R. and S. Miyamoto. 2011. Reclamation of saline, sodic, and boron-affected soils. In: W. W. Wallender and K. K. Tanji, editors, Agricultural salinity assessment and management, 2nd ed. ASCE Manuals and Reports on Engineering Practice No. 71. ASCE, Reston, VA. p. 655-686.

Klaus, J., E. Zehe, M. Elsner, C. Kuells and J.J. McDonnell. 2013. Macropore flow of old water revisited: Experimental insights from a tile-drained hillslope. Hydrol. Earth Syst. Sci. 17: 103-118.

Kohne, J.M., H.H. Gerke and S. Kohne. 2002. Effective diffusion coefficients of soil aggregates with surface skins. Soil Sci. Soc. Am. J. 66: 1430-1438.

Kung, K.J.S., E.J. Kladivko, T.J. Gish, T.S. Steenhuis, G. Bubenzer and C.S. Helling. 2000. Quantifying preferential flow by breakthrough of sequentially applied tracers: Silt loam soil. Soil Sci. Soc. Am. J. 64: 1296-1304.

Luxmoore, R.J. 1981. Microporosity, mesoporosity, and macroporosity of soil. Soil Sci. Soc. Am. J. 45: 671-672.

Luxmoore, R.J., P.M. Jardine, G.V. Wilson, J.R. Jones and L.W. Zelazny. 1990. Physical and chemical controls of preferred path flow through a forested hillslope. Geoderma 46: 139-154.

McDonnell, J.J. 1990. A rationale for old water discharge through macropores in a steep, humid catchment. Water Resour. Res. 26: 2821-2832.

Miller, R.J., J.W. Biggar and D.R. Nielsen. 1965. Chloride displacement in panoche clay loam in relation to water movement and distribution. Water Resour. Res. 1: 63-&.

Mori, Y., A. Suetsugu, Y. Matsumoto, A. Fujihara and K. Suyama. 2013. Enhancing bioremediation of oil-contaminated soils by controlling nutrient dispersion using dual characteristics of soil pore structure. Ecol. Eng. 51: 237-243.

Nachabe, M.H. 1998. Refining the definition of field capacity in the literature. J. Irrig. Drain. Eng. 124: 230-232.

Nielsen, D.R., J.W. Biggar and J.N. Luthin. 1966. Desalinization of soils under controlled unsaturated flow conditions. Sixth Congr. Int. Comm. on Irrig. and Drainage, New Delhi. 19: 15-24.

Nielsen, D.R., M.T. Vangenuchten and J.W. Biggar. 1986. Water-flow and solute transport processes in the unsaturated zone. Water Resour. Res. 22: S89-S108.

Nimmo, J.R. 2010. Theory for source-responsive and free-surface film modeling of unsaturated flow. Vadose Zone J. 9: 295-306.

Oster, J.D., Willards.Ls and G.J. Hoffman. 1972. Sprinkling and ponding techniques for reclaiming saline soils. T.ASAE 15: 1115-1117.

Rekika, D., J. Caron, G.T. Rancourt, J.A. Lafond, S.J. Gumiere, S. Jenni, et al. 2014. Optimal irrigation for onion and celery production and spinach seed germination in histosols. Agron. J. 106: 981-994.

Rengasamy, P. 2006. World salinization with emphasis on australia. J. Exp. Bot. 57: 1017-1023.

Shock, C.C. and F.X. Wang. 2011. Soil water tension, a powerful measurement for productivity and stewardship. Hortscience 46: 178-185.

Smith, A.D. 2008. Evaluating tile drainage systems as a method of salt remediation in Alberta. M.Sc. diss., University of Calgary, Calgary, AB.

Stone, W.W. and J.T. Wilson. 2006. Preferential flow estimates to an agricultural tile drain with implications for glyphosate transport. J. Environ. Qual. 35: 1825-1835.

Tuller, M. and D. Or. 2001. Hydraulic conductivity of variably saturated porous media: Film and corner flow in angular pore space. Water Resour. Res. 37: 1257-1276.

van Genuchten, M.T. 1980. A closed-form equation for predicting the hydraulic conductivity of unsaturated soils. Soil Sci. Soc. Am. J. 44: 892-898.

van Schaik, N., S. Schnabel and V.G. Jetten. 2008. The influence of preferential flow on hillslope hydrology in a semi-arid watershed (in the spanish dehesas). Hydrol. Proc. 22: 3844-3855.

Villholth, K.G., K.H. Jensen and J. Fredericia. 1998. Flow and transport processes in a macroporous subsurface-drained glacial till soil - I: Field investigations. J. Hydrol. 207: 98-120.

Wallace, J.S. and C.H. Batchelor. 1997. Managing water resources for crop production. Philos. Trans. R. Soc. B 352: 937-946.

Wang, R.S., Y.H. Kang, S.Q. Wan, W. Hu, S.P. Liu, S.F. Jiang, et al. 2012. Influence of different amounts of irrigation water on salt leaching and cotton growth under drip irrigation in an arid and saline area. Agric. Water Manage. 110: 109-117.

Weiler, M. 2005. An infiltration model based on flow variability in macropores: Development, sensitivity analysis and applications. J. Hydrol. 310: 294-315.

Weiler, M. and F. Naef. 2003. An experimental tracer study of the role of macropores in infiltration in grassland soils. Hydrol. Proc. 17: 477-493.

5.7 Figures and Tables

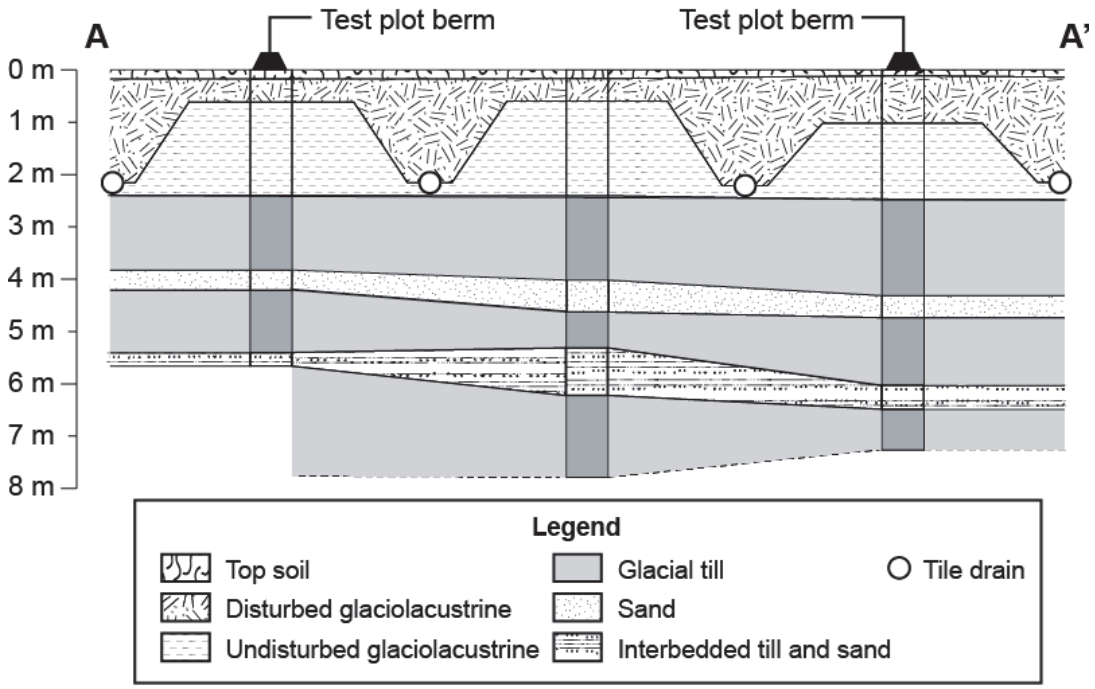

Fig. 5.1. Vertical cross section through the irrigated test plot showing the distribution of unconsolidated geologic materials. Vertical scale is approximate. Horizontal not to scale.

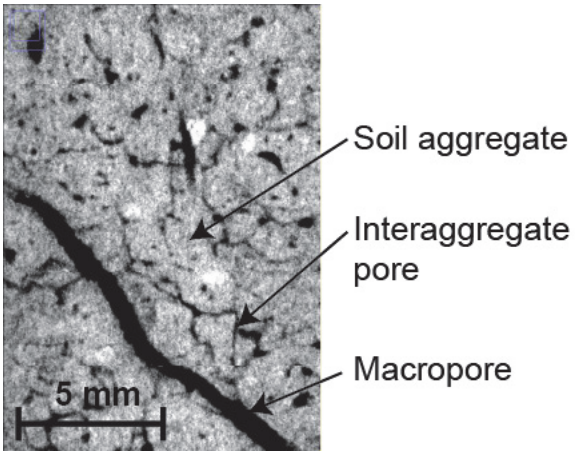

Fig. 5.2. X-ray computed tomogram of intact silt loam subsoil showing soil aggregates (gray), discontinuous interaggregate pores (black), and a relict root hole macropore (black), in vertical cross section.

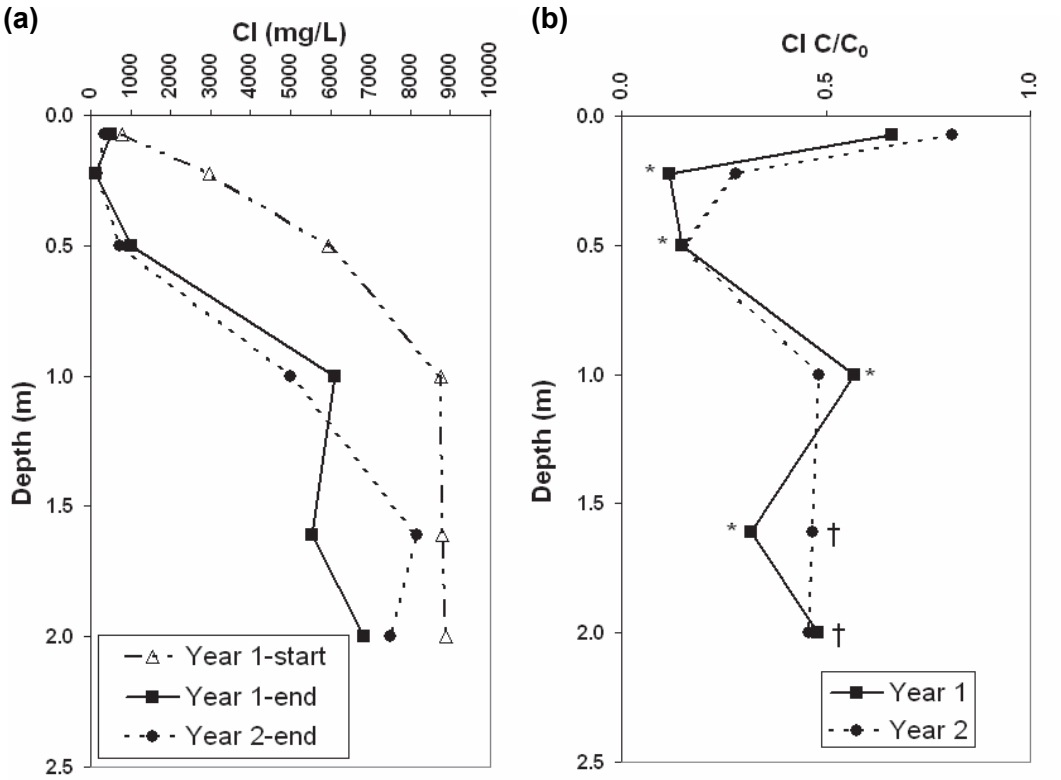

Fig. 5.3. Salt leaching results for the two year irrigation experiment: (a) soil pore water Cl concentrations calculated from saturated paste extract data; and, (b) normalized soil Cl concentrations, C/C_0. Statistical significance of normalized Cl concentration is denoted by: † for α = 0.1, and * for α = 0.05 levels by paired T-test.

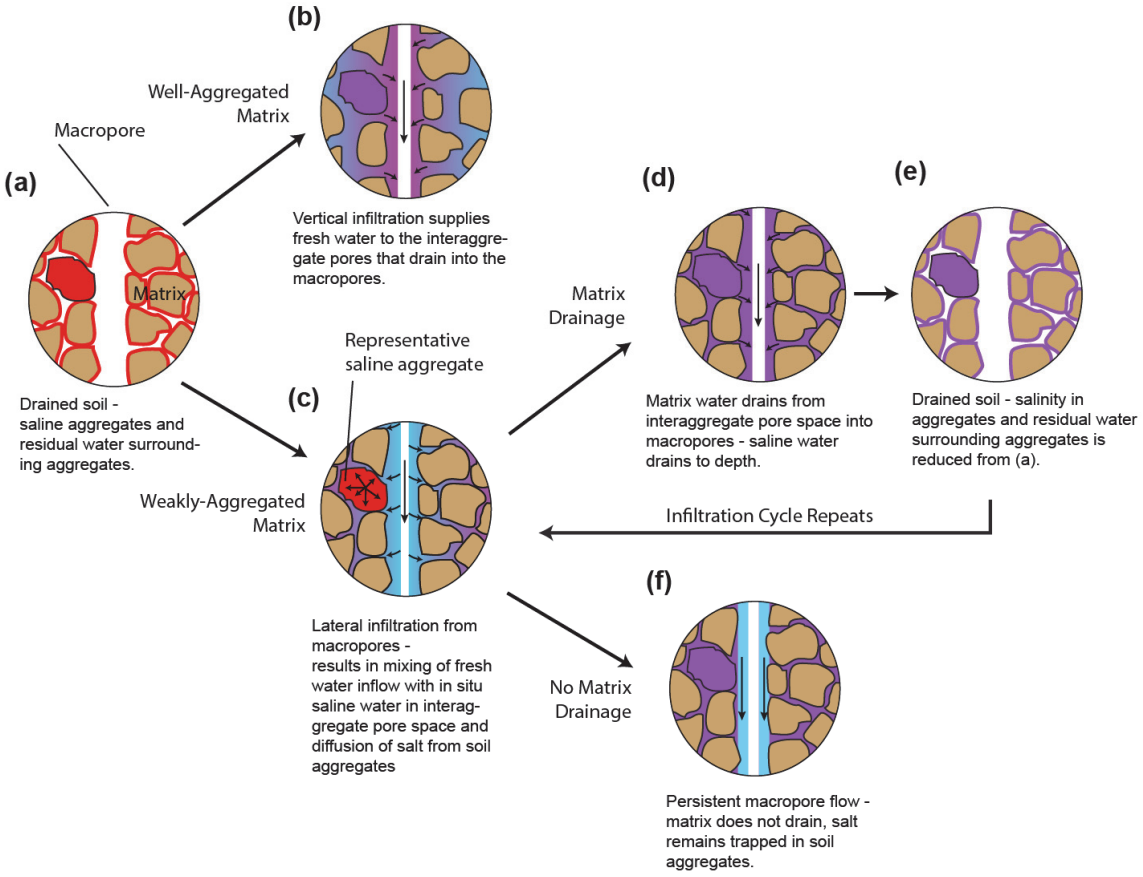

Fig. 5.4. Conceptual model of leaching in fine-grained macroporous soil: (a) drained soil prior to leaching; (b) subsurface macropore flow generation; (c) lateral infiltration from macropore; (d) matrix drainage of saline water into macropore; (e) drained soil of reduced salinity; and, (f) persistent macropore flow restricting matrix drainage and leaching.

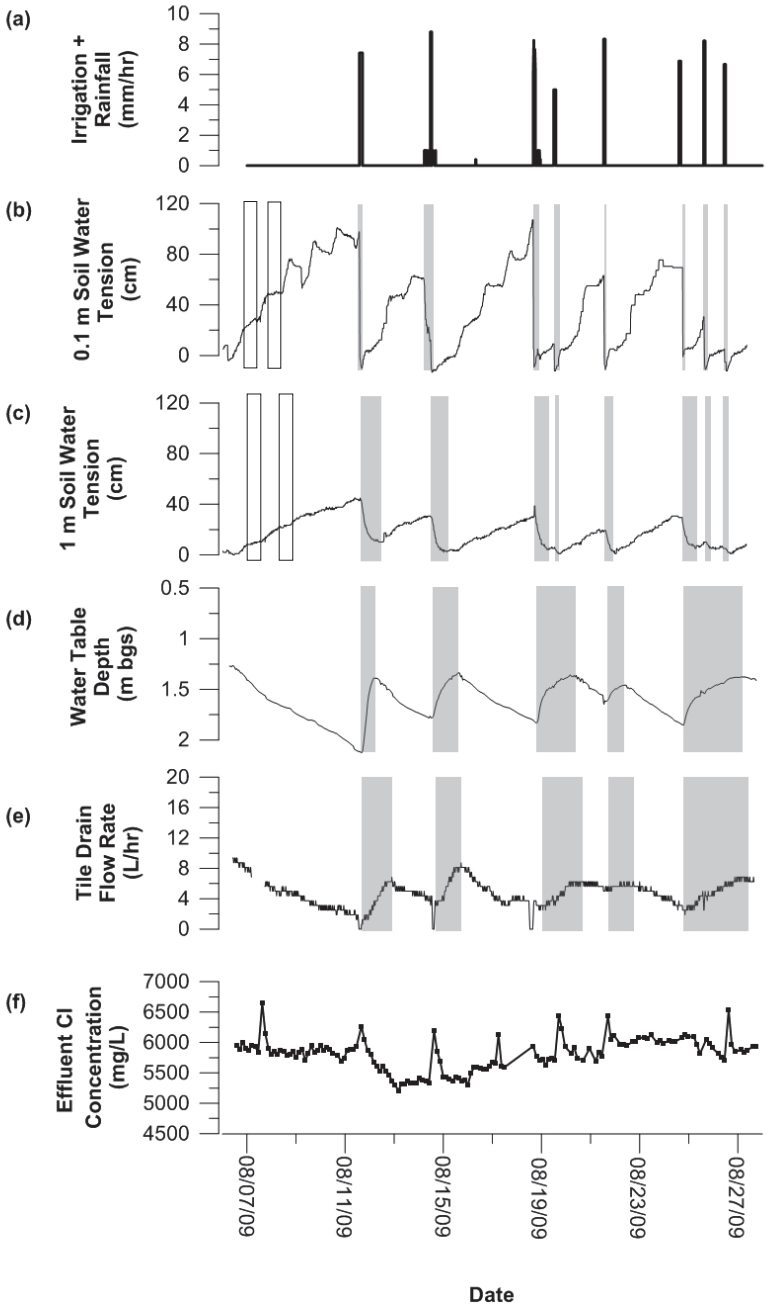

Fig. 5.5. Year 1 irrigation experiment monitoring results for representative 20-d period 7 Aug. to 27 Aug. 2009 showing: (a) intensity of water applied (irrigation + rainfall); (b) soil water tension at 0.1-m depth; (c) soil water tension at 1.0 m depth; (d) water table depth; (e) tile drain flow rate; and, (f) tile drain effluent concentration. Grayed areas in (b) through (e) indicate period of infiltration response. Boxes in (b) and (c) highlight drainage portion of the drying curve.

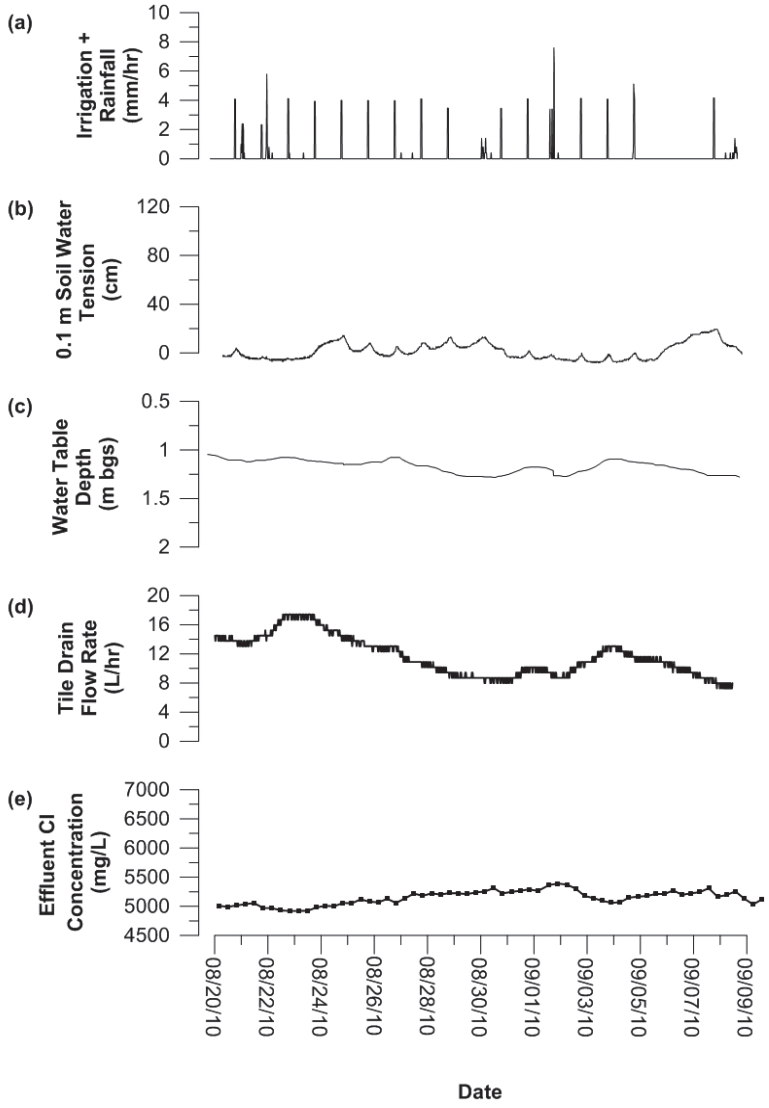

Fig. 5.6. Year 2 irrigation experiment monitoring results for representative 20-d period 20 Aug. to 9 Sep. 2010 showing: (a) intensity of water applied (irrigation + rainfall); (b) soil water tension at 0.1-m depth; (c) water table depth; (d) tile drain flow rate, one-hour moving average; and, (e) tile drain effluent concentration.

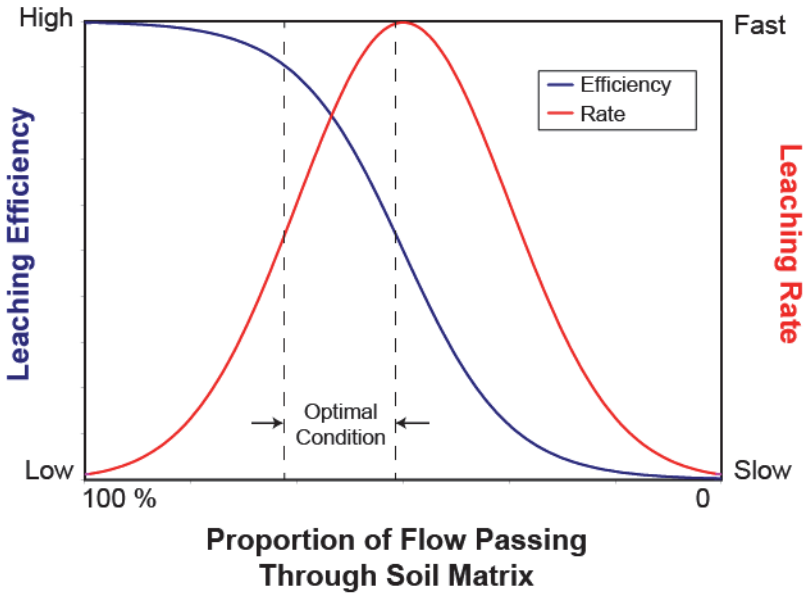

Fig. 5.7. Hypothetical relationship between proportion of soil matrix flow, leaching efficiency and leaching rate in fine-grained, macroporous soil.

CHAPTER 6: CONCLUSIONS AND RECOMMENDATIONS

6.1 Summary of Conclusions

Determination of salinity as EC and sodicity as SAR in gypsiferous soils is complicated by the potential for excess dissolution of gypsum during preparation of the soil SPE. Comparison of SO_4 concentrations measured in the SPE to soil water concentrations from field soil water samples demonstrates that gypsum dissolution produces excess Ca and SO_4 in the SPE. Saturated paste extract EC data may be adjusted by subtracting the excess SO_4 contribution to EC. Saturated paste extract SAR data may be adjusted by subtraction of excess Ca from total Ca, and its relative effect on SAR was determined by equilibrium cation exchange modeling. Adjustment produces a decrease in EC and an increase in SAR relative to that measured in the SPE. As EC and SAR levels decrease towards remediation target levels, the magnitude of the measurement difference increases, hence the relative importance of adjusting for excess gypsum dissolution also increases. Adjusting for gypsum dissolution in the SPE increases the accuracy of measurement of soluble salts (as EC) and sodicity (as SAR), and thereby improves the reliability of data interpretation relative to soil remediation guidelines.

Permeameter testing on intact cores taken from a structured subsoil indicates that diffusion of salt out of low permeability soil aggregates is controlling the rate of saline-sodic swelling and thereby the rate of hydraulic conductivity decrease. Potential causes of increased sensitivity to saline-sodic swelling include: localized loss in hydraulic conductivity in conductive pores causing a disproportionate decrease in bulk soil hydraulic conductivity; or subsoil confinement increasing the degree of internal swelling. Increased sensitivity observed for the intact cores used in this study, suggests that loss of hydraulic conductivity in structured field soils would be underpredicted by conducting similar permeameter tests on repacked soil columns. Additionally, decreases in hydraulic conductivity resulting from macropore disruption are not fully reversible. Uncertainty regarding the reversibility of pore network damage caused by clay swelling, motivates prevention of saline-sodic swelling in field soils before it occurs.

Leaching of salt-affected, fine-grained macroporous soil is complicated by the low hydraulic conductivity of the soil matrix. Results of our plot-scale irrigation experiment demonstrate that efficient leaching is possible in fine-grained, macroporous soil, if water application is appropriate for the soil moisture conditions. Excessive water application and/or poor drainage can result in excessively wet soil moisture conditions that promote preferential flow in macropores. Direct infiltration through macropores may result in inefficient leaching of the soil matrix. Avoidance of excessively wet soil conditions by adjusting water application in response to soil water tension may serve to limit bypass flow and promote efficient leaching of the soil matrix. The key to effective leaching is cycles of infiltration and drainage that transfer saline water from the matrix to the macropores. If persistent macropore flow is generated in the absence of matrix drainage then negligible leaching may result. The optimum duration between irrigation events occurs when matrix drainage has decreased to a negligible rate a few days following infiltration. The SWT value corresponding to the slowing of drainage can be exploited as a setpoint to trigger irrigation. Soil moisture content is therefore cycled through an optimal range for timely leaching. By improving leaching effectiveness, both soil remediation timelines and the amount of applied irrigation water will be reduced. Benefits of efficient leaching include reduced soil remediation costs and improved irrigation water conservation.

6.2 Recommendations for Future Research

The first key finding of this research is the higher degree of sensitivity of intact, structured soil to saline-sodic swelling effects on hydraulic conductivity in comparison to repacked, unconfined soils. This result suggests that in situ subsoil may be more susceptible to significant degrees of hydraulic conductivity loss caused by clay swelling effects on pore structure. A limitation of the current study is the small scale of the 51-mm diameter soil cores used in the permeameter testing. Thereby the swelling effects on hydraulic conductivity observed were limited to relatively small scale soil structure. A logical extension of this research would be to increase the scale of investigation to either large core scale, such as 200–300 mm diameter cores, or plot scale. This increase in scale would increase inclusion of larger scale

soil structure for which the investigation of saline-sodic swelling effects is the primary goal. In particular, the dynamic nature of saline-sodic swelling effects on macropore hydraulic conductivity is of interest from the point of view that macropores are the dominant water conducting pores in fine-grained soil. Therefore, disruption of macropore hydraulic conductivity caused by clay swelling is of importance from a perspective of maintaining good soil drainage during reclamation or remediation of salt-affected soils.

The second key finding of this research is the demonstration of a strong dependency of salt leaching efficiency and rate on soil moisture conditions in fine-grained, macroporous soils. An argument was made for the existence of an optimal range of soil moisture conditions conducive to either maximum leaching efficiency or maximum leaching rate. The complex interaction between macropore flow and leaching of the saline soil matrix coupled with a multitude of potential hydrologic conditions (e.g., irrigation rate, soil moisture, soil drainage, natural precipitation, etc.) makes optimization of this problem well-suited to numerical modeling and simulation. Numerical modeling may include calibration and validation of a model capable of capturing the macropore-matrix water and solute interaction described in the conceptual model. If sufficient accuracy is achieved in the numerical model results, then the effect of various combinations of hydrologic conditions could be simulated. One possible goal of such a simulation exercise would be to develop curves for leaching rate and leaching efficiency vs. measures of dynamic soil moisture condition (e.g., time between infiltration events, magnitude of dry end setpoint, irrigation rate, etc.) that would allow practitioners to readily evaluate the effects on leaching performance.

APPENDIX A: ADJUSTMENT OF SPE SAR FOR EXCESS GYPSUM DISSOLUTION BY EQUILIBRIUM CATION EXCHANGE

Determination of Unadjusted Exchangeable and Total Cation Concentrations

To determine the adjusted soluble Ca concentration and thus the adjusted SAR, total cation concentrations, including both soluble and exchangeable components, must first be determined. By combination and manipulation of Eq. [2.13] and [2.14], the unadjusted NaX concentration in the saturated paste is written as:

$$\mathrm{NaX} = \frac{\mathrm{CEC} \cdot K_G \cdot \mathrm{SAR}}{1 + K_G \cdot \mathrm{SAR}} \qquad [A1]$$

Total sodium concentration, soluble plus exchangeable ($mmol_c\ kg^{-1}$) is then given as:

$$T_{\mathrm{Na}} = \mathrm{Na} \cdot \mathrm{SP} / \rho_w + \mathrm{NaX} \qquad [A2]$$

Multiplication of the soluble Na concentration by the saturation water percentage expressed as a decimal fraction (SP) and division by the density of water (taken to be 1.00 kg L^{-1}) converts the dissolved Na concentration to a $mmol_c\ kg^{-1}$ basis. Exchangeable Ca + Mg can then be determined as the difference between the CEC and NaX:

$$(\mathrm{CaX} + \mathrm{MgX}) = \mathrm{CEC} - \mathrm{NaX} \qquad [A3]$$

Total (Ca+Mg) is thus:

$$T_{(\mathrm{Ca+Mg})} = (\mathrm{Ca} + \mathrm{Mg})\,\mathrm{SP}/\rho_w + (\mathrm{CaX} + \mathrm{MgX}) \quad [A4]$$

Determination of Adjusted Total, Exchangeable and Soluble Cation Concentrations

To adjust total cation concentrations, the amount of excess Ca is taken to be equal to excess SO_4 from gypsum dissolution, Eq. [2.3]. The adjusted total (Ca + Mg) concentration is determined by subtracting excess Ca from the unadjusted total (Ca + Mg) concentration:

$$T_{(\mathrm{Ca+Mg})\mathrm{adj}} = T_{(\mathrm{Ca+Mg})} - \mathrm{Ca}_{\mathrm{excess}}\mathrm{SP}/\rho_w \quad [A5]$$

To calculate the adjusted SAR, adjusted values must first be determined for the soluble and exchangeable Na and (Ca + Mg). This method utilizes an iterative solution. An initial value of adjusted NaX is required to initialize the iteration process. A recommended initial value for $NaX_{corr,1}$ is its unadjusted value taken from Eq. [A1]. Subscripts 1 and 2 are used to denote the variable and target values of NaX_{corr}, respectively. Total Na in the saturated paste is assumed to be constant during the gypsum dissolution process. The adjusted soluble Na concentration is then calculated as the difference between the total Na and the adjusted value for NaX:

$$\mathrm{Na}_{\mathrm{adj}} = (T_{\mathrm{Na}} - \mathrm{NaX}_{\mathrm{adj},1})\rho_w / \mathrm{SP} \quad [A6]$$

The adjusted exchangeable (Ca + Mg) is determined as the difference between the CEC, and the adjusted variable NaX:

$$(\mathrm{CaX} + \mathrm{MgX})_{\mathrm{adj}} = \mathrm{CEC} - \mathrm{NaX}_{\mathrm{adj},1} \quad [A7]$$

The adjusted soluble (Ca + Mg) is then determined as the difference between the adjusted total (Ca + Mg) from Eq. [A5] and the adjusted exchangeable (Ca + Mg) from Eq. [A7]:

$$\left(\mathrm{Ca}+\mathrm{Mg}\right)_{\mathrm{adj}} = [\mathrm{T}_{\mathrm{Ca+Mg,\,adj}} - \left(\mathrm{CaX}+\mathrm{MgX}\right)_{\mathrm{adj}}\,]\,\rho_{\mathrm{w}} / \mathrm{SP} \qquad [A8]$$

With the soluble and exchangeable ion concentrations now adjusted, the adjusted SAR is given as:

$$\mathrm{SAR}_{\mathrm{adj}} = \frac{\mathrm{Na}_{\mathrm{adj}}}{\sqrt{(\mathrm{Ca}+\mathrm{Mg})_{\mathrm{adj}} / 2}} \qquad [A9]$$

The final value of $\mathrm{SAR}_{\mathrm{adj}}$ is calculated using iteration, such as using the Goal Seek tool within an Office Excel spreadsheet (Microsoft, 2003), to solve for the target value of $\mathrm{NaX}_{\mathrm{adj,\,2}}$:

$$\mathrm{NaX}_{\mathrm{adj,\,2}} = \frac{K_{\mathrm{G}} \cdot \mathrm{CEC} \cdot \mathrm{SAR}_{\mathrm{adj}}}{1 + K_{\mathrm{G}} \cdot \mathrm{SAR}_{\mathrm{adj}}} \qquad [A10]$$

subject to the minimization of the difference between estimates of $\mathrm{NaX}_{\mathrm{adj,}}$ ε:

$$\varepsilon = \mathrm{NaX}_{\mathrm{adj,\,2}} - \mathrm{NaX}_{\mathrm{adj,\,1}} \qquad [A11]$$

The iteration of $\mathrm{NaX}_{\mathrm{adj,\,1}}$ and $\mathrm{NaX}_{\mathrm{adj,\,2}}$ continues until a specified tolerance criterion for Eq. [A11] is met. An absolute tolerance of ±0.001 was applied in this study.

This multi-step procedure for SAR adjustment is particularly well suited to implementation in a spreadsheet software program, whereby each numbered equation, Eq. [A1–A11], is entered in a successive column of the spreadsheet. Calculation of $\mathrm{SAR}_{\mathrm{adj}}$ then proceeds quickly on a row by row basis.

APPENDIX B: SOIL WATER CHARACTERISTIC CURVE

Soil water retention was determined on 16 intact, 32-mm diameter soil cores collected over a depth range of 0.3–2.1 m from the glaciolacustrine silt loam layer. A pressure plate extractor (Model 1600, Soilmoisture Equipment Corp.) was used to dry the samples as per the method of Klute (1986). The soil water characteristic curve (SWCC) (drying curve only) was developed using nine pressure steps over a range from 1.2–2000 cm H_2O. The SWCC presented in Fig. B1 was determined by curve-fitting the van Genuchten-Mualem retention model (van Genuchten, 1980) to the measured data using the RETC software program (van Genuchten et al., 1991). Soil water retention parameters are presented in Table B1.

References

Bishop, J.M. 2012. The influence of macropores on flow and transport to subsurface drains in low permeability, salt affected soils. M.Sc. diss., University of Calgary, Calgary, AB.

Klute, A. 1986. Water retention: Laboratory methods. In: A. Klute, editor, Methods of soil analysis. Part 1. Physical and Mineralogical Methods. 2nd ed. Agron. Monogr. 9, Madison, WI. p. 635-662.

van Genuchten, M.T. 1980. A closed-form equation for predicting the hydraulic conductivity of unsaturated soils. Soil Sci. Soc. Am. J. 44:892-898.

van Genuchten, M.T., Leij, F.J. and Yates, S.R., 1991. The RETC Code for Quantifying the Hydraulic Functions of Unsaturated Soils. Version 1.0. EPA Report 600/2-91/065, U.S. Salinity Laboratory, USDA, ARS, Riverside, CA.

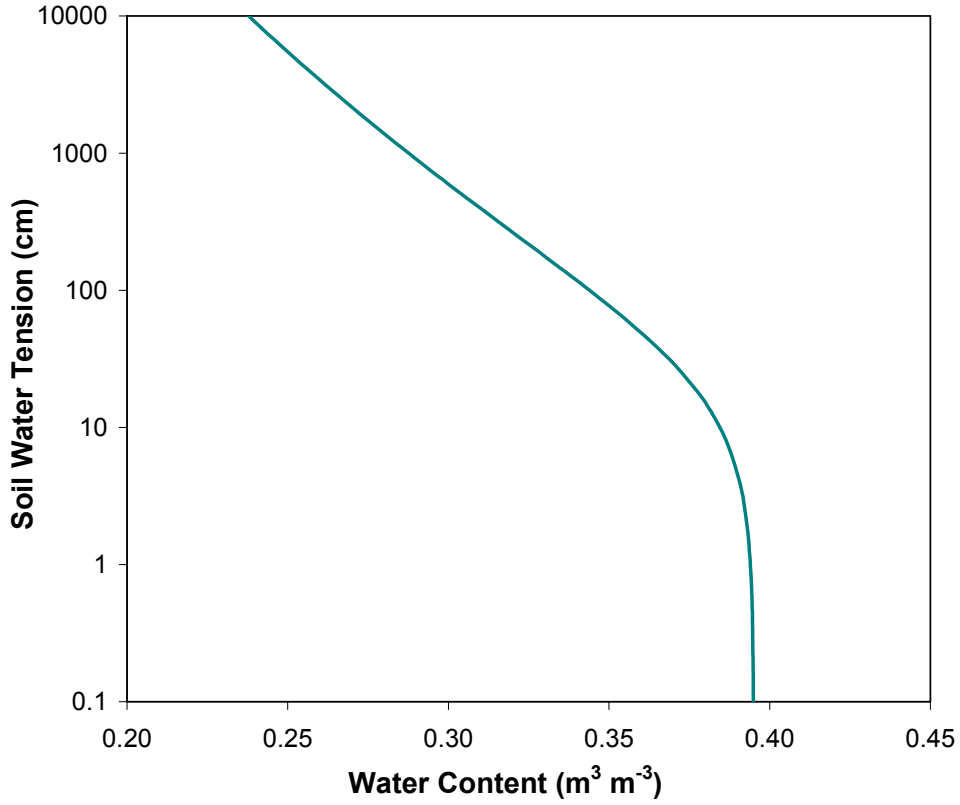

Fig. B1. Soil water characteristic curve (drying) developed for the glaciolacustrine silt loam layer.

Table B1. Input parameters for the van Genuchten-Mualem soil water retention model following van Genuchten (1980), values after Bishop (2012).

θ_R	θ_S	α (m^{-1})	n^Z
0	0.395	4.5	1.08

$^Z m = 1 - 1/n$